CHALMERS

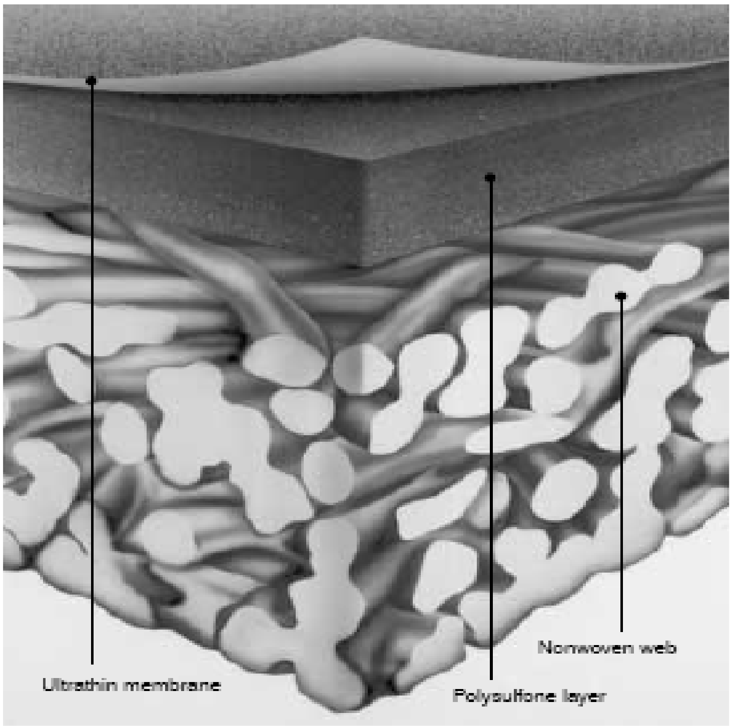

Membrane Characteristics on Flux and Rejection to Nanofiltration

Master's Thesis in the International Master's Programme
Applied Environmental Measurement Techniques

YANG ZHANG

Department of Civil and Environmental Engineering
Water Environment Transport
CHALMERS UNIVERSITY OF TECHNOLOGY
Göteborg, Sweden 2005
Master's Thesis 2005:24

Membrane Characteristics on Flux and Rejection to Nanofiltration

By

Yang Zhang

A Thesis Submitted to

the Department of Water Environment Transport

in Partial of Fulfillment of the Requirements for

the Degree of Master of Science

at

Chalmers University of Technology

Thesis Supervisor

Prof. Bart Van der Bruggen

Chemical Engineering Department
Katholieke University of Leuven, Belgium

Prof. Greg Morrison

Department of Water Environment Transport
Chalmers University of Technology, Sweden

February 2005, Göteborg

Abstract

Membrane technology has a bright future in water and wastewater treatment applications; it is considered one of the most important water treatment techniques in 21st Century. Nanofiltration, a kind of membrane filtration, is taking an important role in water disinfection, reuse of wash water and seawater desalination.

However, fouling is a paramount problem in membrane applications. Recent studies have shown that membrane characteristics such as roughness, internal structure, hydrophobicity and zeta potential influence volume flux and solute rejection as well as fouling behavior. However, the essential relationship between membrane characteristics, performance and solution parameters are lack of synthetic study and still not well understood.

The objective of the thesis is to find out the essential relationship between the characteristics of three different nanofiltration membranes NF, LE, XLE (DOW Filmtec®) and the flux decline, solute rejection as well as membrane fouling. Membrane surface characteristics were detected by adequate measurement techniques. Water flux and solute rejection data obtained in a laboratory-scale crossflow filtration unit at identical initial permeation rates so that the effect of the transverse hydrodynamic force (permeation drag) on the fouling of all membranes is comparable. The data were correlated to the measured membrane surface properties.

Based on the results, the relationship between the surface characteristics of three different membranes, their performance (normalized flux, solute rejection) and solution parameter such as solute concentration, pH value and coupled solutions (salt and colloidal particles) will be discussed and concluded. Micrographs from Atomic Force Microscopy and Scanning Electron Microscopy of the membrane surfaces and cross-sections were also taken to reveal the conclusions by experiment and modeling. At last, revaluation of the three membranes will be performed.

Membrane Characteristics on Flux and Rejection to Nanofiltration

By

Yang Zhang

International Master Programme in Applied Environment Measurement Techniques

Department of Water Environment Transport

Chalmers University of Technology

Göteborg, Sweden

Acknowledgement

This Master Thesis has been done in the Laboratory for Environmental Technology, Department of Chemical Engineering, Katholieke University of Leuven (KUL), Belgium and some supervision during thesis writing from Department of Water Environment Transport, Chalmers University of Technology (Chalmers), Sweden, under the supervision of Professor Bart Van der Bruggen (in KUL) and Professor Greg Morrison (in Chalmers).

First of all, I would like to express my sincere gratitude to my supervisor, Professor Bart Van der Bruggen for his patience and guidance from the preparation to writing of this thesis and. Before I carried out the experiment on membrane filtration I knew quite a few in this area, his guidance really helped me a lot. He also carefully examined my thesis drafts and gave me a lot of very valuable advice.

I would like to appreciate Ir. Katleen Boussu for allowing me to work with her on this very interesting topic. She supervised me when I meet some specific problem during experiment and thesis writing. She also helped me to deal with the AFM, electrokinetic properties of silica particles and membrane zeta potential measurements.

I also want to thank Professor Greg Morrison for accepting to be my supervisor in Chalmers, and discussing about my thesis writing.

I want to show my appreciation to Ir. Leen Breaken, Ir. Jeroen Geens and Madam Michèle Vanroelen. They also helped me a lot during the experiments in the laboratory.

At last, I would like to express my appreciation to Prof. Marianne Nyström from Lappeenranta University of Technology in Finland, for her very valuable comments on my thesis draft.

Table of Content

1. Introduction

1.1 Membrane-“semi-permeable barrier”

A membrane is a kind of filter that is used to separate the suspended or dissolved matter (ions, organics, colloids and so on) in water which at micrometer or nano level, and the common description of the membrane as a “semi-permeable barrier”.

Based on the membranes characteristics (pore size), operation conditions and applications (see Figure 1.1 *Separation performance of different membranes*, and Table 1.1, *Pressure and flux range in different membrane processes*), they can be defined as microfiltration (MF), ultrafiltration (UF), nanofiltration (NF) and reverse osmosis (RO). It is accepted that MF and UF membrane have pores and more open structures and their separation mechanism is “sieve mechanism”, whereas NF and RO are more tight and the mechanism could be described both “sieve mechanism” and charge effect. [15]

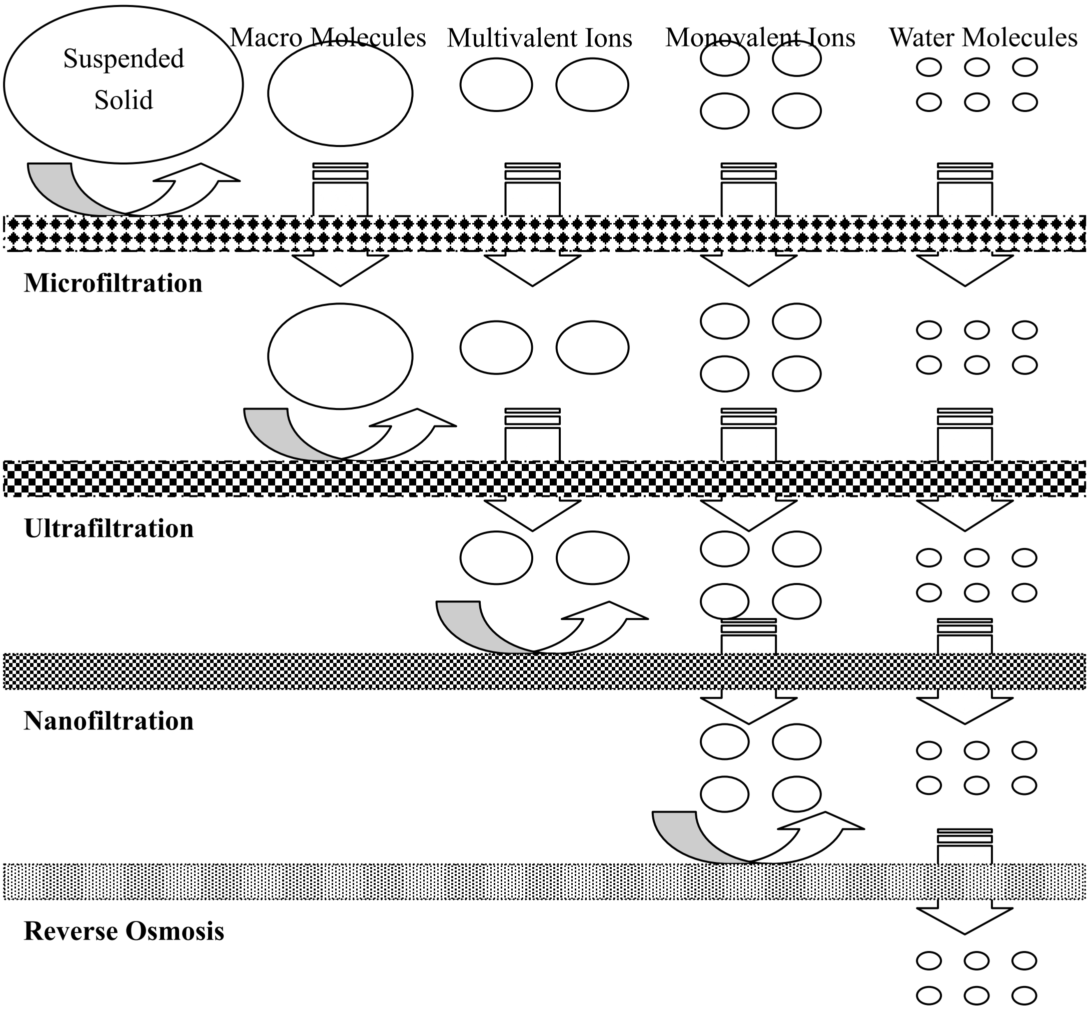

Figure 1.1: Separation Performance of Different Membranes

Table 1.1 Pressure and flux range in different membrane processes[21]

Membrane process	Pressure range (bar)	Flux range ($l.m^{-2}.h^{-1}.bar^{-1}$
Microfiltration	0.1-2.0	>50
Ultrafiltration	1.0-5.0	10-50
Nanofiltration	5.0-20	1.4-12
Reverse Osmosis	10-100	0.05-1.4

At the middle of eighteenth century membrane phenomena were observed and studied, primarily to elucidate the barrier properties and related phenomena rather than to develop membranes for technical and industrial applications.

The first commercial membranes for practical applications were manufactured as bacteria filters in laboratory by Sartorius in Germany after World War I. Although the phenomenon of dialysis had already been known for a long time, the first practical membrane application on hemodialysis was demonstrated by Kolff in the 1940s.

History on the development of membrane processes applications is listed below:

Table 1.2 Development of membrane processes

membrane process	country	year	application
microfiltration	Germany	1920	laboratory use(bacteria filter)
ultrafiltration	Germany	1930	laboratory use
hemodialysis	Netherlands	1950	artificial kidney
electrodialysis	USA	1955	desalination
reverse osmosis	USA	1960	sea water desalination
ultrafiltration	USA	1960	concentration of macromolecules
gas separation	USA	1979	hydrogen recovery
membrane distillation	Germany	1981	concentration of aqueous solutions
pervaporation	Germany/ Netherlands	1982	dehydration of organic solvents

1.2 Nanofiltration membrane

Nanofiltration (NF) is a pressure-driven membrane separation process of witch the first applications started to be used in the last decade. It is a separation process where low molecule weight organics and multivalent ions are retained by a membrane. For nanofiltration, this pressure differences is about 5-20 bar. The structure of nanofiltration membranes in application is usually composites of polymer layers, which is thin selective layer (thickness to 1μm) on thicker nonselective support.

The properties of NF membranes lie between ultrafiltration (UF) and reverse osmosis (RO) membranes. It always can retain molecules which MW about 200-1000, that is to say, the pore diameter of nanofiltration is about 0.7-1.3 nm. The surface of nanofiltration membrane is always charged, it has high retention performance for multivalent ions. But compared to RO, NF membrane has low retention for monovalent ions, this point is important to distinguish NF and RO membrane.

NF membranes have been on the market for about 20 years, and have been applied industrially for 15 years. Today most membrane manufacturers also produce NF membranes. The membranes are made of many different materials, mostly from polymers such as aromatic polyamides, polysulfones, polyethersulfones and substituted poly(vinyl alcohols), poly(acrylonitrile), poly(phenylene oxide) as well as from different modifications of them. NF membranes today can also be made of inorganic materials such as alumina, titania, hematite, and/or silica on alumina or of mixtures of organic and inorganic materials such as zirconia and polyphosphazene.[43]

Membrane applications are found in the production of drinking water (softening, removal of NOM and color) and in industrial water treatment. For nanofiltration, it has used to perform the following separations: hazardous removal from drinking water,[46] metal recovery from effluents,[48] treatment of wastewater from the textile industry,[44] brewery industry,[45] pulp and paper industry,[47] and purification in the pharmaceutical,[49] food and biotechnological industries[50].

Humic substances can be removed from water by a number of different treatment processes because the humic substances are high molecular weight organic molecules carrying a negative charge, like colloids. The conventional treatment method is by coagulation/flocculation separation, but also sorption processes like ion exchange and adsorption on activated carbon as well as membrane filtration processes and oxidation/biofiltration processes can be used. [27]

2 Literature Review

Characterization of the membrane pore structure, such as pore radius, pore density, pore shape, pore length, tortuosity and so on, is very important in view of understanding the process; therefore, and characterization methods must be established. Several characterizing methods have been applied into research, both based on direct instrument observation and experimental methods.

2.1 Methods for membrane structure characterization

There are four methods are applied in the membrane structure characterization, they take important roles to help membranists determine membrane performance and choose an appropriate membrane in a certain application.
Firstly, the microscopy observation method which is the most direct method to characterize the membrane pore structure. Atomic force microscopy (AFM) and scanning electron microscopy (SEM) have been applied for the membrane observation. Secondly, a method based on bubble pressure and gas transport has been applied into the probes. This method can measure the pore size distribution of a membrane under wet condition. The third method is thermoporometry. The temperature of liquid solidification and/or solid melting is lower in smaller pores and thus by measuring the freezing and/or the melting thermodiagram, the pore size and its distribution can be determined in wet environment. These three methods are not directly related with the solute or particle permeation performance, therefore, the fourth and last method is the characterization based on molecular transport through a membrane, which is the most important characteristics of separation membranes. [15]

In the last method, if the relationship between the flux and rejection and the membrane structure is known, the membrane structure (thickness, tortuosity, pore size, pore density etc.) can be characterized (see Figure 2.1).

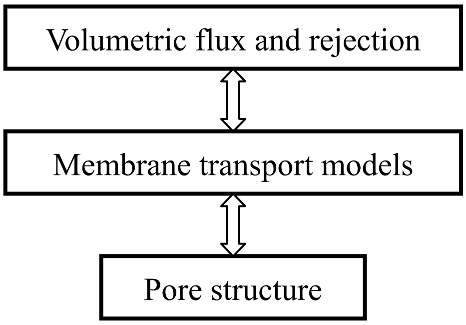

Figure 2.1 Membrane structure characterization by mass transport method

Models which can interpret experimental flux and rejection into membrane pore structure are necessary for the characterization of the membrane.

2.2 Influence of membrane internal structure on transport through membranes

In the past several decades three major approaches have been studied by many membranologists for describing transport phenomena through porous membranes, and each theory has led to its own way for description and modeling of the transport of solute molecules.

The first approach for analysis is based on irreversible thermodynamics derived by Kedem and Katchalsky [16] and Spiegler and Kedem [2].
The second approach is the Stefan-Maxwell multicomponent diffusion equations, which has been introduced into analysis of membrane transport by Peppas and Meadows [18] and Robertson and Zydney [19].
The last approach is called the hydrodynamic model or pore model. It started from the pioneering work done by Ferry in 1936[20].
The former two approaches treat the membrane as a black box, and thus can be applicable to both porous and non-porous membranes. The equations are derived phenomenologically, and they relate inputs and outputs of the membrane and involve the membrane transport properties. The latter is derived from the fundamental hydrodynamic equation for the trans-capillary transport of rigid spheres.

The extended Nernst–Planck model has been used to characterise membranes in terms of both structural and electrical parameters [51]. Recent models have developed this approach to include both steric and hindered transport within the NF pores [52]. Studies of NF membranes using atomic force microscopy (AFM) [53] and nitrogen adsorption–desorption [54] have, however, shown a significant distribution of pore sizes. Cooper and van Derveer investigated the distribution of pores at polysulfone membranes by measuring dextran rejection as a function of molecular weight and found a linear dependency when plotted on log-probability paper, suggesting a log-normal distribution of pores [55].
Mochizuki and Zydney have reviewed the geometric standard deviation (GSD) values that have been reported for many different types of membranes where values ranged considerably from 1.2 to 2.9 depending on both the membrane material and the molecular weight cut-off the membrane. [56]
In contrast, Leypoldt predicted sieving characteristics from measured pore size distributions and concluded that it was not possible to obtain actual distributions from experimental data of sieving coefficient as a function of molecular weight because sieving characteristics were not uniquely dependent on the assumed pore size distribution.[57] Aimar, Meireles, and Sanchez proposed a method for obtaining the log-normal pore size distribution of UF membranes based upon the normalisation of the curves of sieving coefficient against molecular weight with an experimentally measured solute rejection.[58]

Recent work on the theoretical elects of pore size distributions on uncharged solute transport by Mochizuki and Zydney has attempted to quantify solute rejection and flux using log-normal and Gaussian distributions. [56] Saksena and Zydney continued this work to investigate pore size elects in electrokinetic quantities such as zeta potential and electro-osmotic flow. [59]

Van der Bruggen et al. compared the steric hindrance pore model, the model of Zeman and Wales, the log-normal model and an adapted version of the log-normal model by the retention data of a board range of small organic molecules, found out that log-normal model is the most useful model to predict reflection coefficients.[4]

After studied the experimental data by three different membranes, NF70, NTR 7450 and UTC-20 with uncharged molecules, Van der Bruggen and Vandecasteele pointed out that the modelling with molecular weight as a size parameter is nearly as valuable as the modelling with the effective diameter as a size parameter by using the log-normal model.[62]

3 Problem Statement and Research Purpose

3.1 Problem statement:

Fouling is a paramount problem in membrane applications. Recent studies have shown that membrane characteristics such as roughness, internal structure, hydrophobicity and zeta potential influence volume flux and solute rejection as well as fouling behavior. However, the essential relationship between membrane characteristics, performance and solution parameters are lack of synthetic study and still not well understood.

3.2 Purpose:

The objective of the thesis is to find out the essential relationship between the characteristics of three different nanofiltration membranes NF, LE, XLE (DOW Filmtec®) and the flux decline, solute rejection as well as membrane fouling. Membrane surface characteristics were detected by adequate measurement techniques. Water flux and solute rejection data obtained in a laboratory-scale crossflow filtration unit at identical initial permeation rates so that the effect of the transverse hydrodynamic force (permeation drag) on the fouling of all membranes is comparable. The data were correlated to the measured membrane surface properties.

Based on the results, the relationship between the surface characteristics of three different membranes, their performance (normalized flux, solute rejection) and solution parameter such as solute concentration, pH value and coupled solutions (salt and colloidal particles) will be discussed and concluded. Micrographs from Atomic Force Microscopy and Scanning Electron Microscopy of the membrane surfaces and cross-sections were also taken to reveal the conclusions by experiment and modeling. At last, revaluation of the three membranes will be performed.

4. Basic Theory

4.1 Characterization of Membranes

Membrane surface roughness, charge, internal structure and hydrophobicity are the paramount parameters to influence the membrane performance on flux and rejection. The basic theory on these parameters will be introduced below to give a research profile of this thesis.

4.1.1 Membrane Surface roughness

For nanofiltration membranes, membrane surface roughness takes an important role in flux decline and fouling. In filtration of surface water, membrane fouling can be caused by organic compounds and/or particles.

Lee et al [78] pointed out that membrane roughness is considered as a more important factor in membrane organic fouling by controlling interaction between molecules and the membrane surface, compared to the hydrophobic/hydrophilic character of membranes. The significant fouling was caused by adsorption of organics around membrane pores by smaller molecules (pore construction) and/or pore blockage by larger molecules.
For the colloidal fouling, it is proved that the rate and extent of fouling are most significantly influenced by membrane surface roughness. [34] Hoek et al [11] pointed out that when particles approach closer to the membrane, they have a high probability of getting trapped in the valleys of the rough membranes.

4.1.2 Membrane charge

Membrane charge effect is very important to the performance of solute separation. Membrane charge mainly affects the retention of ions, charged molecules and colloids. Donnan Exclusion and DLVO theory are key theories to explain the action of charge effect.

4.1.2.1 Donnan Exclusion:

If charge effects were not present, the equilibrium concentrations of all components would be the same inside the pores as outside if ions are smaller than the pores of the membrane. However, in the case of a negative charged membrane, the stationary phase has a large number of negatively charge groups (R) which tend to attract counterions (Aland repel co-ions (X)). Thus, there is a tendency for positive ions to be pulled into the stationary phase pores and for negative ions to be repelled from them. Due to electroneutrality is maintained, thus anion has to permeate together with cation. This effect is called Donnan exclusion.

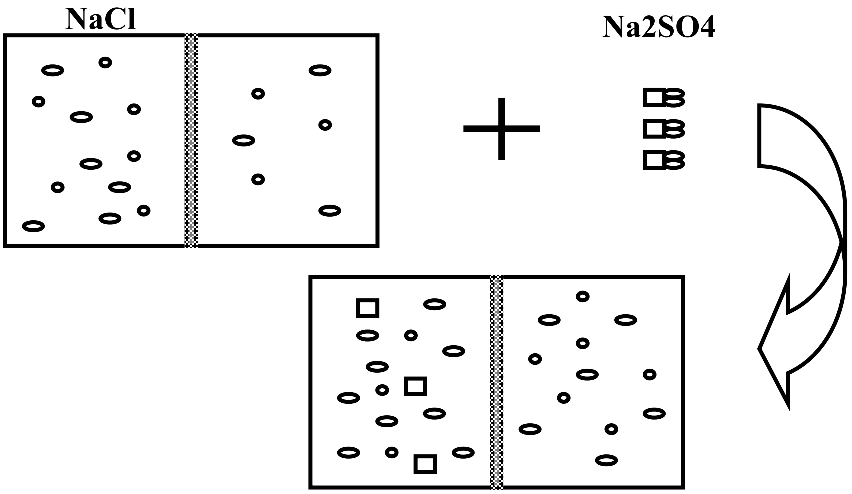

*⬭ =Na^+; ○ = Cl^-; □ = SO_4^{2-}; membrane is negatively charged.

Figure 4.1 Schematic diagram for Donnan Exclusion

In Figure 4.1, suppose the nanofiltration membrane is negatively charged, NaCl retention is about 33% (1/3); if some Na_2SO_4 is added into the left side of the container, due to Donnan Exclusion, SO_4^{2-} "kick" some chloride ions into another side of the membrane, sodium ions have to permeate together with chloride ions, thus, the retention of NaCl increases to 67% (2/3).

Donnan exclusion, which compared to other pressure driven membrane processes has a pronounced effect on the separation in NF. Due to the slightly charged nature of the membrane, solutes with an opposite charge compared to the membrane (counter-ions) are attracted, while solutes with a similar charge (co-ions) are repelled. At the membrane surface a distribution of co- and counter-ions will occur, thereby causing an additional separation. [14]

For negatively charged nanofiltration membranes, suppose only Donnan Exclusion effect available in separation mechanism, the sequence of salts retention should be like below:

$$R_{Na_2SO_4} > R_{NaCl} > R_{MgCl_2}$$

4.1.2.2 DLVO Theory:

Colloids can be present and have different interactions between themselves and to membrane surface.

The publication of the theories of Derjaguin and Landau (1941) and Vervey and Overbeek (1948) directed attention towards understanding the classical problem of colloid stability in both aqueous and non-aqueous media (Appendix 1).

One of the most important features of the theories was the unification they brought to a wide variety of systems which could be called "colloidal" in nature, and the interaction between macroscopic surfaces separated by distances commensurate with colloidal dimensions, typically 1nm - 100nm.

They introduced the fundamental idea that the understanding of complex colloidal phenomenology could be based on the concept of long-range forces; both attractive and repulsive, acting between assemblies of atoms or molecules. Hence, the development of pair potentials, which depend on the nature of the interactions, has been fundamental to progress in the basic science of dispersions.

Membrane separation processes involving interaction of colloidal particles with membrane surfaces have been studied quite avidly over the past decade, leading to considerable insight regarding the dominant particle transport and deposition mechanisms. Most of these studies highlight the paramount importance of colloidal interactions, typically represented in terms of the Derjaguin- Landau- Verwey-Overbeek (DLVO) theory, on particle deposition and fouling phenomena. [11]

4.1.3 Membrane internal structure

Membrane internal structure (such as pore size and its distribution) is an important factor in membrane separation (sieving) mechanism. Steric Hindrance Pore model (SHP model) and log-normal model are usually applied to describe the membrane pore size and its distribution. Van der Bruggen et al [3, 64] adapted the log-normal pore size model. The adapted log-normal model (molecular weight takes instead of molecular radii) is easier to be applied than the log-normal model and fits the experimental data well. [3, 4, 64]

4.1.3.1 Steric Hindrance Pore model (SHP model): [4]

Iwata and Matsuda have shown that if the membrane material contains protruding mobile groups, either naturally or applied by grafting, these groups can form a steric hindrance over the surface and the pores. [30]

The SHP model can thus be used to estimate the membrane pore radius: for a solute with known radius the reflection coefficient is determined and the pore radius can be calculated with equation:

$$\sigma = 1 - H_F S_F \qquad (4.1)$$

with:

$$H_F = 1 + \left(16/9\right)\eta^2 \qquad (4.2)$$

$$S_F = (1-\eta)^2\left[2-\left(1-\eta\right)^2\right] \qquad (4.3)$$

$$\eta = r_s \big/ r_p \qquad (4.4)$$

Where H_F is a “wall-correction parameter” that represents the effect of the pore wall, S_F is a parameter that represents steric hindrance during transport through the pore. The solute radius and the pore radius are symbolized by r_s and r_p respectively.

From Eq. (1) ~ (4), we can get the equation below:

$$\sigma = 1 - \left(1 + \frac{16r_s^2}{9r_p^2}\right)\left(1 - \frac{r_s}{r_p}\right)^2 \left[2 - \left(1 - \frac{r_s}{r_p}\right)^2\right] \quad (4.5)$$

In the Steric Hindrance Pore Model, the reflection coefficient is calculated from the pore size of the membrane and the diameter of the molecule. It is assumed that all the pores have the same size. Therefore, the uniform pore size should not be interpreted as a real value for the diameter of the pores. The calculated pore size corresponds with the pore size of an imaginary membrane with uniform pores, for which the retention of uncharged molecules is equal to retention with the real membrane. In reality, not every pore has the same cylindrical diameter; the model is an approximation of the membrane's structure.

The membrane is thus represented as a bundle of cylindrical pores through which molecule in solution can permeate. During the transport these molecules encounter a certain amount of steric hindrance and interactions with the pore wall. A molecule which is smaller than the diameter of the membrane is partially retained through these effects. A molecule with the same or larger size as the pore diameter is completely retained.

4.1.3.2 Log-normal Model and Its Adapted Formation: [3]

Log-normal distribution used for the calculation of the reflection coefficient as a function of the effective molecular diameter.

In the Log-normal Model, no steric hindrance in the pores or hydrodynamic lag is taken into account, and the value of σ (reflection coefficient) reflects the fraction of membrane pore that are smaller than the molecules in solution. The equation that calculates the reflection coefficient with a molar radius r* is:

$$\sigma(r) = \int_0^r \frac{1}{S_p\sqrt{2\pi}} \frac{1}{r} \exp\left(-\frac{\left[\ln(r) - \ln(\bar{r})\right]^2}{2S_p^2}\right) dr \quad \text{(eq. 4.6)}$$

This equation involves two variables, S_p and $\bar{r}$, where S_p is the standard deviation on the pore size distribution. This standard deviation is measure for the distribution of pore size. As the retention curve corresponds to an integrated log-normal distribution, a small "S_p" represents a large slope of the retention and the large "S_p" represents a small slope. $\bar{r}$ is the size of molecule that is 50% retention, namely average membrane pore size.

Although the molecular weight is not a direct measure of the dimensions of a molecule, it still reflects the molecular size, and it is a readily accessible parameter, whereas complicated calculations are necessary to obtain the effective diameter. However, the log-normal model can be adapted by taking the correlation between

molecular weight and the diameter of the molecule into account. This relation was already derived for the Stokes diameter and was determined for the effective diameter here. The equation for the correlation was found as d_S =A(MW)^B, where A=0.065 and B=0.438. This correlation is valid for the molecular weight range where nanofiltration typically operates (up to7600 Da, this is a very big molecule for nanofiltration) and is similar to the equation found for the Stokes diameter.
The equations of the log-normal model can be written as:

$$\sigma(MW) = \int_0^{MW} \frac{1}{S_{MW}\sqrt{2\pi}} \frac{1}{MW} \exp\left(-\frac{\left(\ln(MW) - \ln(\overline{MW})\right)^2}{2S_{MW}^{\ 2}} \right) dMW \quad \text{(eq. 4.7)}$$

In the equation and the tables, $\sigma(MW)$ is the reflection coefficient of a molecule to the membrane, S$_{MW}$ is the standard deviation which is proportional parameter here, $\overline{MW}$ is the average molecular weight where the retention is 90% under this molecular weight.

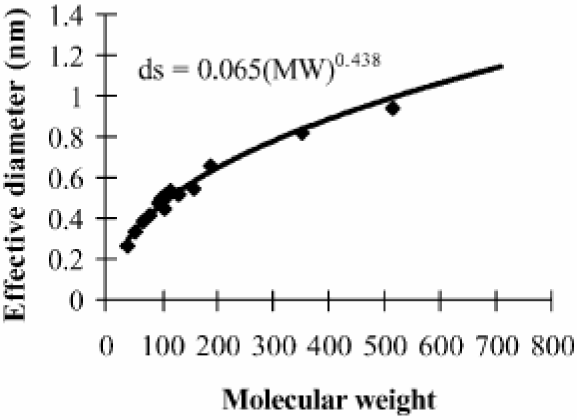

Figure 4.2: Correlation between molecular weight and effective diameter [3]

4.1.4 Membrane hydrophobicity

Membrane hydrophobicity is proved to take an important role in the retention of organic compounds due to the compounds can adsorb on the membrane surface and inside the pores. [32, 80, 81]

Previous research [32, 81] showed that the logarithm of the octanol–water partition coefficient ($\log K_{OW}$) (for more information about K_{OW}, see appendix 6) correlates well with adsorption on the membrane for molecules with a comparable molecular weight below the molecular weight cut-off (MWCO) of the membranes, indicating that hydrophobicity of the compounds influences the evolution of the permeate concentration in time.

Dipole moment of organic molecules is a parameter witch reflects the hydrophobicity of organic molecules. Van der Bruggen et al. [76] proved that the influence of the dipole moment of organic compounds on rejection.

4.2 Separation Mechanisms [1, 14, 21]

Uncharged compounds

Nanofiltration combines removal of uncharged components on nanoscale with charge effects between solution and the membrane. The removal of uncharged components may be a result from size exclusion, as known from ultrafiltration, or may be a result from differences in diffusion rates in a non-porous structure, which depend also on molecular size. According to the Stokes – Einstein law, expressing an inverse proportionality between the diffusion constant and the size of a component, the diffusion rate will be smaller for a larger component, resulting in an effect similar to size exclusion. The charge effect, on the other hand, results in removal of (mainly multivalent) ions, the former effect results in the removal of uncharged organic species.

It is usually accepted that the rejection of uncharged (organic) molecules is determined by the size of the dissolved molecules compared to the size of the membrane pores [63, 76]. Other physicochemical effects such as dipole interactions may also play a role. All models to describe the rejection of organic molecules that have been proposed are based on the sieving mechanism, and neglect other interactions [3]. These models make use of a parameter representing the size of the molecule (or a related parameter such as the diffusion coefficient), and a method to account for pore size distribution or steric hindrance. Rejections can be predicted, but the accuracy can be low when components are used that interact strongly with the membrane or cause fouling. In contrast, rejection of ionic components in NF is obtained in a totally different way: ions are rejected as a result of charge interactions between the membrane surface and the ions (Donnan exclusion). The divalent ions (hardness, sulphates) are more efficiently removed. For tight NF membranes, size exclusion can provide an additional ion rejection [5].

Ions

The NaCl rejection of membranes decreases with nanofiltration increasing salt concentration, which is a typical phenomenon if electrostatic interactions are involved in the rejection mechanisms. The distribution between the bulk on the feed side and the pore entrance is calculated using the Donnan distribution, the transport in the pore is described with the extended Nernst-Planck equation and the Donnan distribution is again applied for the distribution at the permeate side.

Basic definitions in transmembrane hydrodynamics and solute transport [21]

When there's no osmotic pressure difference across the membrane ($\Delta\pi = 0$), the transmembrane flow occurs because of the pressure difference (ΔP). This can be described as:

$(J_V)_{\Delta\pi=0} = L_1 \cdot \Delta P$ (eq. 4.8)

or

$L_1 = \left(\frac{J_V}{\Delta P}\right)_{\Delta\pi=0}$ (eq. 4.9)

L_1 is called the hydrodynamic permeability or water permeability of the membrane and is often referred to as L_P.
When there is no hydrodynamic pressure difference across the membrane ($\Delta P = 0$), the transmembrane flow occurs because of the osmotic pressure difference:

$(J_d)_{\Delta P=0} = L_2 \cdot \Delta\pi$ (eq. 4.10)

or

$L_2 = \left(\frac{J_d}{\Delta\pi}\right)_{\Delta P=0}$ (e.q 4.11)

L_2 is called the osmotic permeability or solute permeability and is often referred to as ω.
The reflection coefficient, σ, can be derived from steady-state permeation measurements. When no volume flux occurs ($J_V = 0$) under steady state conditions then:

$L_1 \cdot \Delta P + L_2 \cdot \Delta\pi = 0$ (eq. 4.12)

or

$(\Delta P)_{J_V=0} = -\frac{L_2}{L_1}\Delta\pi$ (eq. 4.13)

In the steady state (eq. 4.12), when the osmotic pressure difference equal to the hydrodynamic pressure difference, there is no solute transport across the membrane, the membrane is called completely semipermeable (L_1=L_2).
But membranes are always not completely semipermeable, so it can be described as the ratio L_2/L_1, this ratio is equal to reflection coefficient (σ) in quantity, that is to say:

$\sigma = -\frac{L_2}{L_1}$ (eq. 4.14)

Reflection coefficient σ is a measure of the selectivity of a membrane and usually has a value between 0 and 1.
$\sigma = 1 \Rightarrow$ ideal membrane, no solute transport
$\sigma < 1 \Rightarrow$ not a completely semipermeable membrane: solute transport
$\sigma = 0 \Rightarrow$ no selectivity

Volume flux (J_V) and solute flux (J_S) can be described as:

$$J_V = L_P\left(\Delta P - \sigma\Delta\pi\right) \quad \text{(eq. 4.15)}$$

$$J_S = \overline{C_S}\left(1-\sigma\right) J_V + \omega\Delta\pi \quad \text{(eq. 4.16)}$$

The solute transport through the membrane is indicated by three parameters: water (hydrodynamic) permeability L_P, solute permeability ω, and reflection coefficient σ.

If the solute is no completely retained by the membrane then the osmotic pressure difference is not $\Delta\pi$ but $\sigma \cdot \Delta\pi$.
When testing the pure water flux ($\Delta\pi = 0$) with different operation pressure, the schematic plot of volume flux as a function of the operation pressure like below:

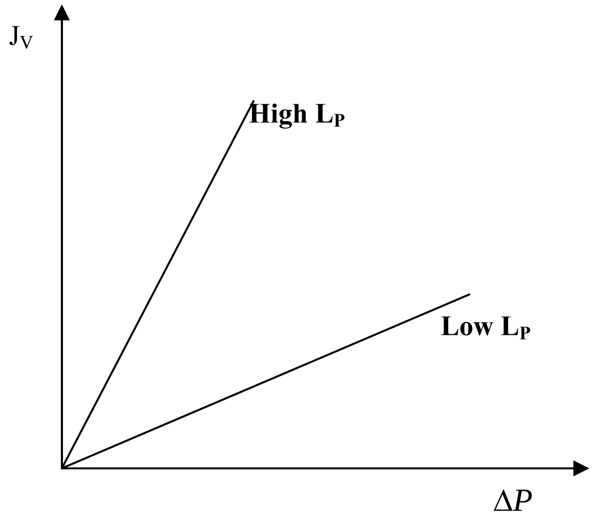

Figure 4.3: Schematic plot of volume flux as a function of the operation pressure

Higher L_P indicates that the membrane has more loose structure.
From the equation 4.1.9, the following equation can be obtained:

$$\frac{J_S}{\Delta c} = \omega + (1-\sigma)J_V \frac{\bar{c}}{\Delta c} \quad \text{(eq. 4.17)}$$

where Δc is the concentration difference between the feed and the permeate and $\bar{c}$ is the mean logarithmic concentration, $\bar{c}$ can be described as:

$$\bar{c} = \left(c_f - c_p\right)/\ln\left(c_f / c_p\right) \quad \text{(eq. 4.18)}$$

From the equation 4.17, the relationship of the parameters can be indicated as the figure below:

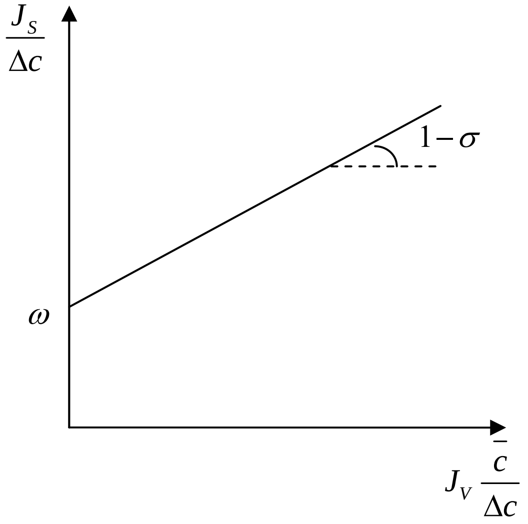

Figure 4.4: Relationship of the parameters in eq. 4.17

Mass transfer in nanofiltration [14]

A representation of the mass transfer process occurring in NF is given in Figure 4.3.

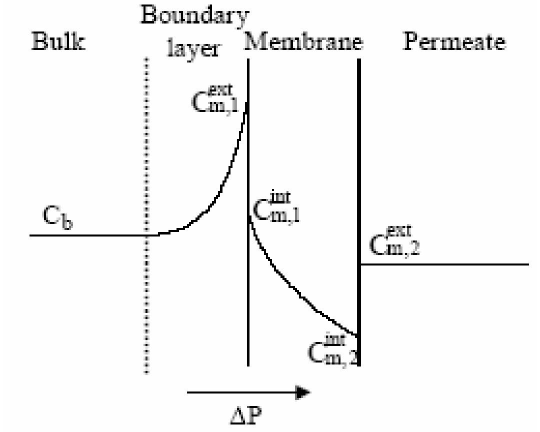

Figure 4.5: Mass transfer through nanofiltration [14]

When an external pressure ΔP is imposed on a liquid which is adjacent to a semi-permeable membrane, solvent will flow through the membrane. The general terms that are used in the description of membrane separation processes are the solvent flux (J) and the rejection (R). The solvent flux is given by:

$$J = \frac{\Delta P}{\eta R_{tot}} \quad \text{(eq. 4.19)}$$

in which ΔP is the effective transmembrane pressure [N/m^2], η the permeate viscosity [Pa.s] and R_{tot} the total resistance towards solvent flow [m^{-1}].

A neutral solute dissolved in the solvent at a concentration level C_b will also flow towards the membrane. If the membrane exhibits rejection for the solute, partial permeation will occur and non-permeated solute accumulates in the boundary layer, and hence a concentration profile develops. Then, the equilibrium with back diffusion takes place. This phenomenon is called concentration polarization. The solute distributes at the membrane/solution interface and will be transported through the membrane by convection and diffusion. At the permeate side, a second distribution process will occur and a final concentration of solute in the permeate, $C_{m,2}^{ext}$, will be reached. For the characterization of solute behaviour the rejection is used, given by:

$$R = 1 - \frac{C_{m,2}^{ext}}{C_b} \quad \text{(eq. 4.20)}$$

In nanofiltration, the distribution of a non-charged solute at the boundary layer/membrane interface is considered to be determined by a steric exclusion mechanism. Steric exclusion is not typical for nanofiltration but applies to ultrafiltration and microfiltration too. Due to its size a solute only has access to a fraction of the total surface area of a pore. This causes a geometrical exclusion of the solute from the membrane. A separation between solutes will only be accomplished when the solutes have a difference in size.

Osmotic Pressure

The retention of ions and small organic molecules in nanofiltration causes osmotic pressure, due to concentration difference. This pressure has to be counterbalanced by the applied transmembrane pressure. Therefore, the pressure needed to obtain a given water flux will be higher, or the water flux at a given transmembrane pressure will be lower. Thus, the osmotic pressure causes flux decline, but this is due to a decrease of the driving force instead of an increase of the resistance against mass transport. This can be expressed by the phenomenologic equation for the water flux, originally introduced by Kedem and Katchalsky: [16]

$$J_V = L_P(\Delta P - \sigma\Delta\pi) \quad \text{(eq. 4.21)}$$

If the reflection coefficient (σ), the maximal retention of the component at an “infinite” pressure, can be assumed to be equal to 1, the water flux would be 0 when the applied pressure equals the osmotic pressure. The extent to which the osmotic pressure will play a role is determined by the retention of the components in the solution, their concentration, and their molecular mass.

Colloids stability

Due to the DLVO interaction (also mentioned in Section 4.1.2.1) between colloids, they get stable state in aqueous solution. The interaction forces are caused by surface zeta potential of silica colloids. Hence, zeta potential is a paramount parameter to describe the stability of silica particles in solution.

It is repulsive forces which keep the silica particles from aggregating; zeta potential reflects those forces and it is a measure of dispersion stability. Higher zeta potential implies more stable dispersions. The zeta potential zero is defined as the isoelectric point (IEP). The isoelectric point is a very important measure and relates strongly to stability. Zeta potential changes with salt concentration, pH and surfactant concentration. For zeta potential of silica particles, low values can indicate colloid instability which could lead to aggregation.

4.3 Modelling of Transport

4.3.1 Spiegler-Kedem Equation [4]

An interpretation of the transport mechanisms through a nanofiltration membrane is necessary for the description of the retention of uncharged molecules. Transport of uncharged molecules is a combination of diffusion and convection. This is expressed in the transport equations of Spiegler and Kedem [2] for water flux and for the flux of a dissolved component:

$$J_V = L_P(\Delta P - \sigma\Delta\pi) \qquad (4.22)$$

$$J_S = -P\Delta x \frac{\Delta c}{\Delta x} \pm (1-\sigma)J_V c \qquad (4.23)$$

Diffusion is represented by the first term in Eq. (4.23); the second term represents the contribution of convection to the transport of uncharged molecules.

The retention of a given molecule can be calculated from Eqs. (4.22) and (4.23) as:

$$R = \frac{\sigma(1-F)}{1-\sigma F} \qquad (4.24)$$

$$F = \exp\left(-\frac{1-\sigma}{P}J_V\right) \qquad (4.25)$$

where R is retention; J_v is water flux(l/h m^2); P is solute permeability(l/h m^2) and σ is reflection coefficient. The solute retention R is given as a function of the water flux J_v and the solute permeability P.

The permeability P is a measure of the transport of a molecule by diffusion and convection. The reflection coefficient σ of a given component is the maximal possible retention for that component. Only the ratio of solute radius to pore radius determines the reflection coefficient. [5] Reflection coefficient can be derived from either experimentally or mathematically.

From Eqs. (4.24) and (4.25), it can be seen that the reflection coefficient corresponds with retention at an infinite water flux. The resulting curve for the reflection coefficient as a function of the molecular diameter (retention curve) can be used to estimate the maximal retention that can be obtained by a given membrane.

From Eq. (4.24) it appears that the retention increases with increasing water flux and reaches a limiting value σ at an infinitely high water flux.

4.4 Membrane Fouling

4.4.1 Resistance Model and Hagen-Poiseuille equation [22]

Resistance model is commonly used to describe phenomena of flux decline. For nanofiltration, the water flux is written as:

$$J = \frac{\Delta P}{\eta R_{tot}} \quad \text{(eq. 4.26)}$$

where, ΔP , driving force; η , viscosity; R_{tot} , total resistance.

The flux decline that was found in the experiments should be explained by an increase in the total resistance against mass transport.

Another popular model to describe the water flux is the **Hagen-Poiseuille equation** (ideal conditions):

$$J = \frac{\varepsilon r^2}{8\eta\tau}\frac{\Delta P}{\Delta x} \quad \text{(eq. 4.27)}$$

here, the membrane resistance depends on the porosity (ε), the tortuosity (τ), the pore radius (r), and the membrane thickness (Δx).

The Hagen-Poiseuille equation is valid when pure water is applied to the membrane. When solutions of organic molecules in water are applied, the water flux will often be lower. Different mechanisms of flux decline can be distinguished [21, 23]. Adsorption inside the pores or at the membrane surface narrows the pores. When the molecules have a similar size as the pores, permeation can lead to pore blocking, a phenomenon that can be enhanced or caused by adsorption. Pore blocking has been observed for ultrafiltration, where macromolecules are filtered. For the filtration of non-macromolecular components with nanofiltration, this phenomenon has not yet been described.

The total resistance is the sum of different individual resistances, i.e., *R*tot= *R*p + *R*a + *R*m + *R*g + *R*cp + *R*i + *R*d (*R*p, resistance due to pore blocking; *R*a, resistance due to adsorption inside the pores; *R*m, membrane resistance (intrinsic); *R*g, resistance caused by the formation of a gel layer; *R*cp, concentration polarization resistance; *Ri*, resistance caused by specific interactions; *R*d, resistance from deposits on the membrane).

In the ideal case, e.g., filtration of pure water, the membrane resistance (*R*m) is the only resistance involved. This is an intrinsic membrane characteristic that corresponds to the resistance calculated from, for example, the Hagen-Poiseuille equation and does not change during filtration or by changing the feed solution. It reflects the minimal resistance of the system against mass transport and thus determines the maximal water flux at a given pressure. The other phenomena can only make pores narrower (or the membrane thicker), resulting in an increase of the total resistance or the addition of an extra resistance term to the intrinsic membrane resistance.

The gel layer resistance, the adsorption resistance, the pore blocking resistance, the deposition resistance, and the concentration polarization resistance depend strongly on the type of feed solution that is used. In this case, the gel layer resistance is not present, as the formation of a gel layer is related to macromolecules, which are not present.

For uncharged organic compounds, adsorption is the process that is most likely to occur. Molecules can get attached to the membrane pores or to the membrane surface by adsorption or chemisorption. Inside the pores, they narrow the free pathway for the water flow, hence decreasing the net pore opening. From the Hagen-Poiseuille equation, it can be seen that this should lead to a flux decline. When adsorption has a strong effect, it could even lead to pore blocking when the whole cross section of the pore is filled.

4.4.2 Freundlich Equation [22]

The remaining flux decline can be explained by adsorption inside the membrane pores or at the membrane surface, possibly enhanced by pore blocking. Freundlich equation is employed to describe the pore blocking and adsorption inside the membrane pores. Formation of Freundlich equation is shown below:

$$q = K_f c^n \quad \text{(eq. 4.28)}$$

where c is the concentration of the component to be adsorbed at equilibrium and q is the amount of the component that is adsorbed on the material, divided by the amount of material. K_f and n are empirical constants. If it is assumed that adsorption and flux decline are proportional, q in the Freundlich equation can be replaced by the flux decline ΔJ :

$$\Delta J = K_f c^n \quad \text{(eq. 4.29)}$$

Typical adsorption isotherm:

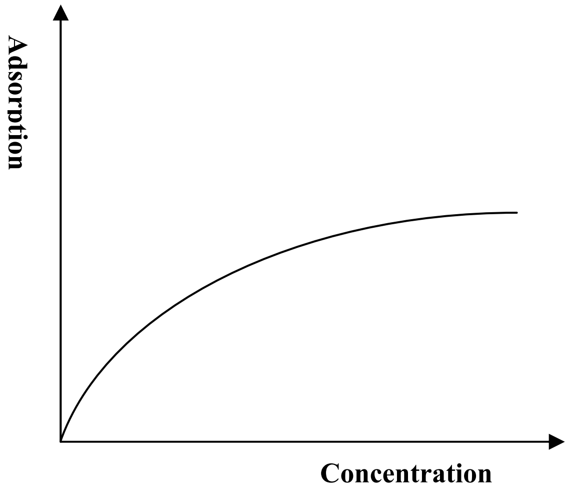

Figure 4.6: Typical adsorption isotherm

5. Experiments Methods and Materials

Three polymeric nanofiltration membranes were studied: NF, LE and XLE, which were supplied by DOW Filmtec®.

5.1 Basic Information about the Membranes

Membrane materials:

- XLE (Commercial code: FT30) membrane made from 1, 3 phenylene diamine
- NF (Commercial code: unknown) is made from piperazine and trimesoyl chloride (TMC).

The surface chemistry change is due to one being an aromatic polyamide and the other being an aromatic aliphatic polyamide.

XLE (FT30):
1, 3 phenylene diamine:

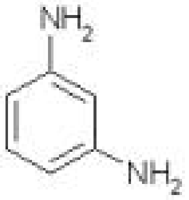

Figure 5.1: 1, 3 phenylene diamine

The FT30 membrane gives excellent performance for a wide variety of applications including low-pressure tapwater purification, single-pass seawater desalination, chemical processing, and waste treatment. (Product information of FT30 by DOW Filmtec®, Form No. 609-01020-604)

Some solute rejection on membrane FT30:

Table 5.1: FT30 (XLE) retention performance from the manufacturer website

Solute	Molar mass (g/mol)	Rejection (%)
Sodium chloride NaCl	58	99
Silica SiO_2 (50 ppm)	60	98
Calcium chloride $CaCl_2$	111	99
Magnesium sulfate $MgSO_4$	120	>99
Ethanol	46	70
Isopropanol	60	90
Lactic acid (pH=2)	90	94
Lactic acid (pH=5)	90	99
Glucose	180	98
Sucrose	342	99

Note: Solute rejection (approximate) 2,000 ppm solute, 225 psi (1.6 MPa), 77°F

(25°C) (unless otherwise noted).
Membrane type: Thin-film composite polyamide
Maximum operating pressure: 1,000 psi (6.9 MPa)
Maximum operating temperature: 113°F (45°C)
pH range, continuous operation: 2 - 11
The FILMTEC FT30 membrane consists of three layers: an ultra-thin polyamide barrier layer, a microporous polysulfone interlayer, and a high-strength polyester support web. (www.dow.com)

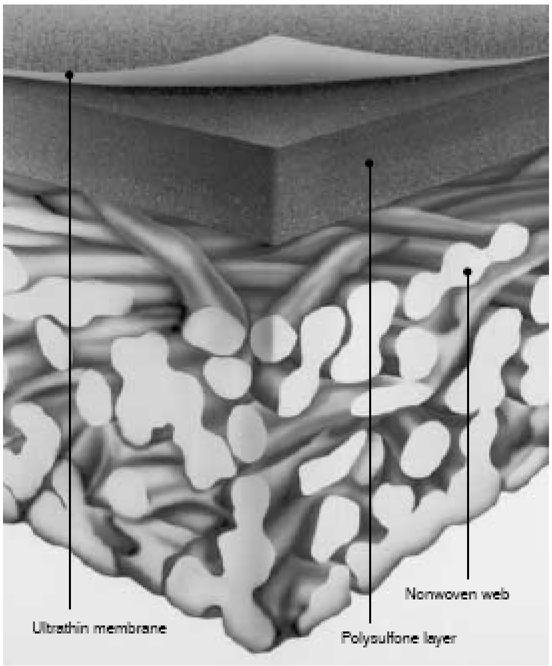

Figure 5.2: FT30 membrane composite (From FT30 Membrane Description, DOW Filmtec®, Form No. 609-01010-704)

The major structural support is provided by the non-woven web, which has been calendered to produce a hard, smooth surface free of loose fibers. Since the polyester web is too irregular and porous to provide a proper substrate for the salt barrier layer, a microporous layer of engineering plastic (polysulfone) is cast onto the surface of the web. The polysulfone coating is remarkable in that it has surface pores controlled to a diameter of approximately 15nm. The FT30 barrier layer, about 200nm thick, can withstand high pressures because of the support provided by the polysulfone layer. Because of its barrier layer thickness, FT30 is very resistant to mechanical stresses and chemical degradation. (From FT30 Membrane Description, DOW Filmtec®, Form No. 609-01010-704)

For NF and LE, the information is very limited, but it is possible to get some comparison and conclusions after analysis the data from literatures and the lab experiments.

Some information about NF

TMC Molecular Formula: $C_6H_3(COCl)_3$

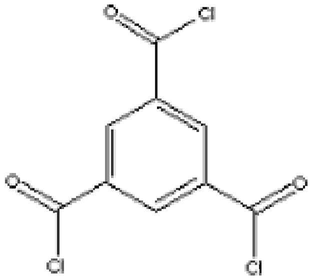

Figure 5.3: trimesoyl chloride (TMC)

Piperazine Molecular Formula: $C_4H_{10}N_2$

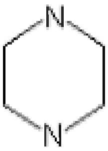

Figure 5.4: Piperazine

Retention measurements of single salt solutions (NaCl, Na_2SO_4, $CaCl_2$) were carried out at different feed concentrations. An 8 bar pressure difference was applied.

5.2 Experiments

5.2.1 Membrane Surface Zeta Potential

Membrane charge is caused by dissociation of basic or acid functional groups or adsorption of ions to the surface. One of the most important effects by membrane charge is to influence the distribution of ions between bulk and membrane by attraction-repulsion interactions, resulting in ion retentions that are higher for multivalent ions than monovalent ions. [39] This attraction repulsion interaction can be explained by Donnan exclusion which plays an important role in retention of monovalent and multivalent ions by nanofiltration.
Zeta potential measurements were used to determine the surface charge of nano-filtration membranes. Instrument measurement by Streaming Potential Analyzer and lab-scale experiment by filtrating salts was carried out to compare the results with the measurements. The instrument measurements and filtration results and comparison are discussed in Chapter 6 Results and Discussion.

The hydrodynamic flow of an electrolyte solution over the membrane surface due to a pressure gradient and ion movement, results in the occurrence of a streaming potential.
Streaming potential analysis is a good method for studying on the interaction between charged particles and membrane such as fouling phenomena, but it only measures the

external membrane surface, so it is not fit to determine the charge inside membrane pores.

By varying the applied pressure (ΔP) the streaming potential (ΔE), which had been generated by a flow of ions due to ΔP, was measured with a digital multimeter and the data were recorded using a microcomputer.
The zeta potential was obtained from the $\Delta E - \Delta P$ slope of a plot using the following Helmholtz-Smoluchowski equation: [25, 26]

$$\frac{\Delta E}{\Delta P} = \frac{\varepsilon \zeta}{\eta \lambda} \quad \text{(eq. 5.1)}$$

where ζ is the zeta potential, η is the solution viscosity, ε and λ is the permittivity and electrical conductivity of the solution, respectively. The KCl concentration in the outer solution was 0.01M throughout the measurements. The pH of the outer solution was regulated from 3 to 12 by adding HCl or KOH.
The measurements were carried out three times for each experimental point, and the mean value (± standard deviation) of each experimental point was indicated.

5.2.2 Electrokinetic Properties and size of Silica Colloids

The Dynamic Light Scattering experiments (For principles, see Appendix 2) were applied to determine the silica particles in function of the pH, with and without NaCl. Autosizer 4700, Malvern Instruments, dynamic and static light scattering - to measure the size of nano-particles and the molecular weight of polymers [35].

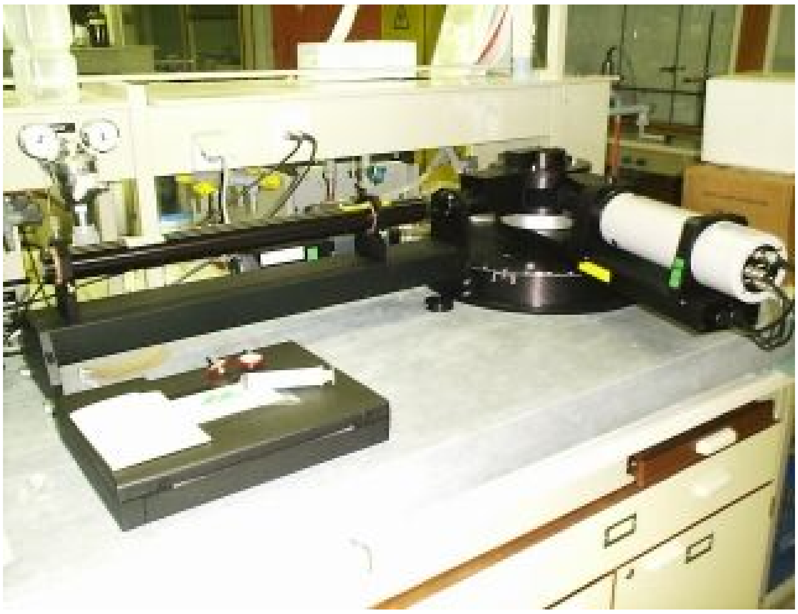

Figure 5.5: Autosizer 4700 for Dynamic Light Scattering Experiments

The size of the particles in each condition was measured three times.
Zeta potential of the silica colloids was measured by Matec ESA9800 Zeta potential analyzer. The method for this measurement is the ESA (the electro-acoustics) effect.

Because of an alternating electrical field, the particles will oscillate in suspension (the used suspension was a 10vol% solution). Due to the oscillation, the particles will generate a sound wave. The dynamic electrophoretic mobility can be calculated out of the amplitude and the phase of the sound wave in function of the frequency of the electrical field.

Figure 5.6: Matec ESA9800 Zeta potential analyzer[76]

5.2.3 AFM Analysis

Roughness of the three membranes was measured by the non contact AFM.

Data were collected from Atomic Force Microscope, then processed in ProScan Software (Proscan elektronische Systeme GmbH, http://www.proscan.de/psi.htm). The "Region Analysis" mode for membrane surface regional analysis was applied on the collected data.

The root mean square roughness (RMS) represents one possibility of quantifying the surface topography by means of an average value.

5.2.4 SEM Analysis

The Scanning Electron Microscope (SEM) Philips XL 30 FEG is available in the Department of Metallurgy and Materials Engineering (MTM) of Katholieke University of Leuven. The working temperature of the emitter is 1800°K, the tip is always kept clean, flashing is never needed, it takes only a minute to become fully operational for a long period. Software for automated point ananlysis, linescans and mapping is available. Data and images can be stored on a harddisc, diskettes or a ZIP. Printouts with a HP560C, as well videoprint output (Sony UP-890) and the use of type 120 negative film on a ultra-high resolution photomonitor offers the users the necessary output possibilities. [31]

The membrane samples were cut in liquid nitrogen to get the cross-section, and both surface samples and cross-section samples were coated with gold for SEM detection.

Figure 5.7: Scanning Electron Microscope (SEM) Philips XL 30 FEG[31]

5.2.5 Contact Angle Measurements

5.2.5.1 Equipment:

Krüss DSA10 Drop Shape Analysis System was applied for the contact angle measurements. This equipment is available in the Laboratory for Environmental Technology, Department of Chemical Engineering, Katholieke University of Leuven.

Figure 5.8: Contact Angle Measuring System G10

The system includes "Contact Angle Measuring System G10" and the software which is applied to process the images acquired by the video camera and analyzes the data. The Sessile Drop Method was applied in the measurement.

System Model: DSA10-Mk2

Serial Number: 2003-4802

Company: Krüss GmbH Germany

5.2.5.2 Basic Measurement Principle:

Hydrophobicity of the membranes is important because a more hydrophobic membrane causes more adsorption of the organic matters and more fouling. To determine the membranes' hydrophobicity, one of the contact angle measurement techniques "the Sessile Drop Method" was applied in the experiment.

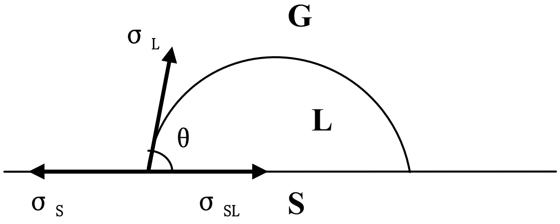

Figure 5.9: Sessile Drop Method

The sessile drop method is applied to determine the contact angle(θ)between the membrane$(S)$and Mili-Q(L). The angle can be expressed by **Young's Equation** below:

$\sigma_L \cdot \cos\theta = \sigma_S - \sigma_{SL}$ (eq. 5.2)

The contact angle(θ) depends on the interfacial tention(σ). In this case, whenθ is large, the membrane surface is more hydrophobic and is harder to be wetted by water.

Possible problem:

The discrepancy of this measurement method can be raised by chemical heterogeneity of the surface, surface roughness or porosity besides some operation discrepancy. It has been found by Nyström *et al.* that the contact angle for a porous membrane is often smaller than for a non-porous surface. [30]

5.2.6 Membrane Performance Testing

Pure water flux testing and retention experiments for ions, small organics and silica colloids were carried out in a laboratory scale test cell (Amafilter®). A schematic diagram of the apparatus is shown in Figure 5.10. A cross-flow filtration cell (effective membrane area is 59 cm^2) containing flat sheet membrane was used. The cross-flow velocity was 6 m/s, which was applied to minimize concentration polarization. All experiments were carried out at a constant temperature of 25°C and constant pressure of 8bar.

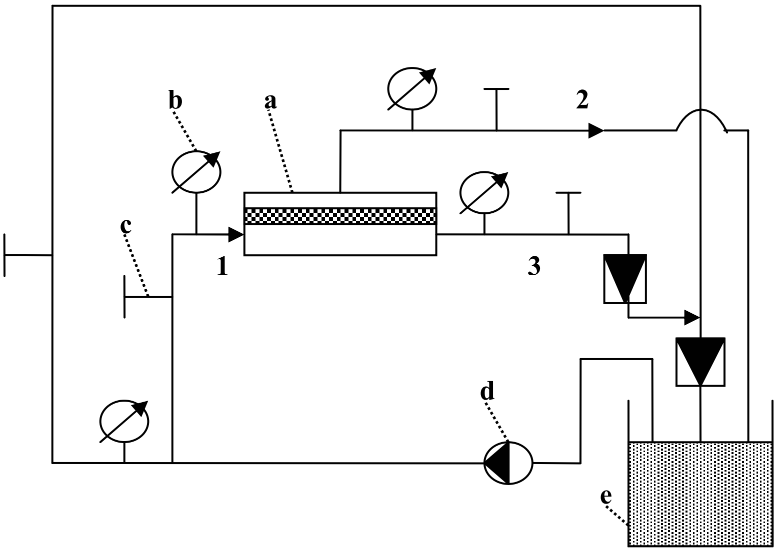

Figure 5.10: Schematic diagram of the test apparatus: (1) feed; (2) permeate; (3) retentate; (a) filtration cell; (b) pressure gauge; (c) pressure valve; (d) pump; (e) feed container; (f) flow meter.

Figure 5.11: The cross-flow filtration cell

5.2.6.1 Pure water flux

Prior to membrane flux test, the membranes were dipped in the DI (Deionized) water for at least 12 hours.

Before data collection, the system was run 15 minutes to make stable.

5.2.6.2 Membrane Rejection Studies:

Prior to rejection test, the membranes were dipped in the DI (Deionized) water for at least 12 hours.

(a) Salts rejection experiments:

Three different monovalent and multivalent salts: NaCl, Na_2SO_4 and $CaCl_2$ were applied for salts rejection experiments. Salt solutions were prepared one night in advance before the experiment and used magnet stirrer to make the solutions stable and equality.

Table 5.2: Effective sizes for different salts calculated from the salt diffusion coefficients

Salt	Diffusion Coefficient (10^{-9} m^2s^{-1})	Effective size (nm)
NaCl	1.61	0.15
Na_2SO_4	1.23	0.20
$CaCl_2$	1.49	0.16

Table 5.3: Stokes radii of several ions [64]

Ion	Stokes radius (nm)
Na^+	0.184
Ca^{2+}	\
Cl^-	0.121
SO_4^{2-}	0.230

* at 25℃

The salts effective sizes were calculated from the salts diffusion coefficient by the Stokes-Einstein equation, the calculation details are described below:
Stokes-Einstein equation:

$$D_S = \frac{kT}{6\pi\eta r} \quad \text{(eq. 5.3)}$$

where, viscosity of water η at 298K of 8.94 x 10^{-4} kg m^{-1} s^{-1}, k is Boltzmann constant, is 1.3806503 × 10^{-23} m^2 kg s^{-2} K^{-1},
For instance, the diffusion coefficient of $CaCl_2$ is 1.49 (10^{-9} m^2s^{-1}), so the effective size of $CaCl_2$ can be calculated as 0.16nm

(b) Organic Compounds Rejection Experiments:

Organic compounds were dissolved into DI water one night in advance before the experiment and used magnet stirrer to make the solutions stable and equality.
Size of organic molecule is decided by both molecular weight and molecular structure.
Six organic compounds were used in this experiment. Some information about these organics is listed below:

Table 5.4: Organic compounds with their diameters and dipole moments [22, 64]

Solute	Molecular Weight (g/mol)	Effective Diameter (nm)	dipole moment (D)
MEK	72	0.42	2.8
EA	88	0.48	1.7
BMK	100	0.52	2.7
Xylose	150	0.55	1.0
Maltose	342	0.82	\
Raffinose	504	0.94	\

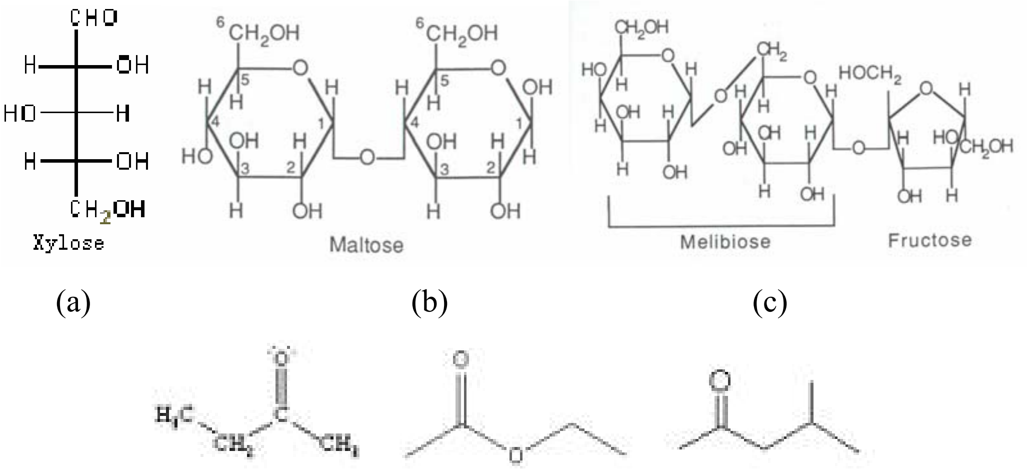

(a) (b) (c)

(d) (e) (f)

Figure 5.12: (a) Xylose, (b) Maltose, (c) Raffinose, (d) MEK, (e) EA, (f) BMK.
*Figure (b), (c) [42]

5.2.7 Analysis apparatuses and methods for ions, compounds, colloids and pH

Adequate apparatuses and methods were applied for analysis of ions, compounds and colloids in this experiment. Details are described below:

5.2.7.1 Conductivity meter for ions

A conductivity meter measures the ionic conductivity (or the resistance) of liquid. The number it gives is the total ion content of the liquid. The device consists a probe which has two platinum electrode plates parallel to each other and separated by some small distance.
Due to the values which measure by conductivity meter are the total ions content, calibration for some specific ion is needed. In the experiment, the effects by different pH values were got rid of by calibration curves (see appendix 8).

5.2.7.2 GC and UV-VIS for organic compounds

Gas Chromatography, HP 5890 with FID/ED detector was applied for determination of organic molecules with low molecular weight; and Shimadzu UV-1601 UV and

VIS spectrophotometer was used to determine the content of sugars in aqueous solution samples. Some details about the measurement methods of these two apparatuses and the experiment procedure are described below:

(a) The experiment with GC, standards, methods and reagents:

The compounds MEK, EA and BMK were detected by Gas Chromatography HP 5890 and adapted software was applied for data analysis. Details for the standards, methods and reagents for detection are listed as following:

MEK, BMK
T_{init}: 100℃， t_{init}: 0.7min
LEVEL1: 70℃/min; 135℃; 0.2min.
LEVEL2: 70℃/min; 160℃; 1.00min.
LEVEL3: 0
FID: Injection: 200℃; Detection: 250℃
Internal Standard: Methanol

EA
Tinit: 100℃; tinit: 0.9min.
LEVEL1: 25℃/min; 125℃; 0.5min.
LEVEL2: 50℃/min; 175℃; 0.9min.
LEVEL3: 50℃/min; 125℃; 0.1min.
FID: Injection: 200℃; Detection: 250℃
Internal Standard: Isopropanol.

Table 5.5: GC methods used for the analysis of organic compounds [64]

Method Number	Method 1	Method 2
T_{init}, t_{init}	100℃, 0.7min	100℃, 0.9min
Heating rate 1 T_1, t_1	70℃/min 135℃, 0.2min	50℃/min 175℃; 0.9min
Heating rate 2 T_2, t_2	70℃/min 160℃, 1.00min	50℃/min 125℃; 0.1min
Internal Standard	Methanol	Isopropanol

The FID detector was operated at 250℃ and the injection temperature was 200℃. Method 1 is used for the determination of MEK and BMK, method 2 is used for the determination of EA. Both methods are used on the HP 5890 Chromatograph.

The principle of gas chromatography is the following:

A sample is vaporized and injected onto the head of the chromatographic column. The sample is transported through the column by the flow of inert, gaseous mobile phase. The column itself contains a liquid stationary phase which is adsorbed onto the surface of an inert solid.

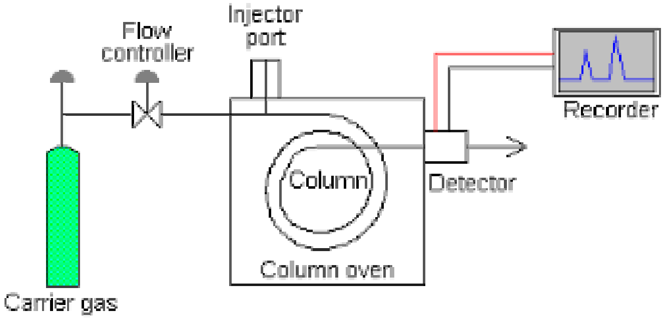

Figure 5.13: Principle of Gas chromatography

(b) The experiment with UV-VIS, methods and reagents:

Sugar detection method is "Phenol sulphuric acid carbohydrate assay" [28], details are listed as following:

Materials:

- Standards: sugar (xylose, maltose, raffinose) 1 mmol/l stock solution
- Use 8, 16, 32, 40, 48 ml solution and make up each sample with DI water to a final volume of 100ml for calibration
- Blank: 100ml water
- Samples: take 0.5ml made up solution (or sample from the experiment) as testing sample

Method:

- Add 0.5ml of 80% Phenol solution (80% Phenol by weight)
- Vortex. Add 2.0 ml concentrated Sulphuric Acid in a stream
- Stand 10 min. in 30℃ Shaking Water Baths
- Read absorbance at 485.0nm, 0.023A in Spectrophotometer

Figure 5.14: UV and VIS Spectrophotometer

The precise solutions (8, 16, 32, 40, 48 mmol/l) of each sugar were made to get the calibration line. One photograph of this procedure is available below as Figure 5.14.

Standard Number	Conc.	Abs.
1	0,0000	0,000
2	0,08000	0,314
3	0,1600	0,775
4	0,2400	1,136
5	0,3200	1,565
6	0,4000	2,011
7	0,4800	2,223
8		

485,0nm 0,0738

Figure 5.15: Photograph of concentration calibration

5.2.7.3 Turbidity meter for silica particles

A turbidity is a measure of the relative clarity of water. That is the reduction in transparency of a liquid caused by the presence of undissolved matter in the liquid. Turbidity increases as a result of silica particles in the water that reduce the transmission of light. So, turbidity is in direct proportion to the concentration of silica colloids in water.

Based on this principle, turbidity meter was applied in the experiment to detect the concentration of silica particles in sample. Each sample was measured three times in turbidity meter and took the average value to minimize the error.

5.2.7.4 pH meter for pH value

The principle of electrometric pH is the determination of the activity of the hydrogen ions by potentiometric measurement using a glass pH indicating electrode coaxially joined to a silver/silver chloride reference electrode.

A pH is a measure of the H^+ activity in water. It is expressed mathematically as shown below:

$$pH = -\log\{H_3O^+\} \quad \text{(eq. 5.4)}$$

where $\{H_3O^+\}$ is the activity of the hydrogen ion.

When the glass detector immersed in solution, the reference electrode makes contact with the sample through the junction, completing electrical contact between the reference electrode, sample and pH indicating electrode. [29]

pH 4.0 and 7.0 buffers were applied before each set of sample measurements to standardize pH electrode. Each experiment sample was measured three times and took the average value.

5.2.8 Experiments on Membrane Fouling Studies

Silica particles filtration experiments:

Commercial silica colloids (AEROSIL®, alkaline dispersion of hydrophilic fumed silica, pH=10) were used for fouling studies (flux and rejection) of the three different membranes.

Zeta Potential Analyzer was applied to detect the zeta potential of silica colloids particles in variation of pH (3, 5, 7, 10 and 12) and ion concentration (NaCl, 0.01, 0.05 and 0.1M) and coupled with silica colloids (30mg/l) and salt (NaCl, 0.05M) in variation of pH (3, 5, 7, 10 and 12). Each membrane in each case was tested for 120 minutes, after 15 minutes to make the system stable.

Prior to membrane fouling test, the membranes were dipped in the DI water for at least 12 hours.

6. Results and Discussion

6.1 membrane characterization

6.1.1 Membrane pore size and roughness

6.1.1.1Measurement and modelling of retention

Membrane pore size is an important characteristic for molecule retention, but it is not possible to measure the pore size directly, as pointed out in Chapter 4. Since several methods based on filtration experiments have been applied for the evaluation, log-normal model is chosen for the calculation of pore size of the membranes in this thesis.

The principle of log-normal pore size model to calculate the membrane pore size has been explained in Chapter 4 Section 4.1.3.2. Six small organic compounds: Methyl Ethyl Ketone (MEK), Ethyl Acetate (EA), Isobutyl Methyl Ketone (BMK), Xylose, Maltose and Raffinose were used in this experiment to detect the characteristics of the membranes (NF, LE and XLE). For the details about the experiments, see Chapter 5, Section 5.2.6 and 5.2.7.

The experimental data for calculation and calculation results as well as discussions will be introduced below.

(a) Experimental Data of Organic Components and Calculation Results:

Table 6.1: Information and Filtration Results of the Organic Compounds

(a) Membrane NF:

Solute	MW	Effective Diameter (nm)[4,64]	Rejection (%)	(J/J_V)*100
MEK	72	0.42	23.38	99.98
EA	88	0.48	17.43	101.36
BMK	100	0.52	52.46	89.89
Xylose	150	0.55	89.37	91.82
Maltose	342	0.82	99.44	95.27
Raffinose	504	0.94	99.83	99.07

(b) Membrane LE:

Solute	MW	Effective Diameter (nm)[4,64]	Rejection (%)	(J/J_V)*100
MEK	72	0.42	67.40	90.95
EA	88	0.48	77.73	90.36
BMK	100	0.52	95.15	84.50
Xylose	150	0.55	97.78	95.07
Maltose	342	0.82	99.20	92.81
Raffinose	504	0.94	99.69	95.96

(c) Membrane XLE:

Solute	MW	Effective Diameter (nm)[4,64]	Rejection (%)	(J/J_V)*100
MEK	72	0.42	69.97	100.36
EA	88	0.48	76.99	72.25
BMK	100	0.52	98.22	88.63
Xylose	150	0.55	96.65	88.67
Maltose	342	0.82	99.69	95.96
Raffinose	504	0.94	99.90	86.54

(b) Calculations by Log-normal Pore Size Model:

The log-normal pore size model was applied to calculate the membranes cut-off and the reflection coefficients to the organic molecules. The retention of organics used in the log-normal model is the retention at 120min (the final experimental data).
Equation of log-normal pore size model used:

$$\sigma(MW) = \int_0^{MW} \frac{1}{S_{MW}\sqrt{2\pi}} \frac{1}{MW} \exp\left(-\frac{\left(\ln(MW) - \ln(\overline{MW})\right)^2}{2S_{MW}{}^2} \right) dMW \quad \text{(eq. 6.1)}$$

In the equation and the tables, $\sigma(MW)$ is the reflection coefficient of a molecule to the membrane, S_{mw} is the standard deviation, $\overline{MW}$ is the average molecular weight where the retention is 90% under this molecular weight, MW(50) (see Appendix 3) is the average molecular weight where the retention of organics for the membrane is 50%. More information about this method, see Chapter 4, Section 4.1.3.2.

The experimental rejections were fitted to the eq.6.1.1 with the standard deviation and molecular weight as parameters. Results showed that the molecular weight cut-off (MWCO) of LE and XLE is almost the same, LE 100, XLE 98, while the MWCO of NF is higher: 155. This means that the membranes have very tight pores, at the lower end of nanofiltration range as it is usually defined (MWCO ca. 150 to 1000)
From the equation below:

$$d_S = A\left(MW\right)^B \qquad \text{(eq. 6.2)}$$

where A=0.065, B=0.438

S_p=S_{MW}*B (eq. 6.3)

where, S_p is the standard deviation (nm)
Using the MWCO which is calculated by the log-normal model and equation 6.2, the average pore size of the membrane can be calculated:

Table 6.2: Calculated membrane pore size by log-normal model

Membrane	NF	LE	XLE
Average pore size (nm)	0.59	0.49	0.48
Standard deviation (nm)	0.14	0.16	0.16

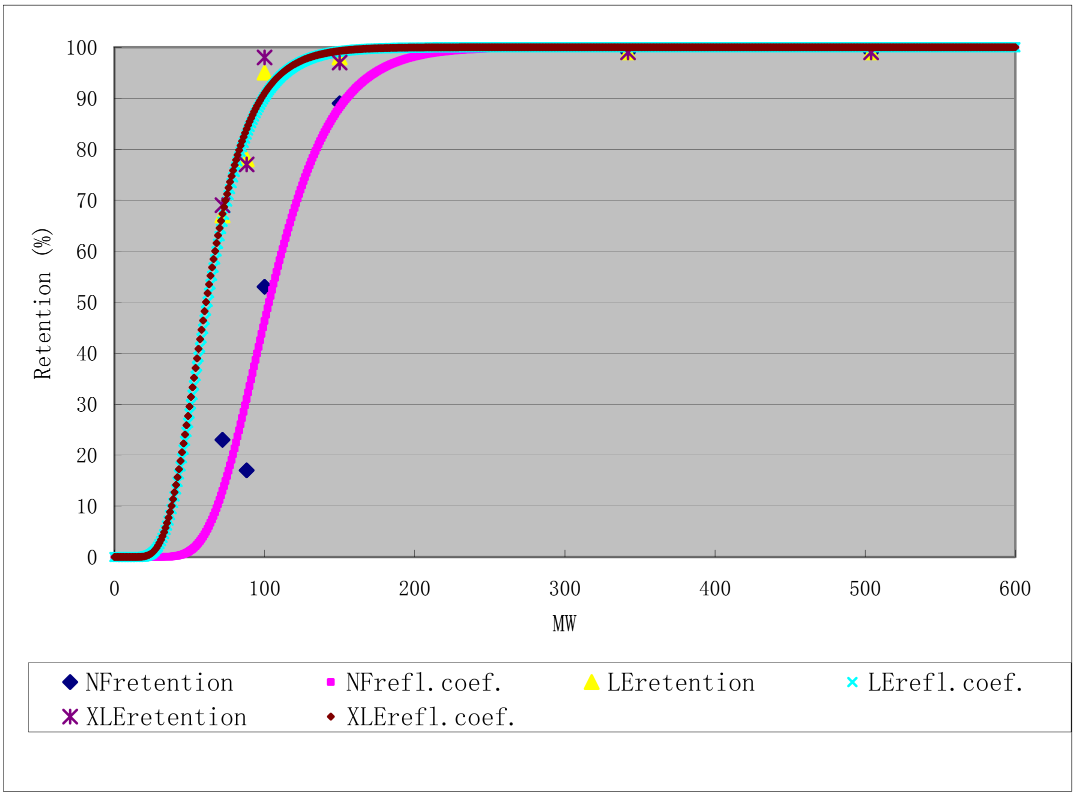

Figure 6.1: Modelling of reflection coefficient of NF, LE and XLE as a function of molecular weight (MW)

The modelling curves in Figure 6.1indicate that reflection coefficients to organic molecules of NF are the smallest and cut-off is the largest while LE and XLE are almost the same.

6.1.1.2 SEM Measurements:

Scanning Electron Microscopy is one of the most direct methods for membrane structure characterization; the membrane internal structures (such as membrane pore size and membrane fibers) are always clearly shown in SEM micrographs. (This method also introduced in Section 2.1)

(1) Pore size:

Membrane NF:

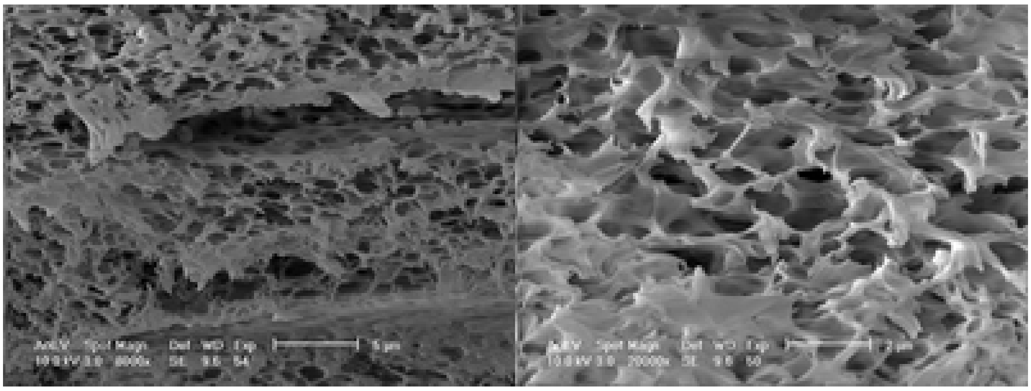

(a) (b)

Figure 6.2: SEM Images: Membrane microstructure of NF (a) (5μm) and (b) (2μm)

Membrane LE:

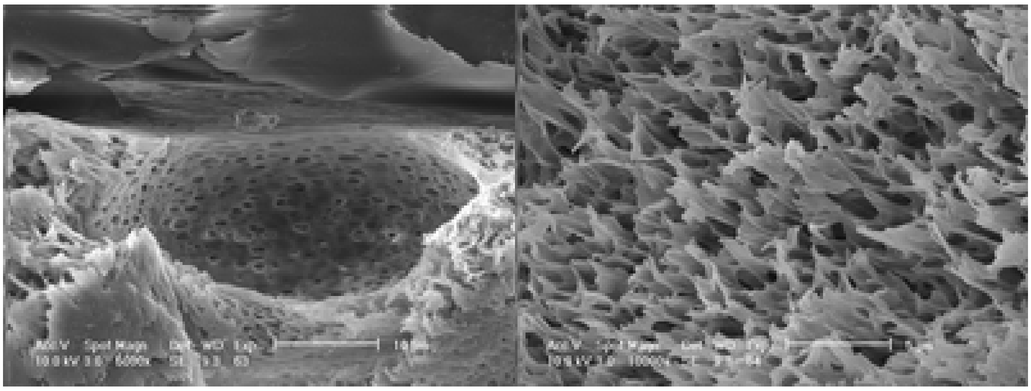

(a) (b)

Figure 6.3: SEM Images: Membrane microstructure of LE. (a) (10μm) shows the membrane pores of the barrier layer; (b) (5μm) shows the fiber of the barrier layer of membrane LE

Membrane XLE:

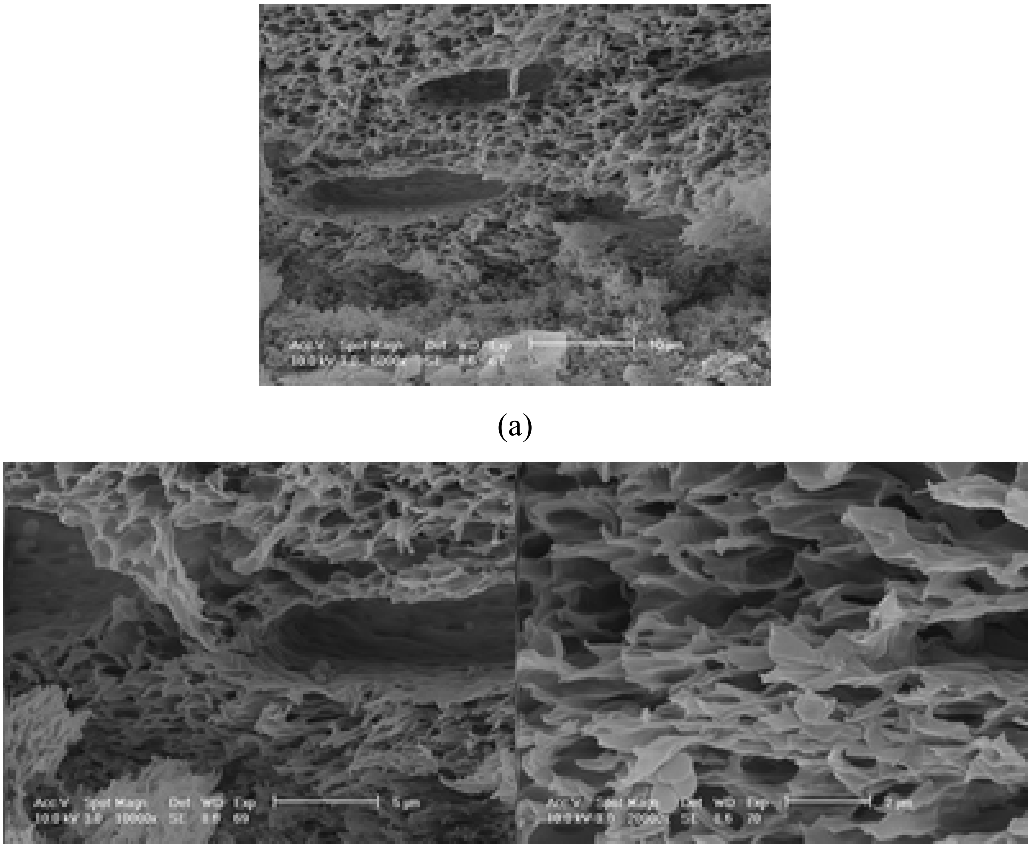

(a)

(b) (c)

Figure 6.4: SEM Images: Membrane microstructure of XLE. (a) (10μm) and (b) (5μm) show the membrane pores of the barrier layer; (c) (2μm) shows the fiber of the barrier layer of membrane XLE

As shown in the SEM cross-section images, NF has the most open microstructure while LE and XLE don’t have much difference in structure.

(2) Membrane Surface Roughness:

Membrane NF:

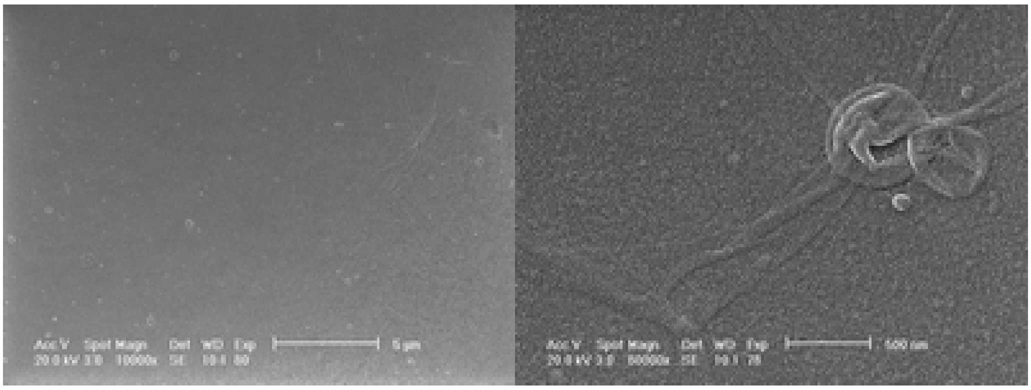

(a) (b)

Figure 6.5: SEM Images: Membrane Surface of NF. (a) (5µm) and (b) (500nm) show the surface of NF. Surface of membrane NF is very smooth.

Membrane LE:

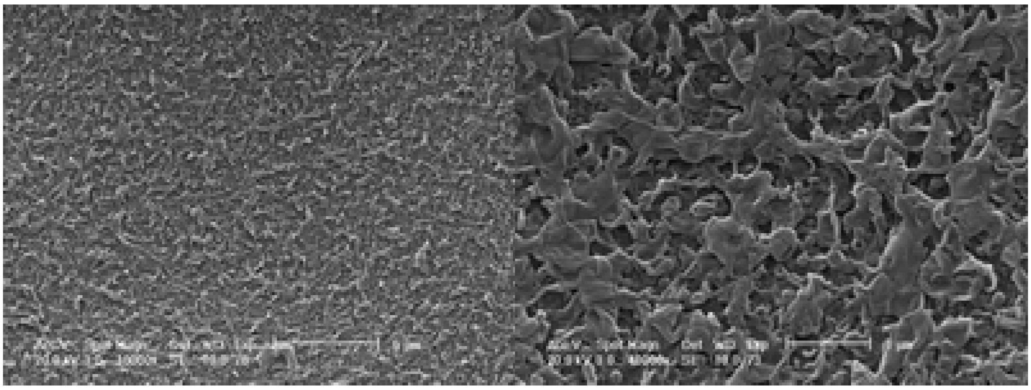

(a) (b)

Figure 6.6: SEM Images: Membrane Surface of LE. (a) (5µm) and (b) (1µm) show the surface of LE. Surface of membrane NF is very rough.

Membrane XLE:

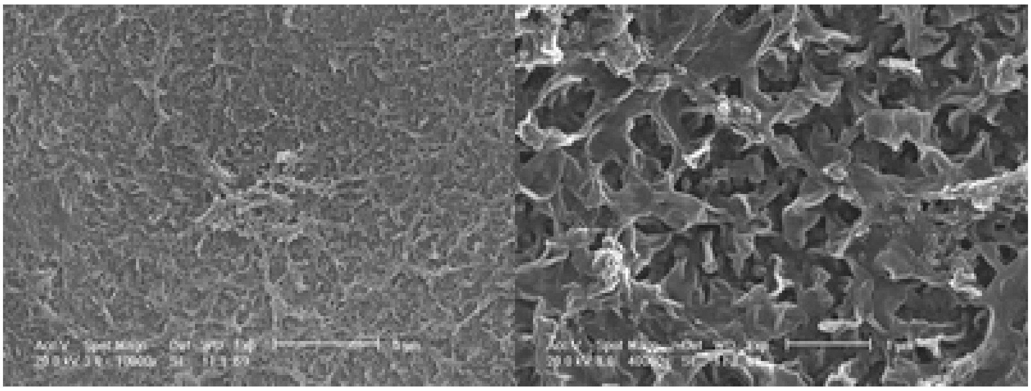

(a) (b)

Figure 6.7: SEM Images: Membrane Surface of XLE
(a) (5µm) and (b) (1µm) show the surface of XLE. Surface of membrane NF is very rough, and it seems more rough than LE

6.1.1.3 AFM Measurements:

Roughness of the three membranes was measured by non contact AFM.

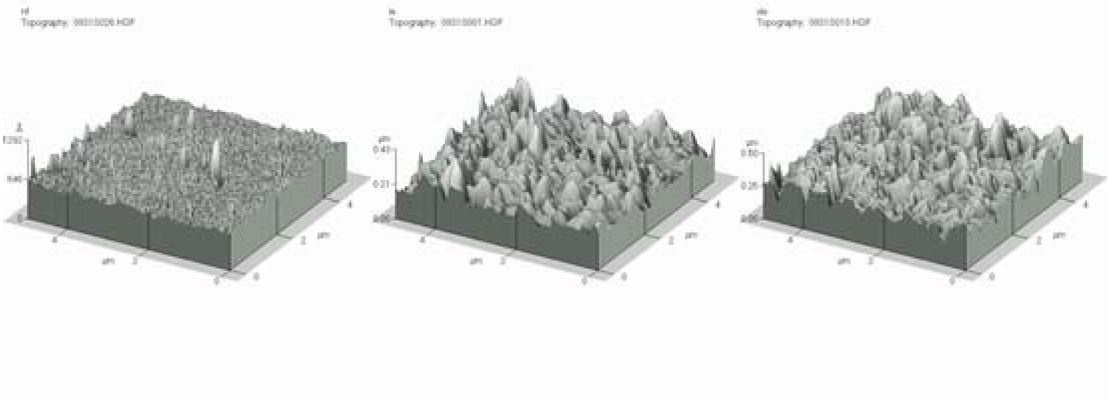

(a) (b) (c)

Figure 6.8: AFM images of (a) NF, (b) LE and (c) XLE. At X and Y axis, the dimension is both 2µm/division, while at Z axis, it depends on the roughness.

Measurement results (Unit: Angström):

Table 6.3: AFM measurement results on three membranes

Range	NF	LE	XLE
0.5 µm*0.5µm	20.8	108.0	207.5
1µm*1µm	28.1	219.1	264.7
3µm*3µm	41.5	330.5	511.0
5µm*5µm	46.0	384.0	609.0

From the results above, it can be easily seen that NF is the smoothest membrane and XLE is the roughest membrane. The roughness differences of the three membranes are remarkable. This conclusion fits the SEM images quite well. Based on the conclusion which mentioned that membrane surface roughness directly affects membrane fouling from former researchers, [33, 34] it can be easily deduced that the range-to-valley difference of XLE may cause the most severe fouling by particles and organic compounds.

6.1.2 Electrokinetic Properties of Membranes

Because the separation principle of nanofiltration membranes is combined with both sieving mechanism and charge effect, the membrane's electrokinetic characteristic is very important for ions, molecules and colloids retention as well as membrane fouling phenomena.

The electrokinetic properties of the three membranes were analyzed by Zeta Potential Analyzer. NF was measured two times, LE and XLE measured three times as a function of pH. The measurement results are shown below:

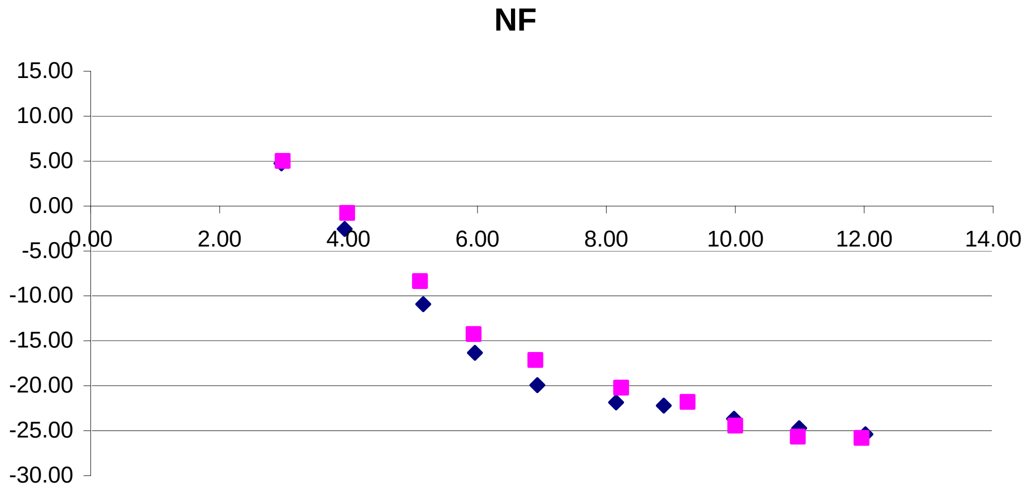

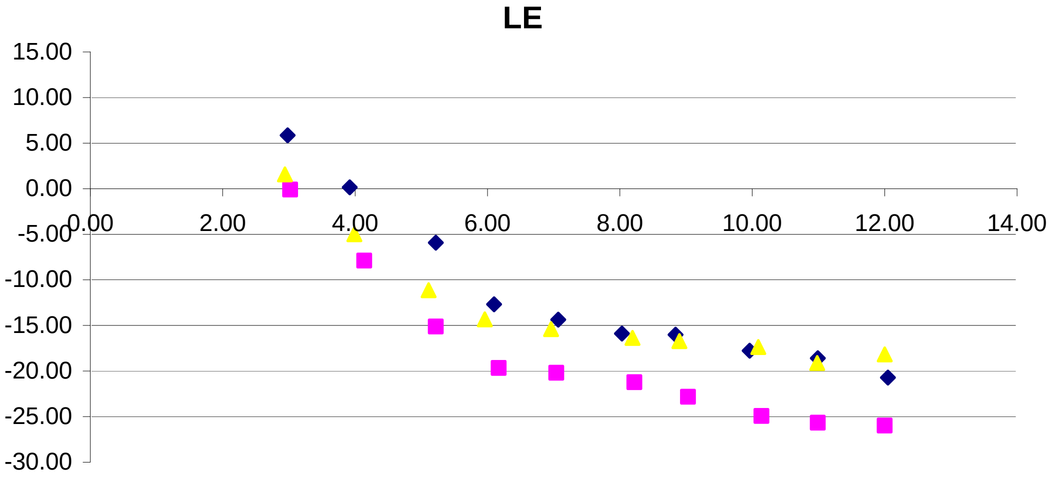

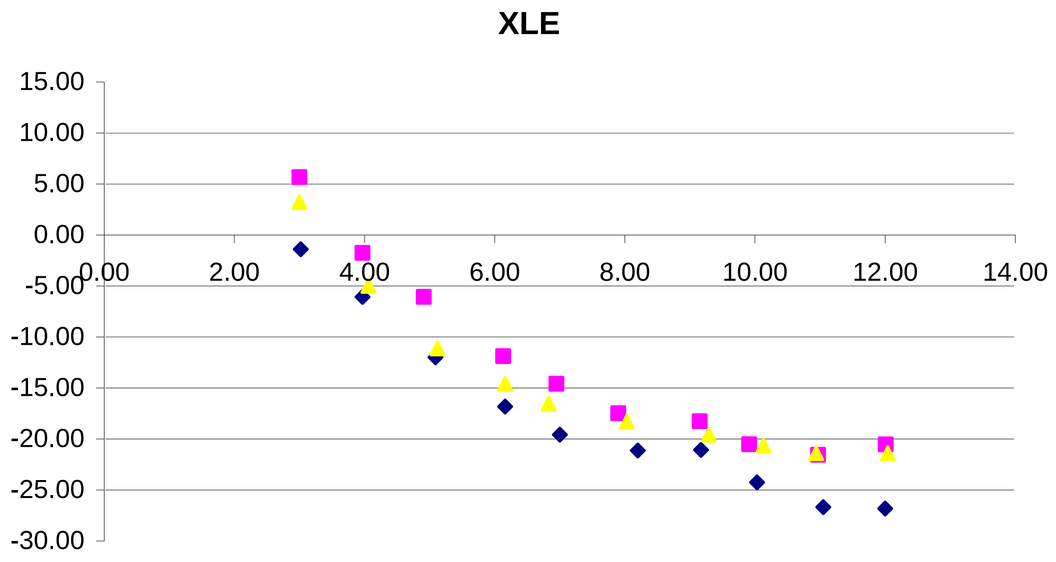

Figure 6.9: Zeta Potential Analysis of NF, LE and XLE

Experimental data are available in appendix 4.

6.1.3 Membrane Hydrophobicity

Membrane hydrophobicity was detected by contact angle measurement with sessile drop method, the principle see Chapter 5, Section 5.2.5.2.

Because of the chemical heterogeneity of the surface, surface roughness or porosity besides some operation discrepancy by the manufacturer and measurement differences, contact angle measurement values with the same piece of membrane may have some differences, so it is better to take the average value of the different measurements. The average measurement results are shown below:

Table 6.4: Contact Angle of the three Membranes

Membrane NF:

Theta(L)[deg]	Theta(R)[deg]	Theta(M)[deg]
38.4	**39.1**	**38.8**

Membrane LE:

Theta(L)[deg]	Theta(R)[deg]	Theta(M)[deg]
62.0 ± 3.66	**62.1 ± 3.99**	**62.0 ± 3.82**

Membrane XLE:

Theta(L)[deg]	Theta(R)[deg]	Theta(M)[deg]
54.62	**54.57**	**53.35**

As shown in Table 6.8, this is evident that membrane NF is the most hydrophilic membrane while LE is the most hydrophobic.

6.2 Membrane Performance on Salts and Small Organic Compounds Rejection

6.2.1 Membrane Performance on Salts Retention

6.2.1.1 Different salts retention comparison:

Ion retention by nanofiltration membranes can be explained by Donnan exclusion, the charge effect.

Based on the principle of Donnan exclusion, for the negatively charged membrane, higher charge of anion means more repulsion and causes higher retention; higher charge of cation means the membrane is more compressed and causes lower salt retention.

Three typical salts for the experiment, NaCl, Na_2SO_4 and $CaCl_2$ were applied for the retention comparison; the concentration of feed is 0.05M for each.

Most membranes are negatively charged, but when the pH value is low, some of the membranes may turn to positively charged [38]. This effect will be introduced and discussed in the experiment of membrane zeta potential analysis and the testing of NaCl retention with pH variation.

Ion retention by three nanofiltration membranes:

8bar, 25℃, 6m/s, Salts: 0.05M

Table 6.5: Salts retention by NF, LE and XLE

Membrane	NF	LE	XLE
Charge	Negative	Negative	Negative
Cut-off	155	100	98
Pore size	0.59	0.49	0.48
NaCl	57.93	92.31	94.21
Na_2SO_4	94.99	95.03	98.34
$CaCl_2$	64.17	95.40	96.92

*Rejection: average rejection

The results indicate that the retention of Na_2SO_4 is the highest while NaCl is the lowest, which is not an expected order and cannot be explained by Donnan exclusion. Since the results cannot be explained by Donnan exclusion, it may be because of the sieving effect. This can be explained by the ion size or diffusion coefficient. Nyström et al. suggested that the higher retention for $CaCl_2$ than for NaCl ($R_{(Na2SO4)}$=95%, $R_{(CaCl2)}$=70%, $R_{(NaCl)}$=45%)can be explained by the different ion size of Ca^{2+} and Na^+.[6] While Peeters et al. suggested that the higher retention of $CaCl_2$ that NaCl can be explained by the different diffusion coefficients of the salts.[65] Schaep et al. [5] determined that the membrane with lager pores, the effect of transport by diffusion could not be neglected. For Stokes radii of the ions, see Table 5.3 in Chapter5 Section

5.2.6.2. The diffusion coefficients in water of the salts used are listed below:

Table 6.6: Diffusion coefficient in water of the salts used in experiment

Salt	Diffusion Coefficient (10^{-9} m^2s^{-1})
NaCl	1.61
Na_2SO_4	1.23
$CaCl_2$	1.44

No matter which is the main cause of the discrepancy to Donnan exclusion sequence by the three salts in the experiment; sieving mechanism takes an important role in this phenomena.

6.2.1.2 Different pH for NaCl Retention:

HCl (volumetric solution, 1mol/L) was applied for the variation of pH in feed; pH analyzer was used for measurement. Calibration curves are available in appendix 8.

8bar, 25℃, 6m/s, NaCl: 0.05M

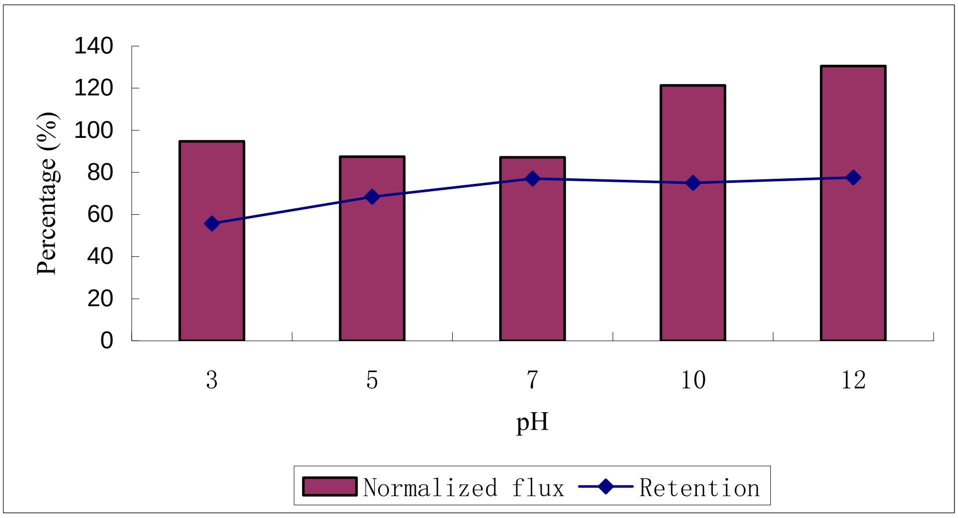

(a) NF

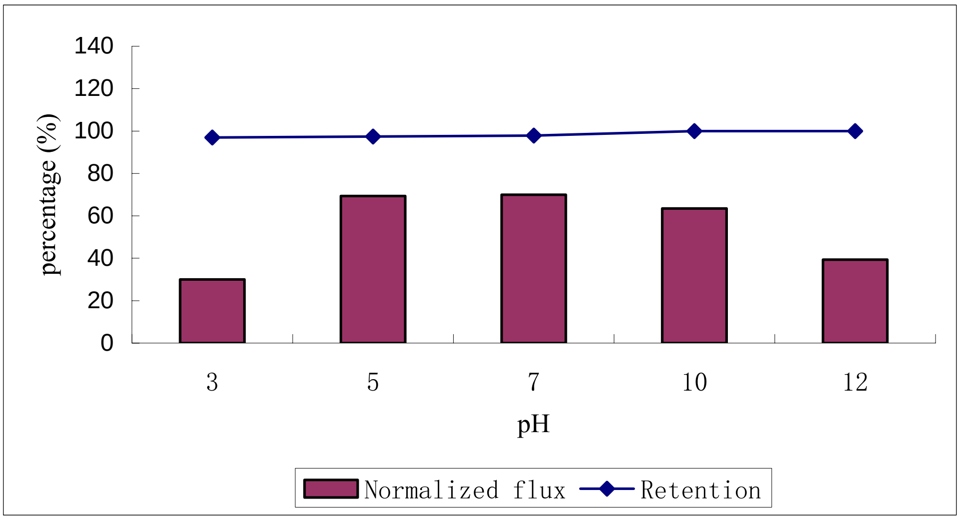

(b) LE

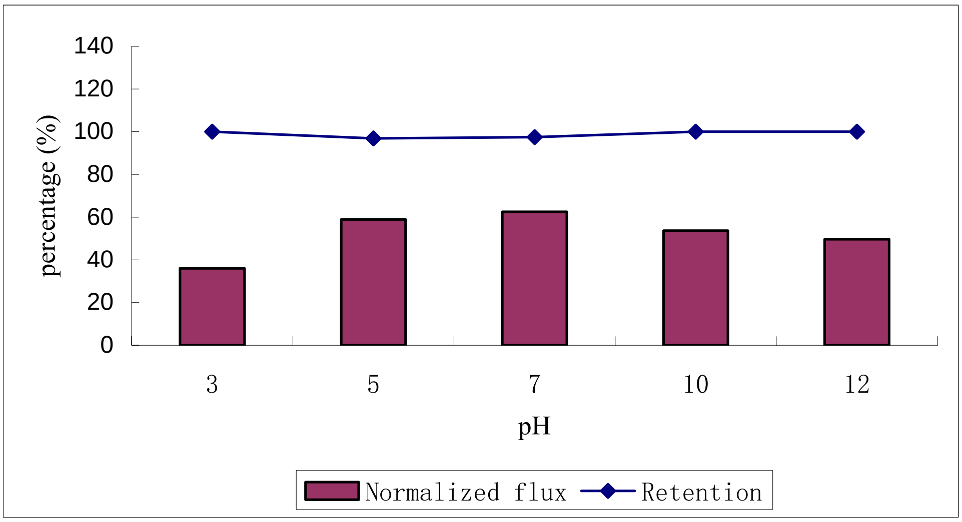

(c) XLE

Figure 6.10: Normalized flux and NaCl retention in different pH background

Experimental data are shown in appendix 9.

As shown, the retention of NaCl increases with the increase of pH value. It is displayed in Figure 6.9 that during the pH range of 3-7, the negative charge of the three membranes increase sharply, whereas, when pH higher than 7, the negative charge increase slowly. This agrees the experiment results in Table 6.10 quite well.

It is clear to reveal that the salts retention increase with the increase of membrane charge.

6.2.1.3 Different NaCl Concentration (Different Ion Strength):

Concentration with 0.01M, 0.05M and 0.1M NaCl were used for ion strength influence to retention experiment.

8bar, 25℃, 6m/s

Table 6.7: NaCl Retention under Different Concentration

Membrane	NF	LE	XLE
NaCl, 0.01M	85.77	95.89	96.79
NaCl, 0.05M	57.93	92.31	94.21
NaCl, 0.1M	50.84	92.15	94.68

*Retention: average retention

Retention of NaCl decrease with the increase of concentration in feed, this attributed to the “shield effect” (because concentration polarization can be neglected due to high feed flow). When the ion strength is high enough, it may “shield” the change effect of the membrane (membrane charge is affected by the background ion strength) and decrease the salt retention.

As shown, membrane NF is the most affected membrane on NaCl retention, because NF has the largest pore size. Less charge effect, less retention.

6.2.2 Membrane Performance on Small Organic Compounds Retention

Six small organic compounds were applied to detect the membrane pore size as well as other characteristics.

Table 6.8: Organic compounds retention with membrane NF, LE and XLE

Membrane	NF	LE	XLE
MEK	21.67	62.33	69.24
EA	14.42	69.08	76.16
BMK	53.84	93.55	97.19
Xylose	86.83	98.05	96.44
Maltose	98.46	99.04	99.58
Raffinose	99.36	99.79	99.79

*Retention: average retention

As exhibited in Table 6.5 and 6.8, although the effective sizes of the organic compounds are much larger than the ions, the retention is usually lower. This is due to the charge effect of the membranes. As it explained in Section 6.2.1.2 and Section 6.2.1.3, this may also depend on the pH value and the salt concentration. This reveals that charge effect is the paramount role in ion retention.

As shown in Table 6.8 and Figure 6.11 (a), (b) and (c) below, the sequence of organic compounds retention is almost as the same order as their molecular weight.

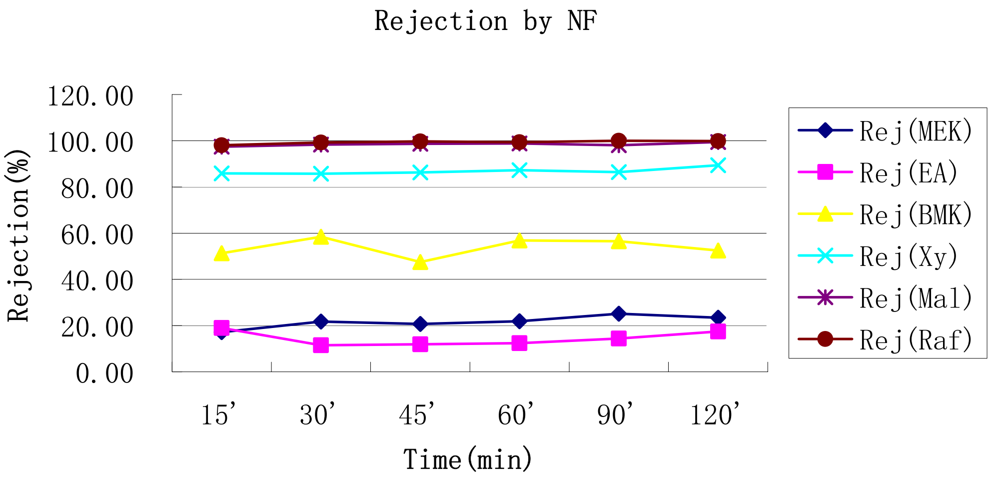

(a) Rejection of organics by NF

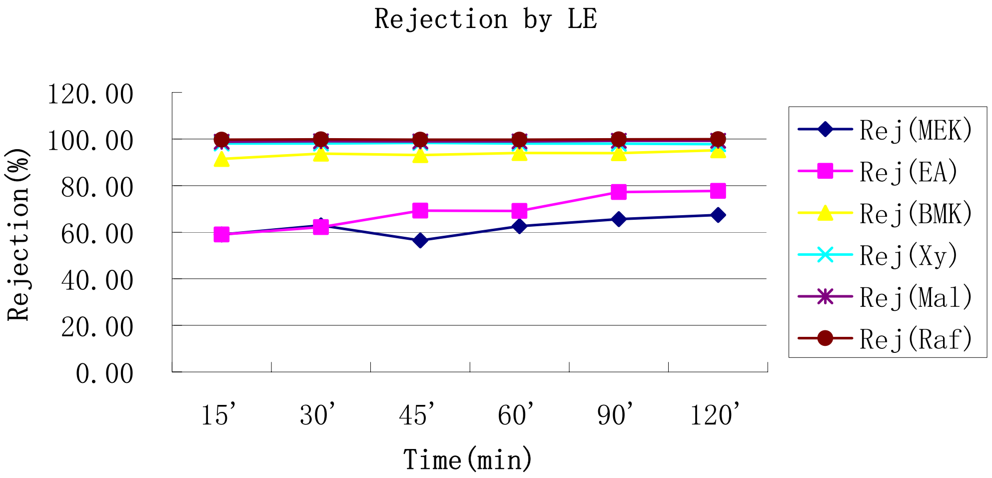

(b) Rejection of organics by LE

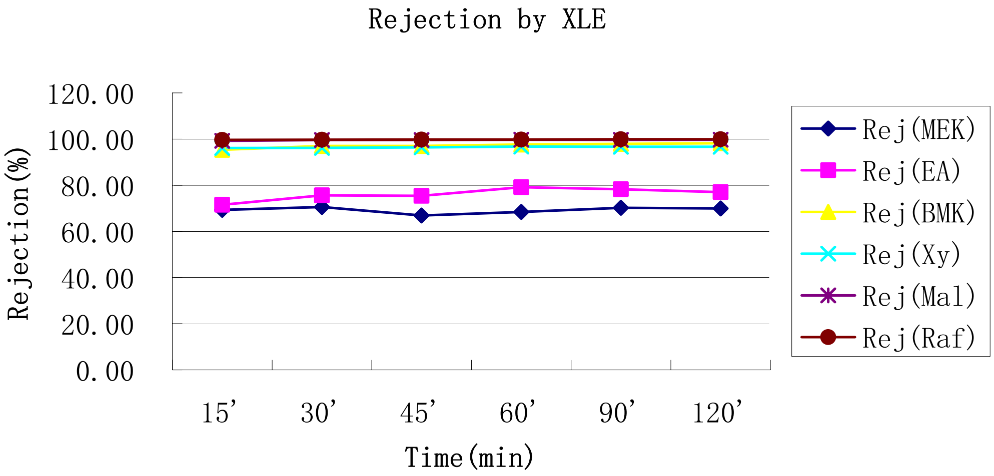

(c) Rejection of organics by XLE

Figure 6.11: Rejection of organic compound by membrane NF, LE and XLE

It also appears that with NF filtration, the retention of ethanol acetate with the retention of MEK has a considerable difference to the order of molecular size, this may be caused by the dipole moment of ethanol acetate (1.7) is much lower than MEK (2.8) (see Chapter 5, Section 5.2.6.2). Charge effect takes a role in the retention of organics if the membrane is charged sufficiently.

The result indicate that retention of small organic molecules is attributed to both sieve mechanism (membrane pore size and structure) and charge effect, sieve mechanism takes a paramount role while charge effect should not be neglected.

6.2.3 Organic Fouling Studies

In the organic fouling experiment, the gel layer resistance is not present, as the formation of a gel layer is related to macromolecules, which are not present here. In all experiments, synthetic solutions of organic components in pure water were used, so that suspended solids do not occur; this contribution to resistance against mass transport is thus avoided. Concentration polarization can be neglected because of the experimental conditions (high flow velocity and low solute concentration). The only factors that remain are the membrane resistance, pore blocking, and adsorption. (see the fouling model in Section 4.4)
For uncharged organic compounds, adsorption is the process that is most likely to occur. Molecules can get attached to the membrane pores or to the membrane surface by adsorption or chemisorption. Inside the pores, they narrow the free pathway for the water flow, hence decreasing the net pore opening. From the Hagen-Poiseuille equation, it can be seen that this should lead to a flux decline. When adsorption has a strong effect, it could even lead to pore blocking when the whole cross section of the pore is filled. The discussion is presented below:

6.2.3.1 Basic theory with organic fouling and flux decline:

Organic compounds may foul the membrane in the filtration process and cause the flux decline, shorten the lifetime of membrane. Organic fouling is an important point for the application of membrane technology and many investigations have been employed. Since flux decline is a major characteristic of fouling phenomena, organic fouling studies in this thesis are concentrating on the flux data.

Hagen-Poiseulle equation is commonly applied to describe the pure water flux through the membrane.

Hagen-Poiseulle equation is shown below:

$$J = \frac{\varepsilon \cdot r^2}{8 \cdot \eta \cdot \tau} \cdot \frac{\Delta P}{\Delta x} \quad \text{(eq. 6.4)}$$

It can be easily seen that the pure water flux through a membrane is determined by the membrane characteristics: ε, τ, r, Ds, the applied pressure ΔP and the viscosity of solution η (here is pure water, viscosity of water is decided by temperature). For more information, see Chapter 4 Section 4.4.

Resistance model is one of the most popular models, which is employed for flux decline caused by membrane fouling.

For nanofiltration, the water flux is written as:

$$J = \frac{\Delta P}{\eta R_{tot}} \quad \text{(eq.6.5)}$$

where, ΔP, driving force; η, viscosity; R_{tot}, total resistance.

The total resistance is the sum of different individual resistances, i.e., *R*tot= *R*p + *R*a + *R*m + *R*g + *R*cp + *R*i + *R*d (*R*p, resistance due to pore blocking; *R*a, resistance due to adsorption inside the pores; *R*m, membrane resistance (intrinsic); *R*g, resistance caused by the formation of a gel layer; *R*cp, concentration polarization resistance; *Ri*, resistance caused by specific interactions; *R*d, resistance from deposits on the membrane). For the details, please see Chapter 4 Section 4.4.

The total resistance exhibits that fouling related with the membrane structure, adsorption and pore blocking, organic compounds deposition, formation of gel layer, concentration polarization and some specific interaction.

For the experiments, the concentration of the organic compounds was very low (2mmol/l), so that osmotic pressure could be neglected. The Freundlich equation is used to describe the membrane pore blocking and adsorption.

Freundlich equation can be described for flux decline as below:

$$\Delta J = K_f c^n \quad \text{(eq. 6.6)}$$

where *c* is the concentration of the component to be adsorbed at equilibrium and *q* is the amount of the component that is adsorbed on the material, divided by the amount of material. K_f and n are empirical constants. For detailed information, check Chapter 4 Section 4.4.

6.2.3.2 Experimental data and discussion:

Six small organic compounds, MEK, EA, BMK, xylose, maltose and raffinose were filtrated with the three membranes to find out the components correlated with flux decline and fouling.

Some information about the organic compounds which relative with this fouling experiment are listed below:

Table 6.9: Information about organic compounds applied in the experiment

Solute	MW (g/mol)	Eff. Dia. (nm)	dipole moment (D)
MEK	72	0.42	2.8
EA	88	0.48	1.7
BMK	100	0.52	2.7
Xylose	150	0.55	1.0
Maltose	342	0.82	\
Raffinose	504	0.94	\

Experimental data (normalized flux) are supplied below:
8bar, 25℃, 6m/s, conc.: 2mmol/l

Table 6.10: Normalized flux of organic compounds filtration with NF

Time	MEK	EA	BMK	Xylose	Maltose	Raffinose
15'	102.16	101.17	94.13	101.33	96.71	99.36
30'	99.65	104.50	92.73	96.23	98.48	99.32
45'	101.59	103.55	94.92	95.80	97.65	99.18
60'	99.19	103.43	93.97	95.37	95.43	99.64
90'	100.85	100.21	91.54	93.01	95.88	99.41
120'	99.98	101.36	89.89	91.82	95.27	99.07
Average	100.57	102.37	**92.87**	95.59	96.57	99.33

Table 6.11: Normalized flux of Organic Compounds Filtration with LE

Time	MEK	EA	BMK	Xylose	Maltose	Raffinose
15'	95.92	100.05	90.56	99.34	99.09	95.82
30'	96.23	98.20	89.77	100.10	96.42	95.21
45'	95.47	95.94	88.01	98.81	93.24	92.11
60'	93.73	95.08	86.89	97.66	94.64	91.49
90'	90.13	92.90	87.30	96.58	93.52	88.59
120'	90.95	90.36	84.50	95.07	92.81	92.81
Average	93.74	95.42	**87.84**	97.93	94.95	92.67

Table 6.12: Normalized flux of Organic Compounds Filtration with XLE

Time	MEK	EA	BMK	Xylose	Maltose	Raffinose
15'	110.18	77.03	95.72	94.56	102.26	89.50
30'	109.48	74.37	93.21	92.04	100.31	86.31
45'	109.21	72.98	91.96	91.00	99.24	87.90
60'	106.79	72.88	89.97	90.29	98.94	88.00
90'	102.24	72.43	89.77	89.51	97.61	86.51
120'	100.36	72.25	88.63	88.67	95.96	86.54
Average	106.38	**73.66**	91.54	91.01	99.05	87.46

As shown in Table 6.10, the normalized flux of membrane NF when filtrating MEK and EA and membrane XLE when filtrating MEK is higher than 100%, this may because of the charge of organic molecule (small charged organic molecules can be sorbed by the membrane and might increase the flux[6]) or experimental error. Data of normalized fluxes in Table 6.10 also indicate that NF has the largest flux.

The data also show that the flux decline with membrane NF is quite small, compared to the data in Table 6.11 and 6.12 with LE and XLE. This can be explained by the fact that NF is more hydrophilic than LE and XLE; flux decline with LE is the largest of the three, this is explained by the fact that LE is the most hydrophobic membrane.

It is pointed out in the literature[40] that flux decline is expected when organic components with a high dipole moment are present, preferably with a size that corresponds to the membrane pore size. In this experiment, components with high dipole moment (MEK, EA and BMK) gave more flux decline, which is also affected by their molecule sizes and membrane's pore size. This is revealed by the experimental data.
The data show that compound BMK has the highest flux decline with NF and LE filtration while ethanol acetate caused the highest flux decline with XLE filtration.
It also reveals that the flux decline with membrane NF and XLE seems correlated with the molecule size. The pore size of NF is 0.59nm, it is close to BMK and xylose, which is corresponding to BMK and xylose have the highest flux decline. And for XLE, the pore size of XLE is 0.48nm, which is close to ethanol acetate, so ethanol acetate has the highest flux decline with XLE filtration.

Whereas, the flux decline with membrane LE seems to have more correlation with the molecule dipole moment than molecule size. Since the dipole moment of the components corresponds with the normalized flux with LE quite well.
So it could be supposed that the organic fouling is attributed to both the membrane characteristics and the solute size and dipole moment.

6.3 Studies on Membrane Fouling by Silica Colloids

In colloidal fouling phenomena to nanofiltration membranes, colloidal particles accumulate on the membrane surface and increase the resistance while decreasing the water yield to water flow through the membrane. Many studies have been carried out in recent decades and some basic principles determined [32, 33, 34]. Adsorption of colloids to the membrane surface is determined by interaction between several physical and chemical factors including operation pressure and temperature, surface physical and chemical properties of the colloids and membranes, feed water chemical composition and so on.

The correlation between membrane surface morphology and the membrane's physical and chemical properties with colloidal fouling will be studied below.

6.3.1 Correlation of Membrane Surface Morphology with Colloids Fouling

Membrane surface morphology such as surface roughness and membrane pore size was proved to have severe influence to membrane fouling phenomena in the past decades [33].

Following, some micrographs on fouled membrane by particles will be shown. These micrographs are the surfaces of the membrane samples, which had filtrated 30mg/l silica colloids for 120min before took the micrographs. These membranes were dried and coated with gold for SEM detection in MTM of KUL.

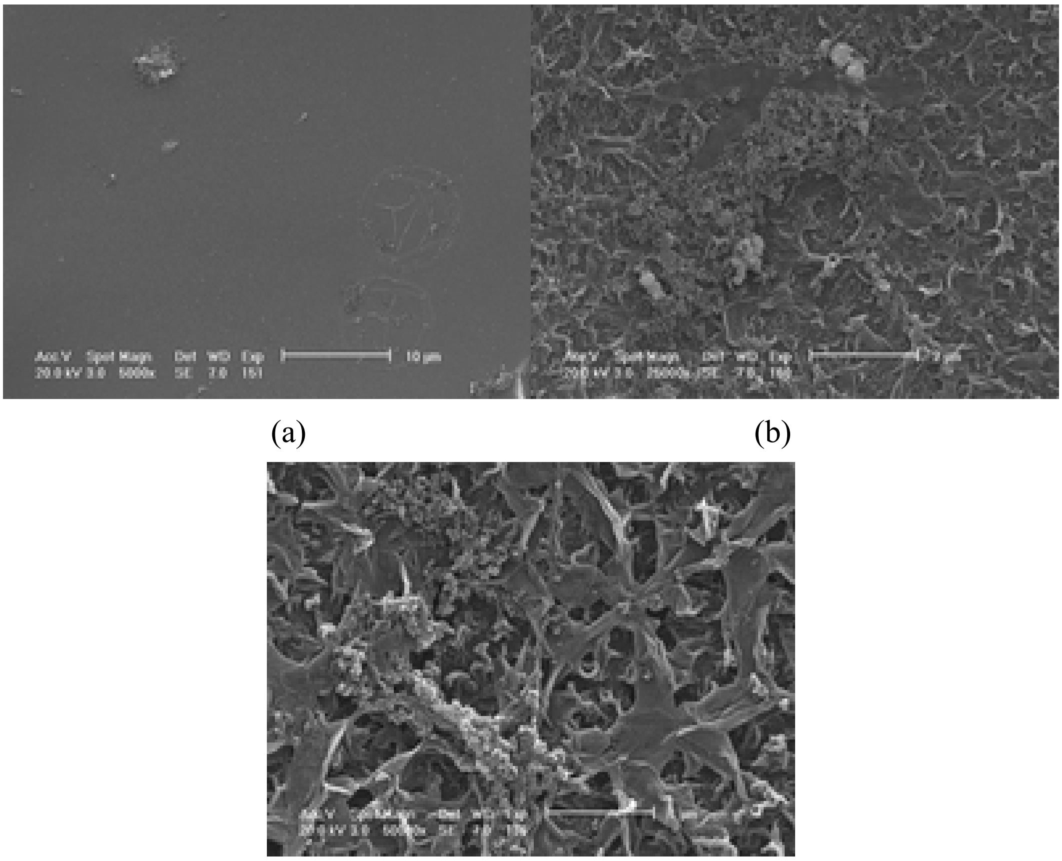

(a) (b)

(c)

Figure 6.12: SEM Images, Particles attached on NF (a) (bar length 10μm), LE (b) (bar length 2μm), XLE (c) (bar length 1μm) after the filtration to silica colloidal solution. The concentration of silica was 30 mg/l.

The SEM micrographs Figure 6.12 (a) (b) and (c) show that the particles mainly accumulated on the ridge structure. The rough membranes adsorbed more particles, the smooth membrane NF had less particles attached on. It can be seen from the photos that all of the membranes were slightly fouled by the particles.

Filtration Experiment Results and Discussions:

Silica colloids were diluted in DI water in neutral condition to 30mg/l, 60mg/l and 90mg/l to detect the colloidal fouling phenomena. Particle size is around 0.12μm.
Because it was too low concentration of the permeate in 30mg/l silica filtration to detect by the turbidity meter, only data of normalized flux are listed.
Experimental data of silica particle filtration are available in appendix 5.

As shown in appendix 5, removal of 90mg/L silica particles is higher than 60mg/L, and flux decline is less severe. Fouling data reveal that membrane XLE is the most seriously fouled, LE is moderately fouled and NF is slightly fouled. This result corresponds with the membrane roughness very well.
It also reveals that membrane fouling increases the retention of colloidal particles due to the cake formation as a “barrier” on membrane.

6.3.2 Correlation of Membrane Physical and Chemical Properties with Colloids Fouling

Membrane surface and chemical properties such as membrane charge, membrane hydrophobicity and membrane chemical composition act important roles in membrane fouling phenomena.

In this thesis, firstly, experimental results on electrokinetic properties of membranes and silica colloids in variation of pH value and salt concentration will be introduced, silica colloids stability in variation of pH value will also be detected to help evaluate the colloidal fouling phenomena.
Secondly, experimental data of salt and colloidal particles retention in variation of salt concentration and pH value as well as normalized flux will be listed.
At last, comparison and discussion which related with the results will be made, and some viewpoints of literatures on colloidal fouling will be introduced.

6.3.2.1 Electrokinetic properties and colloids fouling:

Determination of membrane electrokinetic properties is very important because the properties are reflection of membrane charge, which is a key factor to the retention of charged ion and some uncharged molecules, and it also relative with colloidal fouling due to colloids are always charged.

(1) Membrane Electrokinetic Properties:

Streaming potential analysis was applied to detect the membrane electrokinetic properties, 0.01M KCl was used as electrolyte solution. Each of the three membranes was tested three times and average value was used.

Here is the synthetic chart for membrane zeta potential analysis below:

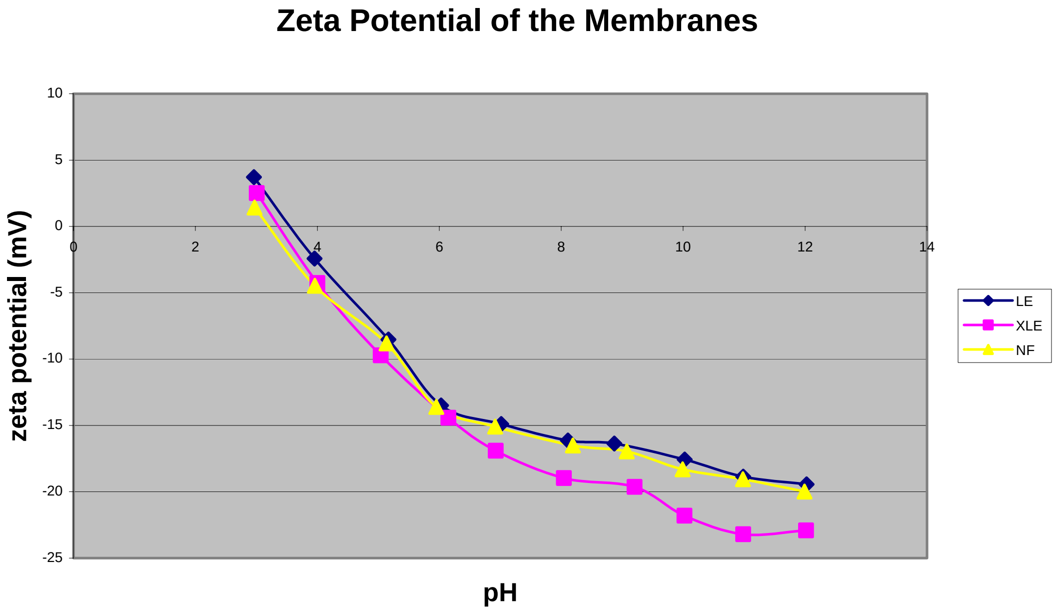

Figure 6.13: Zeta Potential of Membrane NF, LE and XLE as a Function of pH

Figure 6.13 shows the membrane surface zeta potential versus pH, it displays the isoelectric points of the three membranes are quite close, NF pH3, LE pH3.5, XLE pH3.2. The curves as a function of pH are close for NF and LE, but XLE is more negatively charged when pH higher that 6.

(2) Silica Colloids Stability Properties:

To avoid the silica colloidal particles accumulate in some situation in the experiment, silica colloids stability properties were determined under all relative experimental conditions, including as a function of pH value and in variation of NaCl concentration.

The dynamic light scattering experiments were applied for the silica particles stability measurements. The size of the particles in each condition was measured three times.

Results shown below:

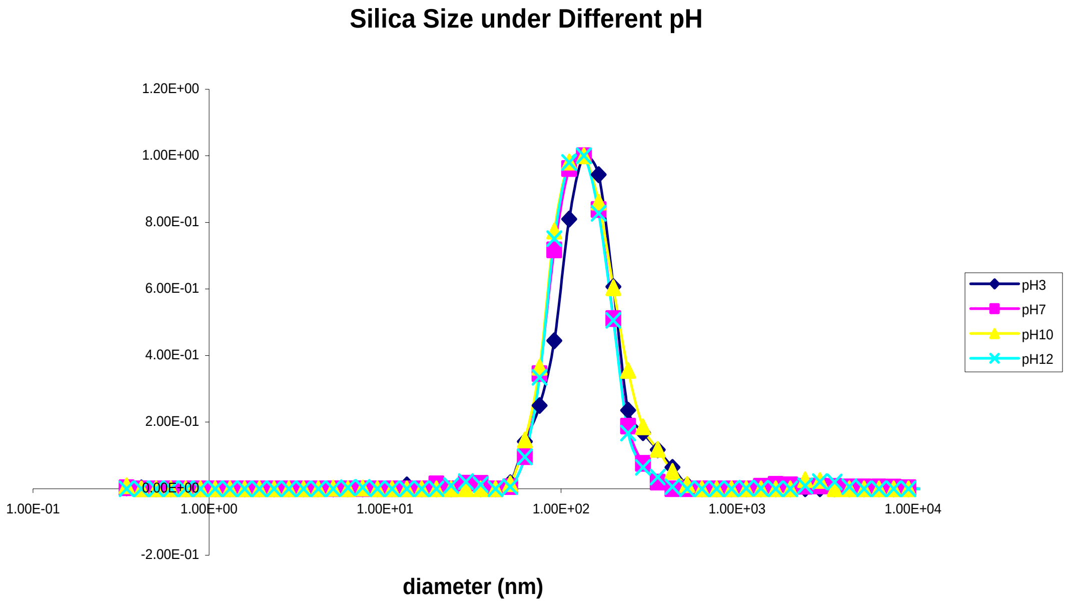

Figure 6.14: Silica Size under Different pH Environment

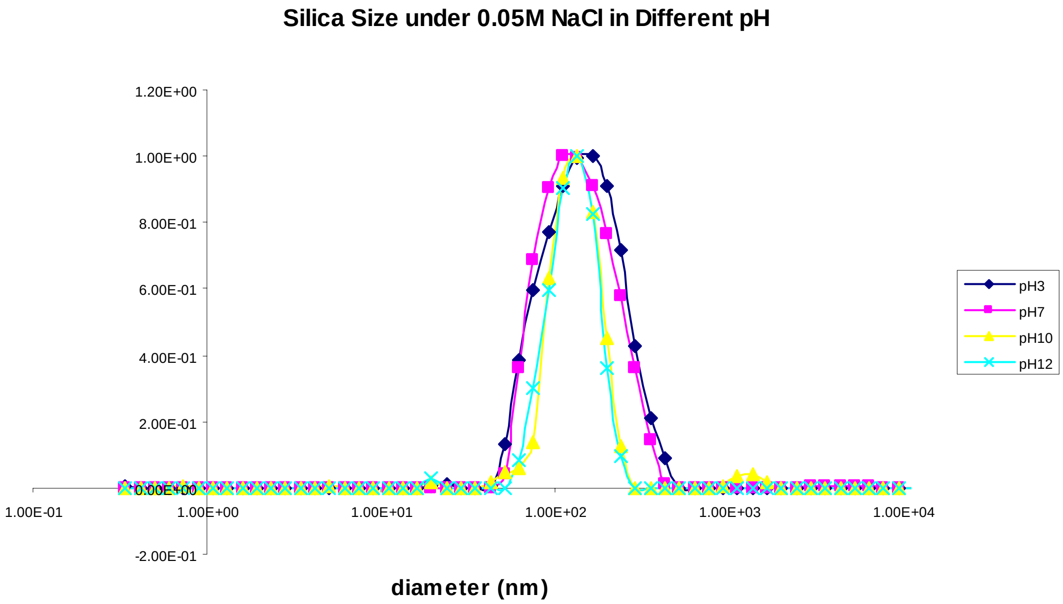

Figure 6.15: Silica Size under 0.05M NaCl in Different pH Environment

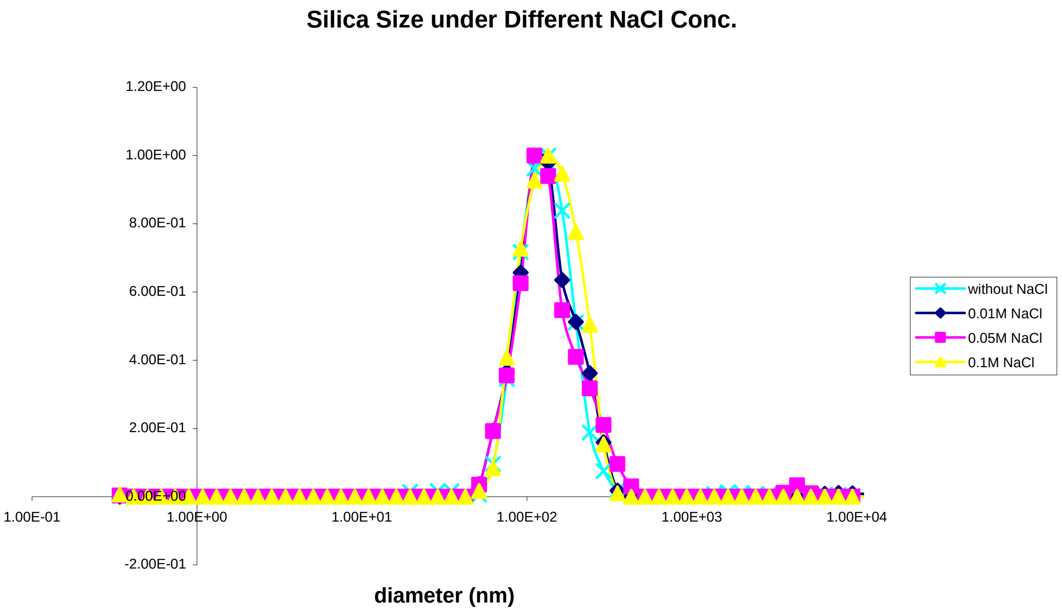

Figure 6.16: Silica Size under Different NaCl Concentration

As shown, the size of the particles stayed always the same, ranging from 111 nm to 140 nm, but this can be due to the instrumental accuracy. However, the size of the particles in the presence of pH3 seems to me a little bit larger than the others (and this with and without 0.05M NaCl). This means at pH3, the stability of silica particles were not as good as they were in other conditions and some particles were aggregated together due to it is close to isoelectric point and low charge effect.

Figure 6.16 shows that silica colloids were really stable from 0.01M NaCl to 0.1M NaCl, due to hydration [36] and steric-like [37] repulsive forces. The critical coagulation concentration of the colloidal suspension was around 1M NaC1 [33].

(3) Silica Colloids Electrokinetic Properties:
The isoelectric point of the membrane and the silica colloids were determined from measurements of electrophoretic mobility as a function of pH with and without NaCl.

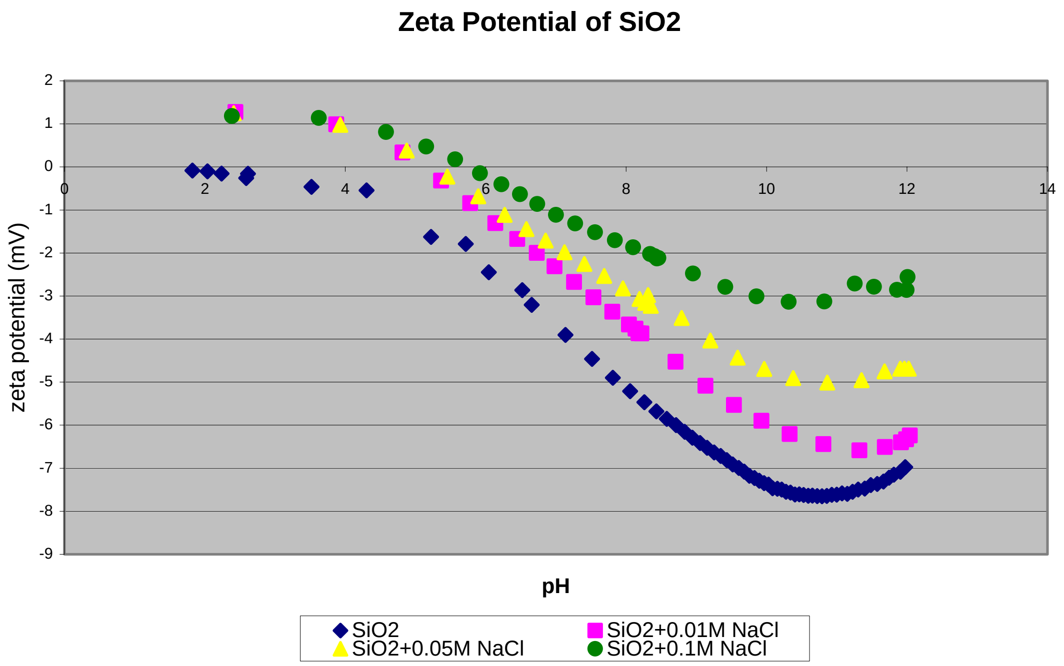

Figure 6.17: Zeta Potential of Silica Colloidal Particles

Figure 6.17 shows the silica colloidal particles zeta potential versus pH, it exhibits the zeta potential variation trend of the silica particles as a function of pH under different salt concentrations. The zeta potential variations of silica particles are attributed to the silica surface chemistry. As shown, silica particles without salt are more charged compare to silica with salt concentration, and the particles are always negatively charged. It can also be deduced from figure 6.17 that for the particles, more salty environment, less negatively charged (in another word, the zeta potential of particles are less “sensitive” to pH variation), although they are almost the same positively charged at pH2. This phenomenon attributes to the electrostatic shield effect by the high concentration salty electrolyte, colloids in more salty environment show less stability. The isoelectric points of SiO_2 with 0.01M NaCl and SiO_2 with 0.05M NaCl are close to pH5, SiO_2 with 0.1M NaCl close to pH6. This means in these points, silica colloids appear to accumulate easily and less interaction with charged membranes.

6.3.2.2 Experiment Results on Membrane fouling for Membrane Surface Physical and Chemical studies:

Silica colloids were diluted in DI water in neutral condition to 30mg/l, 60mg/l and 90mg/l; NaCl or HCl was added before the experiment was carried out to fit for the experimental condition requirements.

All the experiments were performed under the condition of 8bar, 25℃, 6m/s.

(a) Particle rejection in variation of salt concentration:

To demonstrate the shield effect to the membrane and particle charge by NaCl electrolyte, as well as fouling phenomenon upon membranes, particle rejection experiment in variation of salt concentration was performed. Both SiO_2 retention and normalized flux were measured.

Results on particle retention and salt retention will be discussed separately below.

(1) Particle Rejection:

Table 6.13: Flux Decline and SiO_2 Rejection, NaCl 0. 01M, SiO_2 30mg/L

	Membrane NF		Membrane LE		Membrane XLE	
Time	SiO_2 Rejection	Norm.Flux	SiO_2 Rejection	Norm.Flux	SiO_2 Rejection	Norm.Flux
15'	91.39	93.46	91.41	104.24	96.80	97.42
30'	95.35	90.88	97.66	98.32	94.96	**75.92**
45'	93.12	89.88	92.59	96.87	97.55	87.77
60'	96.39	89.88	94.83	94.07	97.48	84.63
90'	95.87	88.93	96.20	94.64	97.55	81.12
120'	94.84	89.73	96.78	88.61	98.30	**66.98**
Average	94.49	90.46	94.91	96.12	97.10	82.31

Table 6.14: Flux Decline and SiO_2 Rejection, NaCl 0.05M, SiO_2 30mg/L

	Membrane NF		Membrane LE		Membrane XLE	
Time	SiO_2 Rejection	Norm.Flux	SiO_2 Rejection	Norm.Flux	SiO_2 Rejection	Norm.Flux
15'	94.50	86.43	96.98	69.39	97.89	71.09
30'	97.52	85.78	98.16	69.99	99.55	66.25
45'	97.34	77.50	97.91	67.49	99.57	69.05
60'	99.47	73.04	99.16	67.41	99.35	69.44
90'	97.87	76.37	98.66	60.72	99.72	60.80
120'	96.63	79.71	98.99	60.96	99.42	60.13
Average	97.22	79.80	98.31	65.99	99.25	66.13

Table 6.15: Flux Decline and SiO_2 Rejection, NaCl 0. 1M, SiO_2 30mg/L

	Membrane NF		Membrane LE		Membrane XLE	
Time	SiO_2 Rejection	Norm.Flux	SiO_2 Rejection	Norm.Flux	SiO_2 Rejection	Norm.Flux
15'	97.22	68.08	94.28	45.92	88.81	48.19
30'	96.89	67.12	98.00	53.81	99.06	56.81
45'	98.22	64.74	99.28	51.99	99.74	53.90
60'	98.00	62.23	99.28	51.78	99.63	41.79
90'	99.11	62.92	97.44	50.57	99.55	36.50
120'	97.89	64.09	98.22	42.99	99.93	52.67
Average	97.89	64.86	97.75	49.51	97.79	48.31

Table 6.13, 6.14 and 6.15 exhibits the slight difference for retention of silica colloids in different salt concentration. However, remarkable differences in the normalized flux are presented.

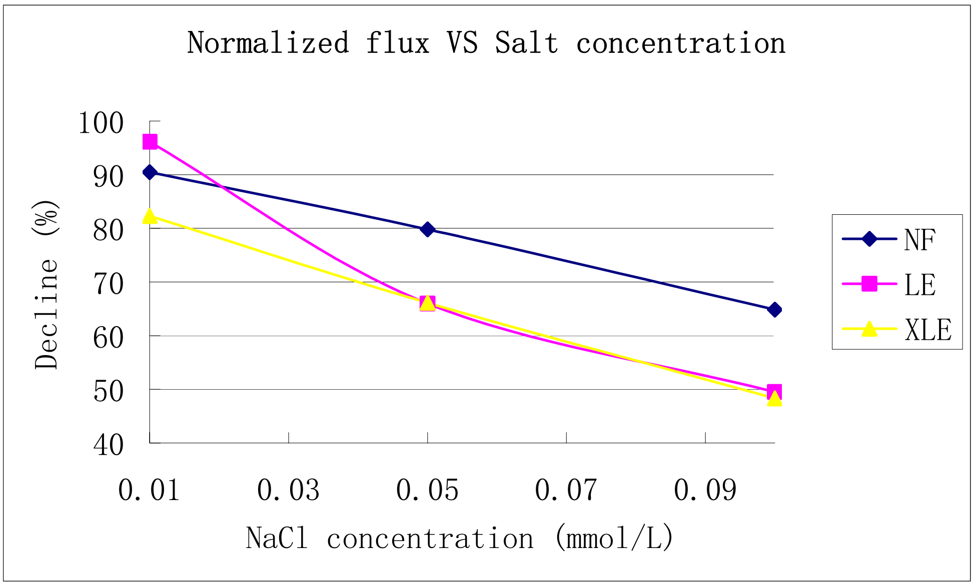

Figure 6.18: Normalized flux versus salt concentration

As shown in the chart 6.18 below, the normalized flux decreases with the increasing of salt concentration. This can be explained by the zeta potential of the silica, which is lower at higher concentrations (less repulsive forces between membrane and particles that prevent fouling). The membranes LE and XLE are more affected than membrane NF. This may be attributed to the fact that LE and XLE have a higher surface roughness. More particles were attached and adsorbed and caused the pore blocking. NF has a much smooth surface, it can prevent particles accumulate onto the surface and block the pores.

(2) Salt Rejection:

Table 6.16: Flux Decline and NaCl Rejection, NaCl 0. 01M, SiO_2 30mg/L

	Membrane NF		Membrane LE		Membrane XLE	
Time	NaCl Rejection	Norm.Flux	NaCl Rejection	Norm.Flux	NaCl Rejection	Norm.Flux
15'	87.90	93.46	96.09	104.24	96.88	97.42
30'	87.90	90.88	96.09	98.32	96.88	75.92
45'	87.90	89.88	96.09	96.87	96.88	87.77
60'	88.71	89.88	96.09	94.07	96.88	84.63
90'	88.71	88.93	96.09	94.64	96.88	81.12
120'	88.71	89.73	96.09	88.61	96.88	66.98
Average	88.31	90.46	96.09	96.12	96.88	82.31

Table 6.17: Flux Decline and NaCl Rejection, NaCl 0.05M, SiO_2 30mg/L

	Membrane NF		Membrane LE		Membrane XLE	
Time	NaCl Rejection	Norm.Flux	NaCl Rejection	Norm.Flux	NaCl Rejection	Norm.Flux
15'	72.76	73.99	93.73	60.63	93.34	59.14
30'	72.51	75.79	94.42	55.98	94.02	59.65
45'	71.78	73.58	94.69	57.16	94.17	57.83
60'	71.01	75.53	94.81	51.76	94.29	56.02
90'	70.34	77.02	95.13	49.96	94.47	54.61
120'	69.62	77.34	95.17	49.81	94.67	52.21
Average	71.34	75.54	94.66	54.22	94.16	56.58

Table 6.18: Flux Decline and NaCl Rejection, NaCl 0.1M, SiO_2 30mg/L

	Membrane NF		Membrane LE		Membrane XLE	
Time	NaCl Rejection	Norm.Flux	NaCl Rejection	Norm.Flux	NaCl Rejection	Norm.Flux
15'	61.10	68.08	88.18	45.92	92.50	48.19
30'	61.01	67.12	91.57	53.81	94.04	56.81
45'	61.56	64.74	91.57	51.99	94.22	53.90
60'	61.56	62.23	91.57	51.78	94.22	41.79
90'	61.93	62.92	91.93	50.57	94.13	36.50
120'	61.56	64.09	91.84	42.99	94.22	52.67
Average	61.45	64.86	91.11	49.51	93.89	48.31

Compared to the salt retention in Table 6.7 in Section 6.2.1.3, it is clear from the figure that the salt retention which is affected by colloids fouling. Also shown in the chart below:

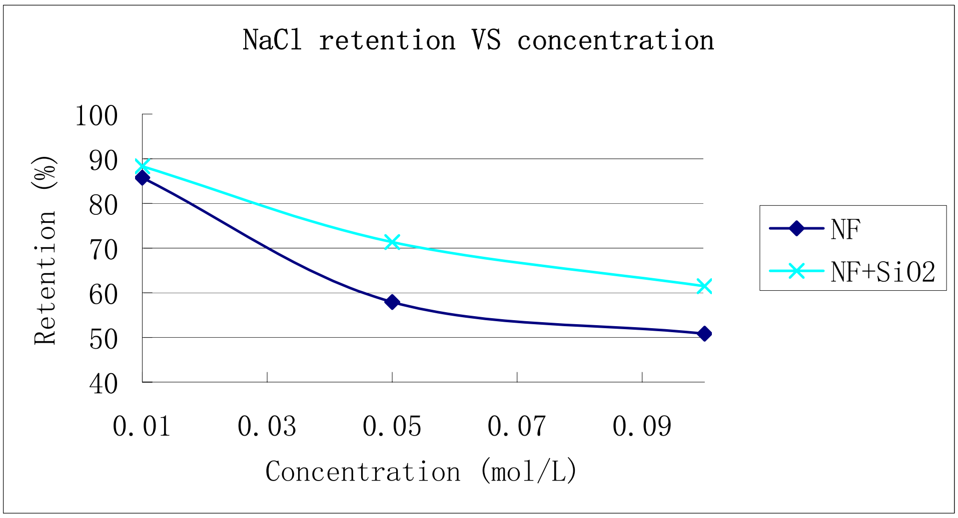

(a) NaCl retention with NF

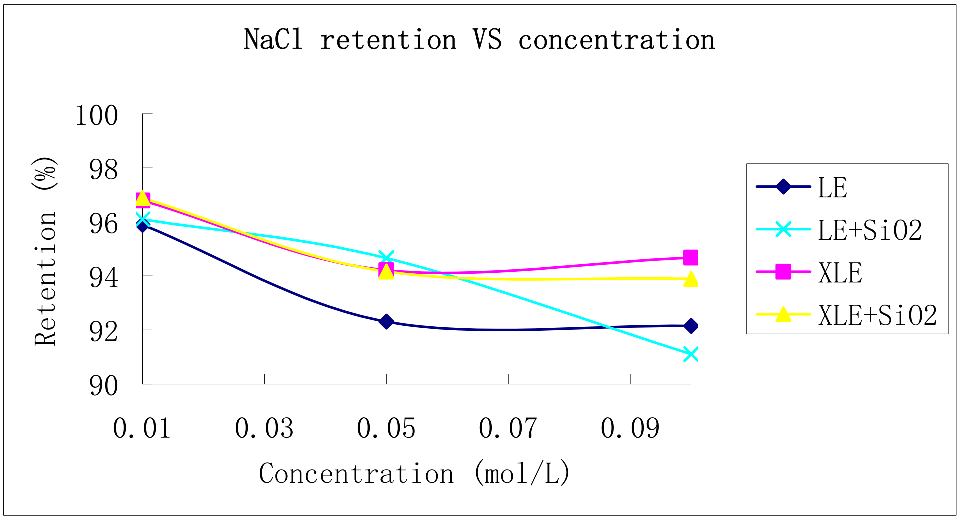

(b) NaCl retention with LE and XLE

Figure 6.19: NaCl retention versus concentration with/without particle effect

Due to membrane NF has larger pores; particles affect the salt retention much severe, it can be seen in Figure 6.19 (a); whereas, for LE and XLE, particles effect is not detected in Figure 6.19 (b) although they were severe fouled by particles which proved by flux decline data.

This may indicate that particles affect the salt retention when the membrane has large pores more than the membrane has small pores, no matter how rough the membrane surface is.

All data show the higher concentration of salt causes the lower retention, this proves the principle: higher electrolyte concentration causes the double layer more compressed and causes lower retention again.

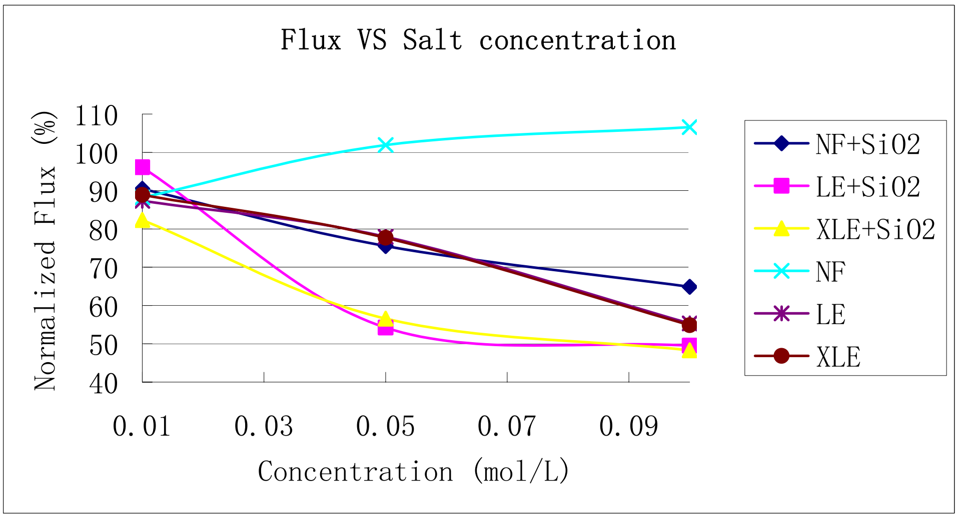

Figure 6.20: Normalized flux versus NaCl concentration

It is clear from Figure 6.20 that the normalized flux decreases with the increase of salt concentration; normalized flux decreases much severe when 30mg/L silica colloids are available in solution than without them. This attributes to the effect of ion strength. Elimelech et al. [67] showed that particle cake thickness, permeability, and porosity generally increased with a decrease in solution ionic strength for a given particle size. Expect for NF without silica particles, all of the results fit for the literatures report quite well.

(b) Particle rejection in variation of pH:

To detect the effect of solution pH value to silica particles retention, the pH was varied from 3 to 12 during filtration of 30mg/l SiO_2. Both retention of silica and membrane normalized flux were measured.
The experimental data for SiO_2 rejection and normalized flux are given below:

Table 6.19: Flux Decline and SiO_2 Rejection, SiO_2 30mg/L, pH=3

	Membrane NF		Membrane LE		Membrane XLE	
Time	SiO_2 Rejection	Norm.Flux	SiO_2 Rejection	Norm.Flux	SiO_2 Rejection	Norm.Flux
15'	95.90	111.81	97.84	99.77	98.59	89.13
30'	98.83	112.56	99.04	76.96	99.62	82.51
45'	99.22	112.54	98.80	91.60	99.62	83.91
60'	98.63	111.51	99.76	87.15	99.81	80.39
90'	98.05	110.14	98.92	84.82	99.91	76.52
120'	98.44	111.75	99.52	83.88	99.81	75.13
Average	98.18	111.72	98.98	87.36	99.56	81.26

Table 6.20: Flux Decline and SiO_2 Rejection, SiO_2 30mg/L, pH≈6 (Normal)

	Membrane NF		Membrane LE		Membrane XLE	
Time	SiO_2 Rejection	Norm.Flux	SiO_2 Rejection	Norm.Flux	SiO_2 Rejection	Norm.Flux
15'	72.73	115.84	99.33	156.68	88.24	141.47
30'	82.87	116.92	96.67	148.57	97.43	110.67
45'	96.50	117.18	97.00	139.16	97.06	117.23
60'	99.30	117.20	99.33	136.10	98.90	114.72
90'	99.65	118.68	99.33	135.80	99.26	117.47
120'	98.60	118.55	97.67	143.32	98.16	114.57
Average	91.61	117.39	98.22	143.27	96.51	119.36

Table 6.21: Flux Decline and SiO_2 Rejection, SiO_2 30mg/L, pH=10

	Membrane NF		Membrane LE		Membrane XLE	
Time	SiO_2 Rejection	Norm.Flux	SiO_2 Rejection	Norm.Flux	SiO_2 Rejection	Norm.Flux
15'	95.23	107.72	98.75	91.13	95.84	125.79
30'	94.76	108.32	99.47	86.03	97.78	121.69
45'	95.63	112.08	98.63	84.98	99.57	118.17
60'	97.22	112.43	98.93	84.31	99.08	113.02
90'	96.82	112.41	99.11	94.43	99.30	102.65
120'	98.49	114.99	99.41	92.20	99.73	95.84
Average	96.36	111.32	99.05	88.84	98.55	112.86

Table 6.22: Flux Decline and SiO_2 Rejection, SiO_2 30mg/L, pH=12

	Membrane NF		Membrane LE		Membrane XLE	
Time	SiO_2 Rejection	Norm.Flux	SiO_2 Rejection	Norm.Flux	SiO_2 Rejection	Norm.Flux
15'	79.91	107.35	82.34	45.54	86.67	38.75
30'	85.82	110.71	89.18	48.24	90.63	43.80
45'	95.74	115.82	83.44	50.79	91.53	44.26
60'	92.67	120.42	84.77	51.05	91.89	45.45
90'	88.18	121.54	82.34	54.75	94.41	47.52
120'	83.92	126.41	89.85	54.79	90.09	48.99
Average	87.71	117.04	85.32	50.86	90.87	44.80

As displayed in the tables, no flux decline is found with membrane NF in all of the pH values. For flux decline of LE and XLE, it shows a strange sequence: less flux decline in neutral condition and severe flux decline in to extreme pH conditions. It could not be explained by recent theories. This may due to some impurities were washed out and block the membrane pores in acidic or basic conditions. Another point is that NF is not easy to be fouled, and membrane volume flux can be increased by increase pH value. It can be proved from the salt filtration in variation of pH experiment, please check Table 6.23 below:

Table 6.23: Normalized flux in NaCl filtration in variation of pH

	NF	**LE**	**XLE**
pH=3	94.97	39.27	37.17
pH=5	88.96	73.87	64.52
pH=7	87.36	74.96	69.39
pH=10	120.09	68.9	61.51
pH=12	126.7	54.08	53.88

As shown in Table 6.19, 6.20, 6.21 and 6.22, the retention of silica particles increases with time; this may be caused by the cake formation with time. Those data also reveal that silica particles have the almost highest retention in pH10 with the three membranes. From Section 6.3.2.1 Figure 6.17 shows the particles have the highest zeta potential in pH10; that means there has the highest repulsion between membrane and silica particles.

(c) Additional Study on Particle Rejection in Salt coupled with pH:

Due to some contradictory results in Section 6.3.2.2 (b), additional studies on particle rejection in salty environment with variation of pH value were carried out. Following discussions will concentrate on the silica particle retention and flux decline. Salt retention will also be discussed and compared with the former conclusions.

To detect the effect of solution pH value to silica particles retention, experiment was set up in variation of pH from 3 to 12 with filtration of 30mg/l SiO_2. For salty environment, 0.05M NaCl was applied. Data are listed below:

Table 6.24: Flux Decline, Salt Rejection and SiO_2 Rejection, SiO_2 30mg/L, NaCl 0.05M, pH=3

	Membrane NF			Membrane LE			Membrane XLE		
Time	R. NaCl (%)	R. SiO2 (%)	J/J_V (%)	R. NaCl (%)	R. SiO2 (%)	J/J_V (%)	R. NaCl (%)	R. SiO2 (%)	J/J_V (%)
15'	56.84	93.74	103.93	86.44	95.09	73.78	82.16	95.65	71.51
30'	58.18	97.65	105.12	88.02	97.66	60.99	83.83	97.83	68.20
45'	59.52	96.87	104.97	89.61	98.99	65.07	85.29	97.43	65.11
60'	60.66	97.46	104.34	90.40	99.22	66.45	86.54	98.12	60.65
90'	61.43	97.65	104.61	91.98	98.99	60.58	89.88	98.42	51.70
120'	64.68	98.83	105.27	93.84	98.21	61.25	91.13	98.52	57.36
Aver.	60.22	97.03	104.71	90.05	98.03	64.69	86.47	97.66	62.42

Table 6.25: Flux Decline, Salt Rejection and SiO_2 Rejection, SiO_2 30mg/L, NaCl 0.05M, pH Neutral

	Membrane NF			Membrane LE			Membrane XLE		
Time	R. NaCl (%)	R. SiO2 (%)	J/J_V (%)	R. NaCl (%)	R. SiO2 (%)	J/J_V (%)	R. NaCl (%)	R. SiO2 (%)	J/J_V (%)
15'	68.69	94.50	102.28	94.26	96.98	82.13	93.47	97.89	84.10
30'	68.86	97.52	101.51	94.43	98.16	82.84	92.96	99.55	78.39
45'	70.42	97.34	91.72	94.61	97.91	79.89	92.96	99.57	81.70
60'	70.07	99.47	86.43	94.78	99.16	79.79	93.13	99.35	82.16
90'	69.90	97.87	90.38	94.78	98.66	71.87	93.13	99.72	71.93
120'	69.38	96.63	94.33	94.78	98.99	72.15	92.78	99.42	71.14
Aver.	69.55	97.22	94.45	94.61	98.31	78.11	93.07	99.25	78.24

Table 6.26: Flux Decline, Salt Rejection and SiO_2 Rejection, SiO_2 30mg/L, NaCl 0.05M, pH=10

	Membrane NF			Membrane LE			Membrane XLE		
Time	R. NaCl (%)	R. SiO2 (%)	J/J_V (%)	R. NaCl (%)	R. SiO2 (%)	J/J_V (%)	R. NaCl (%)	R. SiO2 (%)	J/J_V (%)
15'	80.64	76.47	128.84	100	86.33	80.71	100	93.07	91.83
30'	78.23	78.68	138.32	100	84.90	77.78	100	91.73	88.37
45'	76.43	80.88	140.68	100	80.60	74.72	100	91.47	83.81
60'	75.62	78.19	141.68	100	87.24	73.15	100	90.93	82.27
90'	73.22	81.37	142.00	100	85.94	69.82	100	92.71	77.40
120'	72.41	84.80	144.31	100	82.42	68.82	100	94.22	75.62
Aver.	76.09	80.07	139.31	100	84.57	74.17	100	92.36	83.22

Table 6.27: Flux Decline, Salt Rejection and SiO_2 Rejection, SiO_2 30mg/L, NaCl 0.05M, pH=12

	Membrane NF			Membrane LE			Membrane XLE		
Time	R. NaCl (%)	R. SiO2 (%)	J/J_V (%)	R. NaCl (%)	R. SiO2 (%)	J/J_V (%)	R. NaCl (%)	R. SiO2 (%)	J/J_V (%)
15'	73.26	82.60	152.49	97.17	60.73	66.16	97.24	70.68	59.62
30'	71.03	83.70	159.21	97.60	70.57	53.74	98.43	88.48	54.61
45'	69.84	85.91	161.84	98.04	77.73	62.22	99.03	91.87	48.78
60'	69.69	83.70	163.15	98.33	88.39	64.00	99.32	87.45	52.80
90'	68.95	87.85	166.82	98.62	88.86	54.90	99.62	80.97	46.04
120'	68.35	83.98	169.20	98.62	96.95	60.67	99.92	90.84	50.80
Aver.	70.19	84.62	162.12	98.06	80.54	60.28	98.93	85.05	52.11

*NaCl retention which measured more than 100% is set as 100%.

As shown, the same sequence for flux decline and retention of silica particles appears in the tables. Retention of NaCl increases with pH value, same as Section 5.2.1.2.

6.3.2.3 Comparison between conclusions and literature:

As mentioned, silica particles adsorbed and deposited into the membrane surface forming the cake layer and fouling. This decreases the volume flux. Another side, increasing the ion strength, volume flux decreases due to the increases of cake formation. These conclusions are in agreement with some literatures [67, 68, 69, 70]. Hoek et al. [70] demonstrated that the major cause for flux decline is “cake-enhanced osmotic pressure” in colloidal fouling of nanofiltration membranes.

But Lee et al. [69] pointed out that salt retention decrease when colloidal fouling take place due to the increase of salt concentration polarization by cake formation. The experiments results seem not support this point. As shown in experimental data in Section 6.3.2.2 (b) (2) Table 6.16, 6.17 and 6.18, the retention of NaCl is quite stable.

Yiantsios and Karabelas [71] demonstrated that increase the colloid stability, the membrane would be less fouling. But the experimental data show the results that increase or decrease the pH value (in this case, colloid stability will increase) will both increase the membrane fouling. This may due to the effect of many factors, such as cake formation, concentration polarization, charge effect etc. Increase pH causes depolarization; increase ion strength causes membrane zeta potential increasing. [72] Because of here is a lot of parameters which affect volume flux and salt/colloids retention, it is hard to find disciplines from the experimental data in tables of Section 6.3.2.2 (b) and Section 6.3.2.2 (c). Discussions would be complicated due to many factors act in this case, further studies should be extended.

SiO_2 zeta potential curves (see Section 6.3.2.1, Figure 6.17) in different ion strength have different isoelectric points; this indicates that silica particles adsorb cations in salty environment. But for membranes, their isoelectric points do not be affected by different ion strength. [72] This theory should also pay attention for colloids retention experiments.

6.4 Revaluation for the three membranes

Based on the membrane characteristics studies, it is possible to revaluate these three membranes by their performance and provide some suggestions for their application.

Membrane NF (NF 250)

Membrane NF has very different characteristics to LE and XLE; it is the smoothest and most hydrophilic membrane. Due to these characteristics, it is the most anti-fouling membrane of the three. This can easily be identified from the results of organic and particle fouling experiments.

Membrane charge of the three membranes is relatively close; it can be seen from Figure 6.13 in Chapter 6 Section 6.3.2.1.

Attributed to its larger pore size (0.59nm) and higher molecule cut-off (155) in the three membranes, retention of ion, organic molecules and silica particles is the lowest.

Because of its different characteristics, it has different performance in salt filtration and particle filtration. NF is most affected by “shield effect” of the salty solution. It is also affect severe by particle cake formation.

NF has the highest volume flux.

Due to these characteristics, NF would be a better choice for drinking water treatment.

LE (unknown commercial code)

Membrane LE is generally quite close to XLE, although has some differences.

LE is the most hydrophobic membrane; this means it has less fouling resistance than NF and XLE. LE always has the very high salt removal and volume flux is quite high compared to XLE.

It seems that LE is competent for desalination.

XLE (FT 30)

XLE has a lot of applications recent years, mostly for desalination. Many studies have been carried out on it, [73, 74, 75] the experimental data are agree with the data in those literatures well.

As the manufacturer and literatures said, XLE (FT 30) is a low pressure RO membrane (nanofiltration membrane). It has a good performance in salt retention and good fouling resistance than LE. The disadvantage of XLE is the low volume flux, compared to NF and LE.

7. Conclusion

By using the experimental data from the filtration testing of six small organic compounds, with the log-normal pore size model for calculation, results indicate that membrane NF has the largest average pore size, 0.59nm; LE and XLE are quite similar.

Results from filtration experiments indicate that membrane NF has the most open microstructure while LE and XLE don't have much difference in structure. This has also been indicated in SEM micrographs. SEM and AFM photographs also show that NF is the smoothest membrane and XLE is the roughest membrane. The roughness differences of the three membranes are remarkable. It can be deduced that the range-to-valley difference of XLE causes the most severe organic fouling and it has been proved by organic fouling data.

By sessile method of contact angle measurement to the three membranes, NF is the most hydrophilic membrane while LE is the most hydrophobic.

After the salts (NaCl, Na_2SO_4 and $CaCl_2$) filtration experiment, the results indicate that the retention of Na_2SO_4 is the highest while NaCl is the lowest, which cannot be explained by Donnan exclusion for all of the three membranes. This phenomenon could be explained by the effect by the sieving mechanism. Further experiment results, show that the ion's diffusion coefficient seems quite relative with this sequence.

In the experiment of different pH with NaCl retention, the retention of NaCl increases with the increase of pH value. This is clear to reveal that the salts retention increase with the increase of membrane charge.

In different ion strength to salt retention experiment, retention of NaCl decrease with the increase of concentration in feed, this attributed to the "shield effect" (because concentration polarization can be neglected due to high feed flow). When the ion strength is high enough, it may "shield" the change effect of the membrane and decrease the salt retention. Membrane NF is the most affected membrane, because NF has the largest pore size. Less charge effect, less retention.

In small organic compounds retention experiment, because of the membrane charge effect, although the effective sizes of the organic compounds are much larger than the ions, the retention is usually lower. Charge effect is the paramount role in ion retention while sieve mechanism is more important in organics retention. Charge effect is also taking a role in the retention of organics if the membrane is charged sufficiently and molecule size is close to membrane pore size.

BMK has the highest flux decline with NF and LE filtration while ethanol acetate caused the highest flux decline with XLE filtration. Flux decline with membrane NF and XLE seems correlated with the molecule size. Flux decline with membrane LE seems to have more correlation with the molecule dipole moment than molecule size. Hence, it could be supposed that the organic fouling is attributed to both the membrane characteristics and the solute (organic compounds).

Colloids fouling data corresponds with the membrane roughness. Silica retention increases with the increase of silica concentration, this may due to the cake formation as a “barrier” on membrane.

Membrane surface and chemical properties such as membrane charge, membrane hydrophobicity and membrane chemical composition act important roles in membrane fouling phenomena.

Due to membrane NF has larger pores; particles affect the salt retention much severe. But for LE and XLE which has smaller pores, salt retention is stable. This indicates that particles affect the salt retention when the membrane has large pores more than the membrane has small pores, no matter how rough the membrane surface is.

Normalized flux decreases with the increase of salt concentration; normalized flux decreases much severe when 30mg/L silica colloids are available, due to the effect of ion strengthen.

In the experiment of particle rejection in variation of pH, membrane volume flux can be increased by increase pH value. In pH10, there has the highest repulsion between membrane and silica particles.

In colloidal fouling experiment, results indicate that silica particles adsorbed and deposited into the membrane surface forming the cake layer and fouling, this decreases the volume flux. On the other hand, increasing the ion strength, volume flux decreases due to the increases of cake formation.

8. Recommendations and Future development

Due to some experiment results are not agree with literatures: the retention of NaCl is quite stable; these results seem not support the point by Lee et al. [69]. Experimental data show the results that increase or decrease the pH value (in this case, colloid stability will increase) will both increase the membrane fouling, which does not agree with the opinion by Yiantsios and Karabelas [71]. More experiments should be performed to test these points.

Salts coupled with sugars filtration seems valuable to be carried out to find out the ion and small organic retention, and pH variation conditions would be considerable.

More filtration testing should be performed for monovalent and multivalent salts, $CaSO_4$, $MgSO_4$, $MgCl_2$ and $ZnSO_4$ might be good choices, and pH variation conditions would be considerable.

For colloidal fouling, $Al_2(SO_4)_3$, $FeCl_3$ might be applied to develop the fouling principle by metal ions, and pH variation conditions would be considerable.

Membrane thickness relevant experiment and model comparison could be interesting.

Different methods for membrane reflection coefficient to organic compounds (micro molecule and macromolecule) could be compared by filtration test.

Due to two membranes can have the same average pore size or the same molecular weight cutoff value yet have quite different separation characteristics when there is a difference in the pore size distribution in the membranes, [79] it could be interesting to calculate the pore size distribution of the membranes by adequate models.

References

1. B. Van der Bruggen, C. Vandecasteele, Removal of pollutants from surface water and groundwater by nanofiltration: overview of possible applications in the drinking water industry, *Environmental Pollution 122 (2003) 435–445*

2. *K.S. Spiegler，O. Kedem, Thermodynamics of Hyperfiltration (Reverse Osmosis): Criteria for Efficient Membranes, Desalination, 1, 311 (1966)*

3. B. Van der Bruggen, C. Vandecasteele, Modelling of the retention of uncharged molecules with nanofiltration, *Water Research 36 (2002) 1360–1368*

4. B. Van der Bruggen, J. Schaep, D. Wilms, C. Vandecasteele, A comparison of models to describe the maximal retention of organic molecules in nanofiltration, *Separation Science and Technology, 35 (2000) 169-182*

5. J. Schaep, Bart Van der Bruggen, Carlo Vandecasteele, Dirk Wilms, Influence of ion size and charge in nanofiltration, *Separation and Purification Technology 14 (1998) 155–162*

6. M. Nyström, L. Kaipia, S. Luque, Fouling and retention of nanofiltration membranes, *Journal of Membrane Science 98 (1995) 249-262*

7. G. Hagmeyer, R. Gimbel, Modeling the salt rejection of nanofiltration membranes for ternary ion mixtures and for single salts at different pH values, *Desalination 117 (1998) 247-256*

8. G. Hagmeyer, R. Gimbel, Modeling the rejection of nanofiltration membranes using zeta potential measurements, *Separation and Purification Technology 15 (1999) 19-30*

9. W. R. Bowen, J. S. Welfoot, Modeling of membrane nanofiltration—pore size distribution, *Chemical Engineering Science 57 (2002) 1393 – 1407*

10. J. Qin, M. H. Oo, H. Lee, B. Coniglio, Effect of feed pH on permeate pH and ion rejection under acidic conditions in NF process, *Journal of Membrane Science 232 (2004) 153–159*

11. M. V. Hoek, S. Bhattacharjee, M. Elimelech, Effect of Membrane Surface Roughness on Colloid- Membrane DLVO Interactions, *Langmuir 19, (2003), 4836-4847*

12. http://www.physics.nyu.edu/grierlab/leshouches2/node6.html, accessed in Nov.28, 2004

13. A. Seidel, J. Waypa, M. Elimelech, Role of Charge (Donnan) Exclusion in Removal of Arsenic from Water by a Negatively Charged Porous Nanofiltration Membrane, *Environmental Engineering Science, 18, (2001)*

14. M.K. Timmer, *Properties of nanofiltration membranes; model development and industrial application*, Proefschrift. ISBN: 90-386-2872-2, Techni- sche Universiteit Eindhoven, 2001, Eindhoven, the Netherlands

15. S. Nakao, Determination of Pore Size Distribution 3. Filtration Membranes (Review), *Journal of Membrane Science 96 (1994) 131-165*

16. O. Kedem, A. Katchalsky, Thermodynamic analysis of the permeability of

biological membranes to nonelectrolytes, *Biochem. Biophys. Acta, 27 (1958) 229*

18. N.A. Peppas, D.L. Meadows, Macromolecular structure and solute diffusion in membranes: an overview of recent theories, *Journal of Membrane. Science, 16 (1983) 361-377*

19. B.C. Robertson, A.L. Zydney, A Stefan-Maxwell analysis of protein transport in porous membranes, *Separation Science and Technology, 23 (1988) 1799-1811*

20. J.D. Ferry, Statistical evaluation sieve constants in ultrafiltration, *J. Gen. Physiol., 20 (1936) 95*

21. M. Mulder, *Basic Principle of Membrane Technology (Second Edition)*, Kluwer Academic Publishers, 1996.

22. B. Van der Bruggen, C. Vandecasteele, Flux Decline during Nanofiltration of Organic Components in Aqueous Solution, *Environmental Science and Technology, 35 (2001) 3535-3540*

23. W. Eykamp, In *Membrane Separations Technology, Principles and Applications*; Noble, R. D., Stern, S. A., Eds.; Elsevier: Amsterdam, (1995) 1-43.

24. P. M. Dove, The dissolution kinetics of quartz in aqueous mixed cation solutions, *Geochimica et Cosmochimica Acta, 63 (1999), 3715–3727*

25. J.S. Makie, P. Meares, *Proc. R. Soc. London Ser. A, 232 (1955) 498*

26. M. Hidetoshi, K. Yoshiyuki, T. Akihiko, Pore-surface characterization of amphoteric charged membranes by means of zeta potential measurements, *Colloids and Surfaces A: Physicochem. Eng. Aspects 222 (2003) 165-173*

27. H. Ødegaard, B. Eikebrokk, R. Storhaug, Processes for the Removal of Humic Substances from Water - an Overview Based on Norwegian Experiences, *Water Science and Technology, 40 (1999) 37-46*

28. M. Dubois, K.A. Gilles, J.K. Hamilton, P.A. Rebers, F. Smith, Calorimetric method for determination of sugars and related substances, *Anal. Chem. 28 (1956) 350-356*

29. Website of University of Colorado at Boulder, http://snobear.colorado.edu/, accessed in Feb. 2005

30. J.A. Howell, M. Nyström, *Fouling Phenomena In: Membranes in Bioprocessing: Theory and Application.* Eds. J.A. Howell, V. Sanchez and R. Field, Chapman & Hall, London, 1993, 203-241.

31. Webpage of the Department of Metallurgy and Materials Engineering (MTM) of Katholieke University of Leuven (KUL) http://www.mtm.kuleuven.ac.be/Research/Equipment/Physical/Philips-SEM-XL30-FEG.html, accessed in December, 2004.

32. B. Van der Bruggen, D. Segers, C. Vandecasteele, L. Braeken, A. Volodin, C. Van Haesendonck, How a Microfiltration Pretreatment Affects the Performance in Nanofiltration, *Separation Sci. Technol., 39 (2004) 1443 - 1459*

33. M. Elimelech, X. Zhu, A. E. Childress, S. Hong, Role of membrane surface morphology in colloidal fouling of cellulose acetate and composite aromatic polyamide reverse osmosis membranes, *Journal of Membrane Science 127 (1997) 101-109*

34. E. M. Vrijenhoek, S. Hong, M. Elimelech, Influence of membrane surface

properties on initial rate of colloidal fouling of reverse osmosis and nanofiltration membranes, *Journal of Membrane Science 188 (2001) 115–128*

35. Webpage of the Laboratory of General Biochemistry and Physical Pharmacy, University of Gent, Belgium: http://www.ugent.be/fw/biofys/en/research/equipment, Accessed in December, 2004

36. J.N. Israelachvili, *Intermolecular and Surface Forces*, 2nd edn., Academic Press, London, 1992

37. G. Vigil, Z.H. Xu, S. Steinberg and J. Israelachvili, Interactions of silica surfaces, *J. Colloid Interface Sci., 166 (1994) 367*

38. *Ion Retention in Nanofiltration*, Lab for Environmental Technology, University of Leuven

39. *Determination of the Charge of Nanofiltration Membranes*, Lab for Environmental Technology, University of Leuven

40. *Flux Decline in Nanofiltration*, Lab for Environmental Technology, University of Leuven

41. *Retention Mechanisms of Organic Molecules by Nanofiltration*, Lab for Environmental Technology, University of Leuven

42. http://www.hobbybrouwen.nl/artikel/Koolhydraten.htm, accessed in December, 2004

43. J. Tanninen, M. Nystrom, Separation of ions in acidic conditions using NF, *Desalination, 147 (2002) 295-299*

44. B. Van der Bruggen, B. Daems, D. Wilms and C. Vandecasteele, Mechanisms of retention and flux decline for the nanofiltration of dye baths from the textile industry, *Separation and Purification Technology, 23 (2001) 519-528*

45. L. Braeken, B. Van der Bruggen, C. Vandecasteele, Regeneration of brewery waste water using nanofiltration, *Water Research, 38 (2004) 3075–3082*

46. B. Van der Bruggen, K. Everaert, D. Wilms, C. Vandecasteele, Application of nanofiltration for removal of pesticides, nitrate and hardness from ground water: rejection properties and economic evaluation, *Journal of Membrane Science, 193 (2001) 239-248*

47. S. Platt, M. Nyström, Recovery of brightness in paper mill water, *Desalination, 161 (2004) 123-136*

48. J. Castelblanque, F. Salimbeni, NF and RO membranes for the recovery and reuse of water and concentrated metallic salts from waste water produced in the electroplating process, *Desalination, 167 (2004) 65-73*

49. A. Zhu, W. Zhu, Z. Wu, Y. Jing, Recovery of clindamycin from fermentation wastewater with nanofiltration membranes, *Water Research, 37 (2003) 3718-3732*

50. A. Fähnrich, V. Mavrov, H. Chmiel, Membrane processes for water reuse in the food industry, *Desalination, 119 (1998) 213-216*

51. T. Tsuru, M. Urairi, S. Nakao, S. Kimura, Reverse osmosis of single and mixed electrolytes with charged membranes: Experiment and analysis, *Journal of Chemical Engineering of Japan, 24 (1991) 518–524*

52. W. R. Bowen, A. W. Mohammad, Diafiltration by nanofiltration: Prediction and optimization, *A.I.Ch.E. Journal, 44(8) (1998) 1799–1812*

53. W. R. Bowen, T. A. Doneva, Atomic force microscopy of nanofiltration membranes: surface morphology, pore size distribution and adhesion, *Desalination, 129 (2000) 163–172*

54. C. Combe, C. Guizard, P. Aimar, V. Sanchez, Experimental determination of four characteristics used to predict the retention of a ceramic nanofiltration membrane, *Journal of Membrane Science, 129 (1997) 147–160*

55. A. R. Cooper, D. S. van Derveer, Characterization of ultrafiltration membranes by polymer transport measurements. *Separation Science Technology, 14 (1979) 551–556*

56. S. Mochizuki, A. L. Zydney, Theoretical analysis of pore size distribution effects on membrane transport, *Journal of Membrane Science, 82 (1993) 211–227*

57. J. K. Leypoldt, Determining pore size distributions of ultrafiltration membranes by solute sieving—mathematical limitations, *Journal of Membrane Science, 56 (1987) 339–354*

58. P. Aimar, M. Meireles, V. Sanchez, A contribution to the translation of retention curves into pore size distributions for sieving membranes, J*ournal of Membrane Science, 54 (1990) 321–338*

59. S. Saksena, A. L. Zydney, Pore size distribution effects on electrokinetic phenomena in semipermeable membranes, *Journal of Membrane Science, 105 (1995) 203–215*

60. W. R. Bowen, J. Welfoot, Modelling the performance of membrane nanofiltration—critical assessment and model development, *Chemical Engineering Science 57 (2002) 1121-1137*

61. W. R. Bowen, J. S. Welfoot, Modeling of membrane nanofiltration- pore size distribution effects, *Chemical Engineering Science, 57 (2002) 1393 – 1407*

62. A. E. Yaroshchuk, Recent progress in the transport characterisation of nanofiltration membranes, *Desalination 149 (2002) 423-428*

63. K. Kosutic, B. Kunst, Removal of organics from aqueous solutions by commercial RO and NF membranes of characterized porosities, *Desalination 142 (1) (2002) 47–56*

64. B. Van der Bruggen, *Removal of organic components from aqueous solution by nanofiltration,* Doctoral Thesis, Department of Chemical Engineering, Katholieke University of Leuven, September 2000

65. J.M.M. Peeters, J.P. Boom, M.H.V. Mulder, H. Strathmann, Retention measurements of nanofiltration membranes with electrolyte solutions, *Journal of Membrane Science 145 (1998) 199-209*

66. S.Y. Kwak, M.O. Yeom, I.J. Roh, D.Y. Kim, J.J. Kim, Correlations of chemical structure, atomic force microscopy (AFM) morphology, and reverse osmosis (RO) characteristics in aromatic polyester high-flux RO membranes, *J. Membrane Science 132 (1997) 183–191*

67. R. S. Faibish, M. Elimelech, Y. Cohen, Effect of Interparticle Electrostatic Double Layer Interactions on Permeate Flux Decline in Crossflow Membrane Filtration of Colloidal Suspensions: An Experimental Investigation, *Journal of Colloid and Interface Science 204 (1998) 77–86*

68. M.S. Chun, H. I1 Cho, In K. Songb, Electrokinetic behavior of membrane zeta

potential during the filtration of colloidal suspensions, *Desalination 148 (2002) 363-367*

69. S. Lee, J. Cho, M. Elimelech, Influence of colloidal fouling and feed water recovery on salt rejection of RO and NF membranes, *Desalination 160 (2004) 1-12*

70. E.M. Hoek, A.S. Kim, M. Elimelech, Influence of crossflow membrane filter geometry and shear rate on colloidal fouling in reverse osmosis and nanofiltration separations, *Environmental Engineering Science, 19 (2002) 357- 372*

71. S.G. Yiantsios, A.J. Karabelas, The effect of colloid stability on membrane fouling, *Desalination 118 (1998) 143-152*

72. M. Elimelech, W. H. Chen, J. J. Waypa, Measuring the zeta (electrokinetic) potential of reverse osmosis membranes by a streaming potential analyzer, *Desalination, 95* (1994) 269-266

73. M.J. Kotelyanskii, N.J. Wagner, M.E. Paulaitis, Atomistic simulation of water and salt transport in the reverse osmosis membrane FT-30, *Journal of Membrane Science 139 (1998) 1 16*

74. S. D.N. Freeman, T. F. Storcker, Comparison of two thin-film composite membranes: low pressure FT-30 to very low pressure NF40HF, *Desalination, 62 (1987) 183-191*

75. R.E. Larson, R.J. Petersen, and P.K. Eriksson, Test Results on FT-30 Eight-inch -diameter seawater and brackish water reverse osmosis elements, *Desalination, 46 (1983) 81-90*

76. B. Van der Bruggen, J. Schaep, D. Wilms, C. Vandecasteele, Influence of molecular size, polarity and charge on the retention of organic molecules by nanofiltration, *Journal of Membrane Science 156 (1999) 29–41*

77. Matec Instrument Company, http://www.matec.com/mas/products/esa-9800/, accessed on January, 2005

78. N.H. Lee, G. Amy, J.P. Croue, H. Buisson, Identification and understanding of fouling in low-pressure membrane (MF/UF) filtration by natural organic matter (NOM), *Water Research 38 (2004) 4511–4523*

79. R. Baltus, Characterization of the pore area distribution in porous membranes using transport measurements, *Journal of Membrane Science 123 (1997) 165 - 184*

80. L. Braeken, R. Ramaekers, Y. Zhang, G. Maes, B. Van der Bruggen, C. Vandecasteele Influence of hydrophobicity on retention in nanofiltration of aqueous solutions containing organic compounds, *Journal of Membrane Science (2005), article in press*

81. K. Kimura, G. Amy, J. Drewes, Y. Watanabe, Adsorption of hydrophobic compounds onto NF/RO membranes: an artifact leading to overestimation of rejection, *Journal of Membrane Science 221 (2003) 89–101*

List of Symbols

$\bar{c}$	mean logarithmic concentration
Δc	concentration difference
c_b	solute concentration in feed
c_f	solute concentration of feed
$C_{m,2}^{ext}$	final concentration of solute
c_p	solute concentration of permeate
$\overline{C_S}$	mean solute concentration
ΔE	streaming potential
J	solvent flux
ΔJ	flux decline
J_d	diffusive flux
J_S	solute flux
J_V	volume flux
L_1, L_P	hydrodynamic permeability (water permeability)
L_2, ω	osmotic permeability (solute permeability)
ΔP	pressure difference, applied pressure
q	component absorbed on the membrane
R	rejection (retention)
R_{tot}	total resistance
r_s, r	solute radius

r_p	membrane pore radius
$\bar{r}$	average membrane pore size
S_p	standard deviation on the pore size distribution
Δx	membrane thickness
ε	membrane porosity, permittivity
η	viscosity
λ	electrical conductivity of solution
$\Delta \pi$	osmotic pressure difference
σ	reflection coefficient
τ	membrane tortuosity
ζ	zeta potential

Abbreviations

AFM:	atomic force microscopy
BMK:	isobutyl methyl ketone
Da:	Dalton
DI:	deionized
DLVO:	Derjaguin, Landau, Vervey and Overbeek
EA:	ethyl acetate
FID:	flame-ionisation detection
GC:	Gas Chromatography
GSD:	geometric standard deviation
IEP	isoelectric point
KUL:	Katholieke University of Leuven
MEK:	methyl ethyl ketone
MF:	microfiltration
MW:	molecular weight
MWCO:	molecular weight cut-off
NF:	nanofiltration
RMS:	root mean square roughness
RO:	reverse osmosis
SEM:	scanning electron microscopy
SHP:	steric hindrance pore

TMC: trimesoyl chloride

MTM: Department of Metallurgy and Materials Engineering

UF: ultrafiltration

UV: ultra violet

VIS: visible spectrometry

Summary on Membrane Performance Testing Results

NF:

Pore size: **0.59nm**
Cut-off: **155**
Roughness: the **smoothest** (AFM: **20.8/28.1/41.5/46.0**)
Zeta potential: I.P.: **pH=3**
Hydrophobicity: the **most hydrophilic**, Contact angle: **38.8**
Salts Retention: NaCl: **58%**
    Na_2SO_4: **95%**
    $CaCl_2$: **64%**
Charge effect by pH and ion strength: (NaCl pH3 ~ 12: **55.5 ~ 80%**)
    (NaCl 0.01 ~ 0.1M: **86 ~ 50.8%**)
Organics Retention: MEK (72): **22%**
    EA (88): **14%**
    BMK (100): **54%**
    Xylose (150): **87%**
    Maltose (342): **98%**
    Raffinose (504): **99%**

LE:

Pore size: **0.49nm**
Cut-off: **100**
Roughness: the **medium** (AFM: **108.0/219.1/330.5/384.0**)
Zeta potential: I.P.: **pH=3.5**
Hydrophobicity: the **most hydrophobic**, Contact angle: **62.0 ± 3.82**
Salts Retention: NaCl: **92%**
    Na_2SO_4: **95%**
    $CaCl_2$: **95%**
Charge effect by pH and ion strength: (NaCl pH3 ~ 12: **92.7 ~ 99.9%**)
    (NaCl 0.01 ~ 0.1M: **95.9 ~ 92%**)
Organics Retention: MEK (72): **62%**
    EA (88): **69%**
    BMK (100): **94%**
    Xylose (150): **98%**
    Maltose (342): **99%**
    Raffinose (504): **99.8%**

XLE:

Pore size: **0.48nm**
Cut-off: **98**
Roughness: the **roughest** (AFM: **207.5/265.7/511.0/609.0**)
Zeta potential: I.P.: **pH=3.2**
Hydrophobicity: the **medium**, Contact angle: **53.35**
Salts Retention: NaCl: **94%**
Na_2SO_4: **98%**
$CaCl_2$: **97%**
Charge effect by pH and ion strength: (NaCl pH3 ~ 12: **96.9 ~ 99.9%**)
(NaCl 0.01 ~ 0.1M: **96.8 ~ 94.7%**)
Organics Retention: MEK (72): **69%**
EA (88): **76%**
BMK (100): **97%**
Xylose (150): **96%**
Maltose (342): **99.6%**
Raffinose (504): **99.8%**

Appendix 1

Detailed Explanation of DLVO Theory:

The partition function for N simple ions of charge q_i arrayed at positions $\vec{r}_i$ in the static potential $\phi(\vec{r})$ is:

$$\mathcal{Q} = \mathcal{Q}_0 \int_\Omega d\vec{r}_1 \cdots d\vec{r}_N \, \exp\left[-\beta V\left(\{\vec{r}_i\}\right)\right], \quad (2)$$

where

$$V\left(\{\vec{r}_i\}\right) = \frac{1}{\epsilon} \sum_{i=1}^{N} q_i \phi(\vec{r}_i) \quad (3)$$

is the total Coulomb energy, the prefactor $\mathcal{Q}_0$ results from integrals over momenta, and $\beta^{-1} = k_B T$ is the thermal energy at temperature T. All charged species in the system, including the fixed macroions, contribute to $\phi(\vec{r})$. The macroions also exclude simple ions from their interiors, so their volumes are excluded from volume of integration Ω. Equation (3) implicitly adopts the primitive model, approximating the solvent's influence through its dielectric constant, ϵ.

The partition function can be expressed as a functional integral over all possible simple-ion distributions:

$$\mathcal{Q} = \mathcal{Q}_0 \int' \mathcal{D}n \, \exp\left(-\beta f[n]\right), \quad (4)$$

where $n(\vec{r})$ is one particular simple-ion distribution with action:

$$\beta f[n] \approx \beta V[n] + \int_\Omega n \ln n \, d\Omega. \quad (5)$$

Ω is the volume of the system and the prime on the integral in Eq. (4) indicates that the simple ions' number is conserved: $\int_\Omega n \, d\Omega = N$.

Equation (5) differs from the exact action by terms accounting for higher-order correlations among simple ions. Dropping these terms, as we have in Eq. (5), yields a tractable but thermodynamically inconsistent theory. Minimizing $f[n]$ to implement the mean field approximation yields the Poisson-Boltzmann equation

$$\nabla^2\phi = -\frac{4\pi}{\epsilon}\sum_\alpha n_\alpha q_\alpha \exp\left(-\beta q_\alpha \phi\right), \quad (6)$$

where the subscript n_α is the concentration of simple ions of type α far from charged surfaces.

By considering only one ionic distribution, the mean field approximation neglects fluctuations and higher-order correlations among the simple ions. Even this simplified formulation has no analytic solution except for the simplest geometries. Derjaguin, Landau, Verwey and Overbeek (DLVO) invoked the Debye-Hückel approximation to linearize the Poisson-Boltzmann equation. Solving for the potential outside a sphere of radius a carrying charge $-Ze$ yields

$$\phi(r) = -\frac{Ze}{\epsilon}\frac{\exp(\kappa a)}{1+\kappa a}\frac{\exp(-\kappa r)}{r}. \quad (7)$$

The monotonic decay of correlations within the simple ion distribution is described by the Debye-Hückel screening length, κ^{-1}, given by:

$$\kappa^2 = \frac{4\pi}{\epsilon k_B T}\sum_\alpha n_\alpha {q_\alpha}^2. \quad (8)$$

We will consider only monovalent simple ions with $q_\alpha = \pm e$.

Although the Debye-Hückel approximation cannot be valid near the surface of a highly charged sphere, nonlinear effects should be confined to a thin surface layer. Viewed at longer length scales, nonlinear screening should only renormalize Z and κ.

In this approximation, we obtain the effective pair potential by integrating Eq. (7) over the surface of a second sphere separated from the first by a center-to-center distance r. This integration is facilitated by assuming the second sphere's presence does not disrupt the first sphere's ion cloud. The resulting superposition approximation yields a screened Coulomb repulsion for the effective inter-sphere interaction,

$$U(r) = \frac{Z^2e^2}{\epsilon}\left[\frac{\exp(\kappa a)}{1+\kappa a}\right]^2\frac{\exp(-\kappa r)}{r}. \quad (9)$$

The full DLVO potential includes a term accounting for dispersion interactions. These are negligibly weak for well-separated spheres, however, and are omitted from $U(r)$.

Appendix 2

Dynamic Light Scattering:

When a beam of light passes through a colloidal dispersion, the particles or droplets scatter some of the light in all directions. When the particles are very small compared with the wavelength of the light, the intensity of the scattered light is uniform in all directions (Rayleigh scattering); for larger particles (above approximately 250nm diameter), the intensity is angle dependent (Mie scattering).

If the light is coherent and monochromatic, as from a laser for example, it is possible to observe time-dependent fluctuations in the scattered intensity using a suitable detector such as a photomultiplier capable of operating in photon counting mode.

These fluctuations arise from the fact that the particles are small enough to undergo random thermal (Brownian) motion and the distance between them is therefore constantly varying. Constructive and destructive interference of light scattered by neighbouring particles within the illuminated zone gives rise to the intensity fluctuation at the detector plane which, as it arises from particle motion, contains information about this motion. Analysis of the time dependence of the intensity fluctuation can therefore yield the diffusion coefficient of the particles from which, via the Stokes Einstein equation, knowing the viscosity of the medium, the hydrodynamic radius or diameter of the particles can be calculated.

The time dependence of the intensity fluctuation is most commonly analysed using a digital correlator. Such a device determines the intensity autocorrelation function which can be described as the ensemble average of the product of the signal with a delayed version of itself as a function of the delay time. The "signal" in this case is the number of photons counted in one sampling interval. At short delay times, correlation is high and, over time as particles diffuse, correlation diminishes to zero and the exponential decay of the correlation function is characteristic of the diffusion coefficient of the particles. Data are typically collected over a delay range of 100ns to several seconds depending upon the particle size and viscosity of the medium.

Analysis of the autocorrelation function in terms of particle size distribution is done by numerically fitting the data with calculations based on assumed distributions. A truly monodisperse sample would give rise to a single exponential decay to which fitting a calculated particle size distribution is relatively straightforward. In practice, polydisperse samples give rise to a series of exponentials and several quite complex schemes have been devised for the fitting process. One of the methods most widely used today is known as Non-Negatively Constrained Least Squares (NNLS).

Particle size distributions can be calculated either assuming some standard form such as log-normal or without any such assumption. In the latter case, it becomes possible, within certain limitations, to characterise multimodal or skewed distributions. The size range for which dynamic light scattering is appropriate is typically submicron with some capability to deal with particles up to a few microns in diameter. The lower limit of particle size depends on the scattering properties of the particles concerned (relative refractive index of particle and medium), incident light intensity (laser power and wavelength) and detector / optics configuration.

Dynamic light scattering (also known as Quasi Elastic Light Scattering [QELS] and Photon Correlation Spectroscopy [PCS]) is particularly suited to determining small changes in mean diameter such as those due to adsorbed layers on the particle surface or slight variations in manufacturing processes.

(Webpage of Brookhaven Instruments Limited, Redditch, Worcestershire, the United Kingdom, http://www.brookhaven.co.uk/dynamic-light-scattering.html, accessed in December, 2004)

Appendix 3

Table 1: Calculation results of NF organics filtration of log-normal model

component	Mw	retention	calculated retention	(retention-calculated retention)^2
MEK	72	23	13	100
EA	88	17	31	196
BMK	100	53	46	45
Xylose	150	89	88	0.63
Maltose	342	99	100	0.98
Raffinose	504	99	100	1
				344

a=Smw	0.32
b=MW(50)	103.50
MWCO	155

Table 2: Calculation results of LE organics filtration of log-normal model

component	Mw	retention	calculated retention	(retention-calculated retention)^2
MEK	72	67	66	1.51
EA	88	78	83	24
BMK	100	95	90	23
Xylose	150	98	99	1.37
Maltose	342	99	100	1
Raffinose	504	99	100	1
				51

a=Smw	0.37
b=MW(50)	62
MWCO	100

Table 3: Calculation results of XLE organics filtration of log-normal model

component	Mw	retention	calculated retention	(retention-calculated retention)^2
MEK	72	69	67.32515077	2.80511993
EA	88	77	83.96765443	48.5482082
BMK	100	98	90.99000004	49.1400995
Xylose	150	97	99.2699485	5.152666201
Maltose	342	99	99.99986085	0.999721715
Raffinose	504	99	99.99999954	0.999999071
				107.6458146

a=Smw	0.366429
b=MW(50)	61.50452
MWCO	98

Appendix 4

Experiment data of zeta potential analysis

Table 1: Data of Zeta Potential Analysis of NF, LE and XLE

Average of the different measurements, NF			Average of the different measurements, LE		
pH	zeta	error	pH	zeta	error
2.97	4.88	2.06	2.96	3.71	2.09
3.96	-1.66	0.63	3.96	-2.42	0.98
5.14	-9.63	1.28	5.17	-8.53	1.89
5.95	-15.29	1.50	6.03	-13.50	1.16
6.92	-18.53	1.05	7.02	-14.89	1.28
8.19	-21.02	0.80	8.11	-16.13	0.84
9.08	-22.00	1.67	8.87	-16.37	0.72
9.99	-24.04	4.83	10.03	-17.57	2.65
10.98	-25.19	3.44	10.99	-18.86	3.26
11.99	-25.60	1.94	12.03	-19.44	1.80

Average of the different measurements, XLE		
pH	zeta	error
3.01	2.51	0.45
4.00	-4.27	0.82
5.04	-9.72	1.19
6.15	-14.43	1.12
6.93	-16.90	0.94
8.04	-18.97	1.02
9.20	-19.64	2.44
10.02	-21.80	2.24
10.99	-23.21	1.99
12.02	-22.92	1.46

Appendix 5

Table 5: Results of 30mg/L Silica Particles Filtration

	Membrane NF		Membrane LE		Membrane XLE	
Time	Flux	Norm. Flux	Flux	Norm. Flux	Flux	Norm. Flux
0'	74.56	105.96	52.82	114.08	59.83	121.74
15'	73.96	105.08	49.95	107.87	54.16	110.19
30'	74.53	105.89	47.86	103.36	51.50	104.78
45'	74.93	106.46	47.41	102.39	49.28	100.27
60'	76.29	108.39	46.36	100.12	49.24	100.19
75'	75.47	107.22	45.16	97.54	48.13	97.94
90'	75.80	107.69	43.53	94.02	47.03	95.70
105'	76.53	108.72	41.49	89.61	47.51	96.68
120'	76.32	108.43	42.37	91.51	46.51	94.63

Table 6: Results of 60mg/L Silica Particles Filtration

	Membrane NF		Membrane LE		Membrane XLE	
Time	Norm. Flux	Rejection	Norm. Flux	Rejection	Norm. Flux	Rejection
0'	97.37	\	107.76	\	90.92	\
15'	93.29	\	101.86	\	95.21	\
30'	93.37	94.83	99.61	96.54	92.99	97.83
45'	93.98	\	96.46	\	91.83	\
60'	95.88	95.69	94.79	96.05	87.15	98.38
75'	94.74	\	90.11	\	87.21	\
90'	95.55	95.11	90.95	98.27	86.93	98.92
105'	93.42	\	89.46	\	86.73	\
120'	96.31	95.69	82.90	97.53	85.44	96.39

Table 7: Results of 90mg/L Silica Particles Filtration

	Membrane NF		Membrane LE		Membrane XLE	
Time	Norm. Flux	Rejection	Norm. Flux	Rejection	Norm. Flux	Rejection
0'	97.82	\	105.66	\	98.23	\
15'	100.71	\	100.78	\	94.68	\
30'	101.23	97.81	99.91	98.91	93.63	98.61
45'	99.69	\	99.96	\	92.81	\
60'	100.20	97.09	97.33	98.91	92.10	98.79
75'	100.27	\	95.16	\	90.78	\
90'	99.88	98.00	96.06	98.72	91.38	98.61
105'	97.48	\	94.69	\	89.19	\
120'	98.05	97.81	94.67	99.45	86.18	99.13

Appendix 6

Information on K_{OW} of organic compounds

The octanol-water partition coefficient (K_{OW}) is the ratio of the concentration of a chemical in octanol and in water at equilibrium and at a specified temperature. Octanol is an organic solvent that is used as a surrogate for natural organic matter. This parameter is used in many environmental studies to help determine the fate of chemicals in the environment. The octanol-water partition coefficient has been correlated to water solubility; therefore, the water solubility of a substance can be used to estimate its octanol-water partition coefficient. K_{OW} is always to be applied for describing the hydrophobicity of the organic compounds. In general, hydrophobicity increases with increasing K_{OW}.

Webpage of US Geological Survey: http://toxics.usgs.gov/definitions/kow.html, accessed in Feb. 2005

Appendix 7

Some information on reagents for filtration experiment

NaCl: AnalaR®
BDH Laboratory Supplies, Poole BH15 1TD England.
MW: 58.44g/mol, Lot: K31445433 249
Volumetric Solution

HCl: Hydrochloric Acid, 1mol/L
Geldenaaksebaan 464,
B-3001 Leuven
Lot: 99J110037

NaOH: Sodium hydroxide, 1mol/L
Volumetric Solution
Fisher Scientific UK Limited
Bishop Meadow Road
Loughbough, Leicestershire LE11 5RG UK
Code: J/7620/15
Batch: 0387006

Particles:
ALDRICH
Silica, fumed, 99.8%
Batch# 03318CB
FW: 60.09

Table 8: Silica colloidal particles phyco-chemical data

	SiO_2 content	Stabilisizing Agent	pH-value DIN ISO 787/IX	Viscosity (Brookfield 50 rpm, 20℃)	Aggregate Size (d-50 Wert)	Density (20℃)
Unit	wt.%	\	\	mPa s	μm	g/cm^3
Typical Value	20 ± 1.0	Ammonia	9.5~10.5	≦100	0.12	1.12

VP Disp. W 7520, AEROSIL®
Alkaline dispersion of hydrophilic fumed silica

Methyl Ethyl Ketone (**MEK**)
Art. 822253
C_4H_8O MW: 72.11g/mol
1L=0.8kg
Schuchardt, 8011 Hohenbrunn bei, München

Ethyl Acetate (EA)
EC-NO: 205-500-4
$CH_3COOC_2H_5$, MW: 88.10g/mol
BDH Laboratory Supplies
Poole BH15 1TD England

Isobutyl Methyl Ketone (BMK)
Art. 6146
$C_6H_{12}O$, MW: 100.16g/mol
1L=0.8kg
Schuchardt, 8011 Hohenbrunn bei, München

Appendix 8

Calibration for salt concentration

Table 9: Data of salts concentration for calibration

NaCl

Concentration (mol/l)	0.001	0.002	0.005	0.01	0.02	0.04
Condictivity (μS/cm)	13.71	26.1	61.2	119.6	232	453

Na2SO4

Concentration (mol/l)	0.001	0.002	0.005	0.01	0.02	0.04
Condictivity (μS/cm)	25.5	48.9	112	212	398	747

CaCl2

Concentration (mol/l)	0.001	0.002	0.005	0.01	0.02	0.04
Condictivity (μS/cm)	26.9	52	119.5	231	442	844

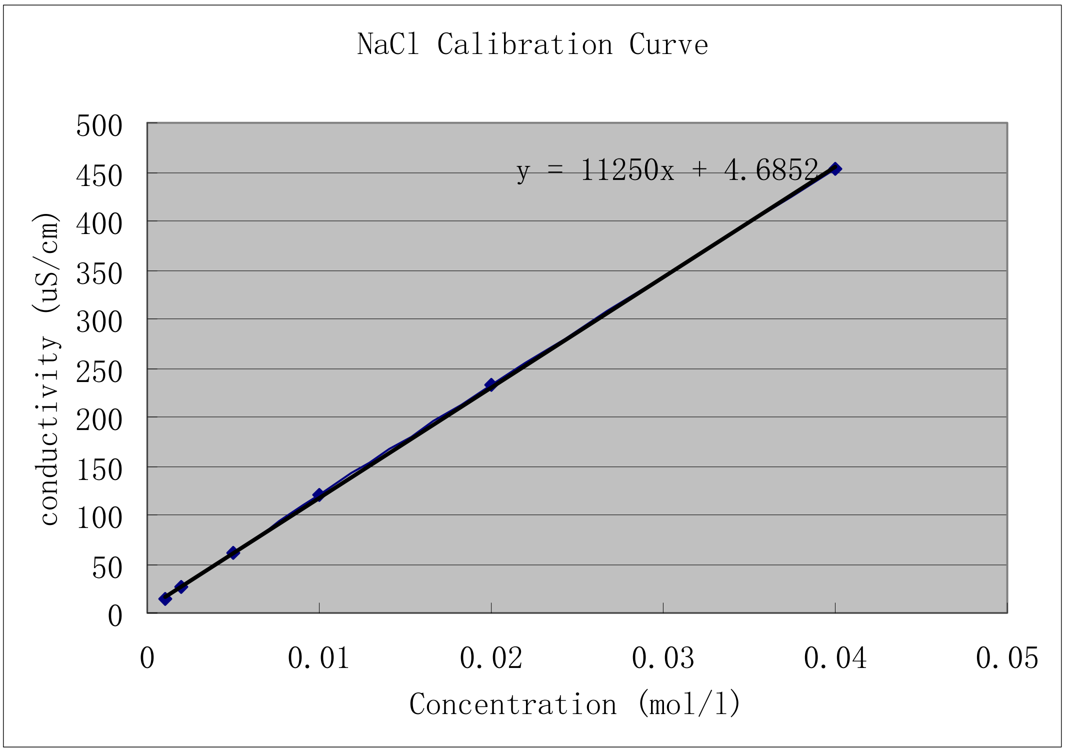

(a)

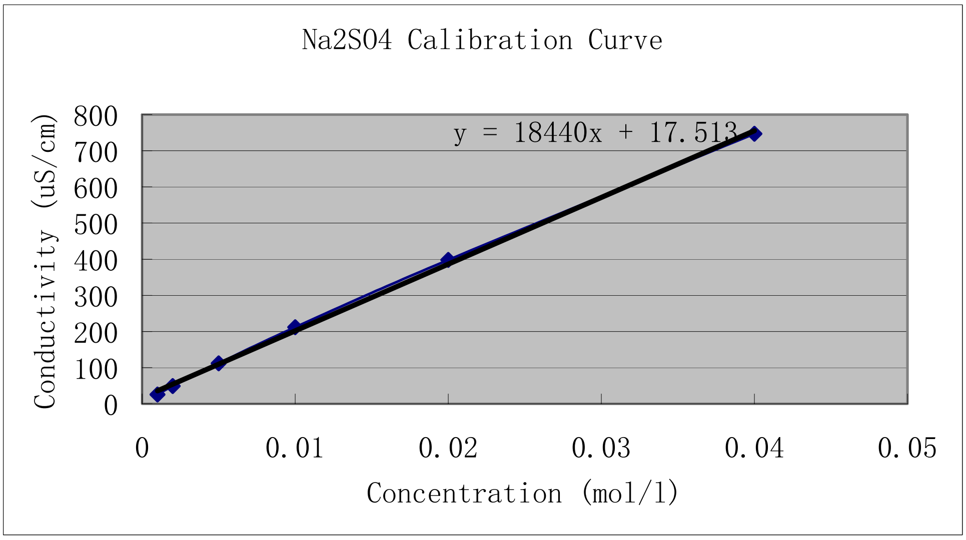

(b)

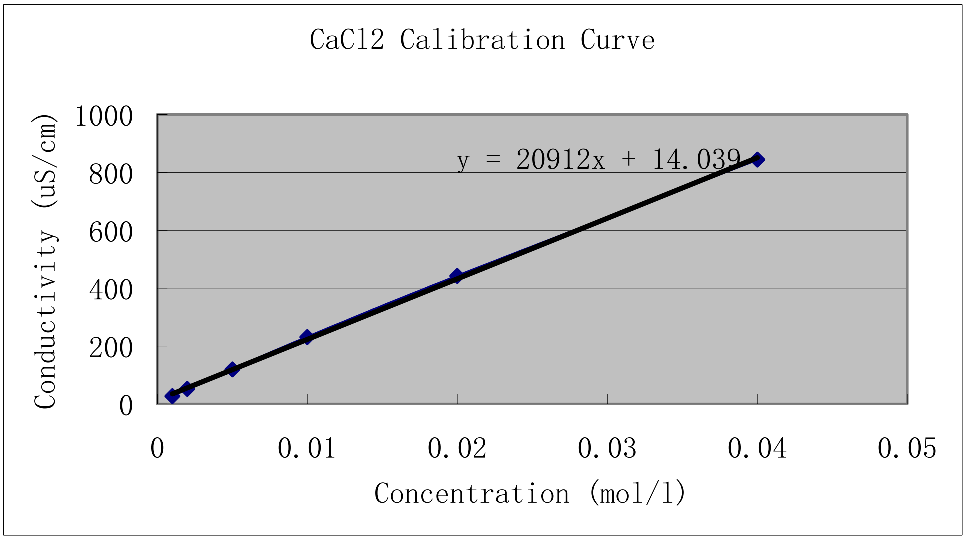

(c)

Figure 1: Calibration curve for salt concentration

Appendix 9

NaCl Retention in Different pH Background

Table 10: NaCl Retention in Different pH Background

Membrane	NF		LE		XLE	
	retention	n. flux	retention	n. flux	retention	n. flux
pH=3	55.74	94.78	96.93	30.04	100	36.00
pH=5	68.41	87.45	97.40	69.38	96.85	58.94
pH=7	77.05	87.19	97.84	69.93	97.51	62.48
pH=10	75.02	121.32	100	63.49	100	53.65
pH=12	77.58	130.53	100	39.32	100	49.65

*For the retention which exceeds 100% in the data, 100% takes place.

**n. flux=normalized flux